INVESTIGATION OF THE CRYSTAL GROWTH AND PROPERTIES OF TUNGSTEN BRONZE TYPE ELECTRO-OPTIC MATERIALS

by

T. M. BRUTON

A THESIS SUBMITTED FOR THE DEGREE OF DOCTOR OF PHILOSOPHY

May, 1971

Science of Materials Section,
Department of Electrical Engineering,
Imperial College of Science and Technology,
University of London

ABSTRACT

The work described in this thesis is the original work of the author except where full acknowledgment has been made.

The significant parameters in determining the conditions for the growth from solution of optical quality, large single crystals of lead tantalate have been measured. Single crystals have been prepared which were suitable for electro-optic measurements. A model for the growth of lead tantalate crystals from solution is proposed. The half wave voltage for several orientations of the crystal has been measured.

The structural and dielectric properties of a new series of tungsten bronze oxides based on the composition $Pb_6Ti_2Nb_8O_{30}$ have been determined and the ferroelectric behaviour of the lead rich compounds has been established.

TO MARGARET

ACKNOWLEDGEMENTS

I should like to thank Dr. E. A. D. White for many helpful discussions and much good advice during the course of this project. I should like to thank Mr. J. D. C. Wood and Mr. K. C. Jeffries, of the Crystal Growth Laboratories, for their technical advice and Prof. J. C. Anderson for his encouragement.

I am grateful to the Director, G.P.O. Research Station, Dollis Hill, for the award of a research studentship and to Dr. M. Faktor and Mrs. S. Ayers of the G.P.O. Research Station for their advice and encouragement.

I should like to thank Mrs. P. Mackellow for typing the manuscript.

The measurements of dielectric constants of $Pb_6Ti_2Nb_8O_{30}$ ceramic discs were carried out by staff of the G.P.O. Research Station and the electro-optic measurements were carried out on equipment on loan from the G.P.O. research station.

TABLE OF CONTENTS

CHAPTER I

1. INTRODUCTION

1.1 The Need for Electro-Optic Materials

The radio, television and telephone links between two major industrial cities in this country require a bandwidth of 200 MHz to transmit the volume of information. This volume is growing exponentially each year and communication systems with very large bandwidths will be needed. A communications system employing an optical frequency carrier wave could possess bandwidth in the 1k MHz region which could accommodate the growth in the volume of information to be transmitted for the foreseeable future.

Such a system is dependent upon the achievement of efficient means of modulation. Modulators using the linear electro-optic effect have been proposed. The linear electro-optic effect was first discovered by F. Pockels (1893) and in this effect a change in the refractive index of a crystal is achieved by the application of an electric field. Although a number of materials have been discovered which exhibit this effect, only a very few have been found to possess a sufficiently strong effect to be of practical importance.

There is a further difficulty as the materials must be available as large single crystals of optical quality. It has been found that many of the materials exhibit a large effect but are not readily prepared as single crystals. Consequently, a better understanding of the conditions necessary for the controlled growth of good quality single crystals is required.

There are potential applications for crystals exhibiting a large electro-optic effect in other fields in addition to communications; in high speed optical digital deflectors; in memories and in optical

display systems. All these potential uses can only be realised when materials possessing large electro-optic coefficients can be easily prepared as optical quality single crystals.

1.2 The Uses of Electro-Optic Materials

The two most important potential applications are as modulators in an optical communication system and as polarisation switches in an optical digital system. In a modulator configuration, a coherent light beam which is polarised at 45° to the principal axes of the crystal is propagated through the crystal. The light beam is divided into two equal components plane polarised at right angles. An electric field applied to the crystal changes the refractive indices of the crystal, usually by differing amounts in the two directions of polarisation. Hence, there is a phase difference between the two components which is dependent on the applied electric field. The electric field can be applied parallel to the light beam (longitudinal effect) or at right angles to it (transverse effect). By suitable choice of the analyser orientation and the crystal's natural birefringence either phase modulation or amplitude modulation can be achieved.

In an optical digital light deflector a series of crystals is arranged with an electro-optic crystal alternating with a strongly birefringent crystal. As for a modulator, a beam is propagated through the crystal as two components which are given a relative phase difference by the field. In general, an eliptically polarised light beam is produced. However, at one value of the field, the half wave voltage, a phase difference of π radians is obtained and a plane polarised beam is produced. If the natural birefringence of the crystal is used, so that with no field applied there is a phase difference of 2π radians, then again a plane polarised beam is obtained. The two resultant plane polarised waves for

phase differences of π and 2π radians are polarised at right angles. Thus, applying the field to the crystal rotates the plane of polarisation by 90^{o}. The birefringent crystal is orientated so that one polarisation is transmitted without deflection and the other is deflected. Hence, for each unit in the series there are two possible positions for the beam which may be switched by a voltage. This is the basis for a high speed optical computer write-in system.

1.3 Other Non-Linear Optical Phenomena

The linear electro-optic effect is one of a number of non-linear optical phenomena which are of technological significance. The most important are second harmonic generation (S.H.G.) and parametric oscillation. In S.H.G. a fundamental wave of frequency ω is transmitted through a non-linear crystal and secondary components of frequency ω_2 and ω_0, are generated. Furthermore, if two waves of frequency ω_1 and ω_2 are propagated through the crystals, then components of frequencies $\omega_1 + \omega_2$ and $\omega_2 - \omega_1$ are generated. This is of practical importance because if ω_1 is an infra red frequency and ω_2 an ultra violet frequency, then $\omega_2 - \omega_1$ will be a visible frequency. Therefore, conversion from infra red to the visible is possible.

In parametric oscillation two waves of differing frequencies are propagated through the crystal. Optical energy can be transmitted from one to the other and the crystal then acts as a light amplifier.

In general a crystal which exhibits one non-linear phenomenon will also exhibit two others, but with differing efficiencies. Thus, when a new material is developed, even if it is poor in respect of one phenomenon, it may be important with respect to another, consequently, it is worthwhile to investigate all the non-linear properties of the material.

1.4 Linear Electro-optic Materials Currently Under Investigation

Only crystals with non-centrosymetric structure exhibit the linear electro-optic effect (4.5). Within this constraint a very wide range of materials has been investigated. These may be broadly classified into five categories:

(1) AB type semiconductors

(2) KH_2PO_4 and its isomorphs

(3) Organic materials

(4) Oxygen-Octahedra ferroelectrics

(5) Miscellaneous materials.

Table 1.1 lists the properties of typical compounds of each category. The oxygen-octahedra ferroelectrics have been the subject of the most intense investigation in recent years. They can be classified into three structure types, each made up of BO^{n-}_6 octahedral units. The three are (1) perovskile type structure; e.g. $BaTiO_3$, (2) pseudo-ilmenite-type structure; e.g. $LiNbO_3$, (3) tungsten bronze structure e.g. $Sr_{0.5}Ba_{0.5}Nb_2O_6$. The tungsten bronze structure materials have been shown to have the highest electro-optic coefficients and the lowest half wave voltages of any of the groups. This has been ascribed by Wemple (1969) to the fact that these materials have the closest packing of BO_6 octahedra. The two best materials that have been so far developed are barium sodium niobate, $Ba_2NaNb_5O_{1.5}$ and strontium barium niobate $Ba_{(1-x)}Sr_{(x)}Nb_2O_6$.

1.5 The Selection of New Materials for Investigation

In addition to the requirement that the crystal should belong to a non-centrosymmetric class, the following criteria define a good electro-optic material.

(1) Low absorption at the relevant frequencies

(2) Large electro-optic coefficients and high refractive indices.

(3) Resistance to optical damage.

(4) Easily grown as large single crystals.

(5) Resistance to atmospheric attack and possessing long term thermical stability.

(6) Low dielectric constant and dielectric losses.

There criteria are obvious except for (3) but are not consistent with one another. Optical damage occurs when the crystal is irradiated in an electric field. The radiation excites electrons from the valence band; due to the internal electric field the electrons migrate through the crystal, in the beam area, and fall into deep traps. The electrons accumulate locally, producing a charge field which produces its own refractive index change which in turn scatters light out of the crystal.

Although it is not possible to predict whether a new material will satisfy all or any of these criteria until large single crystals are grown, there are some grounds for chosing new materials. Miller's rule (Miller, 1964) states the electro-optic coefficient is proportional to the linear dielectric susceptibility. Thus a material possessing tungsten bronze structure and having a large dielectric constant should prove to be a good electro-optic material. One such material is lead metatantalate, $PbTa_2O_6$, which is a tungsten bronze ferroelectric with a dielectric constant of about 800 (Francombe 1958). No measurement of its electro-optic properties has been reported.

It is known that stochiometric tungsten bronzes are not optically damaged by lasers. While a number of different tungsten bronze compositions have been investigated, very little attention has been given to tungsten bronzes of the type $(A1^{2+})_2\ (A2^{2+})_4\ (B1^{4+})_2\ (B2^{5+})_8\ O_{30}$, which is the required composition for a fully-filled tungsten bronze structure. Thus, it might be expected that the composition $Pb_6Ti_2Nb_8O_{30}$ is a tungsten bronze ferroelectric. A study of its dielectric properties in ceramic

form would indicate if further investigation of its growth as single crystals and subsequent measurement of electro-optic coefficient is desirable.

1.6 Crystal Growth of Electro-Optic Materials

On this topic the following quotation from Bergman (1970) is instructive. "The number of materials of any kind which can be grown as large single crystals is very limited indeed. It is, therefore, not surprising that the major bottleneck is not in finding materials to grow but in finding satisfactory ways of growing them." By far the most commonly used method of preparing crystals for electro-optic purposes has been the Czochralski technique. Virtually all the tungsten bronze ferroelectrics have been prepared in this manner. The review of recent electro-optic materials by Spencer (1967) mentions no other growth technique. While the technique has been successful for some materials, it limits the types of material that can be grown. For example, lead is a highly polarised ion and should have a beneficial effect when incorporated into the tungsten bronze structure. However, lead oxide is volatile at high temperatures ($>1000^{\circ}C$) and the Czochralski technique cannot be used. Similarly, non-congruently melting materials cannot be prepared by this technique. The high temperature/solution technique (fluxed melt technique) must therefore be used for such materials; this has been employed with some success in the preparation of many materials for research purposes and has the advantage that small but good quality crystals are obtainable. It has been applied to the growth of potassium tantalum niobate (KTN) from solution in potassium carbonate by Whipps (1970).

1.7 The High Temperature Solution Technique

High temperature solution techniques and aqueous solution tech-

nique are both examples of the same basic principle, that is the addition of a solvent component which lowers the melting point of the pure component to a temperature at which it may be prepared as a single crystal. However, as the solvent is a molten oxide or salt, the solution process must take place at high temperatures (>800^{o}C) as the solvents are liquids only at these temperatures. The technique has proved remarkably successful in the preparation of refractory oxides which are extremely insoluble in room temperature solvents. (White I, 1965). Lead tantalate can only be prepared by this technique (1.13). The high temperature solution technique has limitations due to the problems in maintaining the solution at constant temperature and due to the highly corrosive nature of the solvents which can be contained only in crucibles of platinum or irridium. Furthermore, very little is known of the chemical or physical behaviour of these solutions, and by their very nature they make difficult measurement of their properties. However, Elwell (1967, 1968) has shown where an investigation of the solution's properties is made, a very substantial improvement can be achieved in the size and quality of the crystals grown. The conditions for the growth of large single crystals is discussed in Chapter 2. However, most crystals that have been grown from high temperature solutions have been obtained without any investigation of the solute solvent system. This is a fact deplored by reviewers of the subject (White I, 1965, Roy (1968)) who point out the great value of a systematic study of the properties of the solution.

1.8 The Scope of the Research

In order to grow large single crystals of lead tantalate, it is necessary to find a suitable solvent (criteria of suitable solvents, 2.2). For this reason the solubility of lead tantalate in a number of solvents has been measured. Of these the solvent, lead vanadate $Pb_2V_2O_7$ was most

suitable and further measurements were made on the properties of this solute-solvent system. Experiments to grow single crystals by slowly cooling the solution and by the temperature gradient transport technique, (White, I, 1965) have been performed. A model for the growth of lead tantalate from solution was derived from the experimental evidence. The dielectric and electro-optic properties of the lead tantalate crystals were measured.

The dielectric and structural properties of the system $Pb_6Ti_2Nb_8O_{30}$ have been measured for a varying Ti:Nb ratio. Lanthanum oxide was added to provide charge compensation. Experimental attempts to grow single crystals are described.

LITERATURE SURVEY

1.9 The Linear Electro-Optic Effect

The linear electro-optic effect was first measured by F. Pockels (1893, 1906) in crystals of quartz, tourmaline, potassium chlorate and Rochelle salt. Zwicker and Schirrer (1943 and 1944) reported the d.c. electro-optic coefficients of potassium dihydrogen phosphate and potassium dideuterium phosphate. The effect in these later materials was sufficiently large for their use in practical applications, and their discovery, with the advent of the laser, stimulated the investigation of the variety of materials whose properties are now known.

Nye (1960) derived the dependence of the electro-optic coefficient r_{ijk} on the symmetry of the crystal. He further demonstrated that the change in refractive index of the crystal with electric field was due to the dependence of the dielectric polarisation on higher orders of the electric field. Most theoretical models advanced since that time have tried to derive a mechanism for this dependence.

In a phenomenological model for second harmonic generation Miller (1964) assumed that the free energy of the S.H.G. was dependent upon the amplitude of the polarisation waves of the secondary radiation.

In this way he derived a relation:

$$d_{ijk} = \delta_{ijk}\, {}^{2\omega}\chi_{ii}\, {}^{2\omega}\chi_{jj}\, {}^{\omega}\chi_{kk}\, {}^{\omega}\delta_{ijk}$$

where d_{ijk} is the coefficient of second harmonic generation,

$\chi_{ii}^{2\omega}$ etc. are the linear susceptibilities at the appropriate frequencies.

δ_{ijk} is a constant and was found by Miller to have a similar value for a wide range of materials.

Miller then used Kleinman's relation (Kleinman (1962)) that

$$r_{ijk} = -\frac{4\pi}{n_{ij}^{4}} d_{ijk}$$

to show the dependence of r_{ijk} on the linear optical susceptibilities at the appropriate frequencies.

The classical model of a dielectric material due to Huang was extended by Kelly (1966) to give a non-linear polarisation. Huang's model needed only dipole interactions for the calculation of the susceptibility due to the lattice ions. Kelly extended the treatment to include the quadrupole interactions and hence obtained a polarisation dependent on the electric field. The electronic contribution was calculated using the linear susceptibility and Lorentz type local effective field value, which included the applied field. Experiment results agreed with their theory to an accuracy of within a few per cent.

Kurtz and Robinson (1967) used the anharmonic oscillator model first derived by Bloembergen (1965) to derive an expression for the electro-optic coefficient. In this model, each bonding electron is thought to oscillate with an ultraviolet frequency in a symmetrical potential well to which a small anharmonic term is added. The characteristic frequency of the electron describes the refractive index in the visible region, and the anharmonicity gives rise to a non-linear polarisation. Kurtz and Robinson

then used this and the Kleinman relation to deduce the electro-optic constant. They further extended their treatment to include ferroelectric materials and concluded that the linear electro-optic coefficient depended directly upon the spontaneous polarisation. Garret (1968) has shown that the anharmonic oscillator model provides a valid description for a number of non-linear phenomena. Kurtz and Robinson's treatment is most valid for ionic crystals and Kelley's treatment for covalently bonded crystals.

There are two distinct mechanisms by which the applied electric field changes the refractive index of the crystal. The first is the interaction between the field and the lattice vibrational modes, which in turn through the lattice to bonding electron interaction changes the polarisability at optical frequencies and hence gives a refractive index change. The second mechanism is the direct interaction of the applied electric field with the bonding electrons. Kaminow (1967) has shown that in lithium niobate and lithium tantalate the lattice contributes 90% and the electrons 10%. of the effect.

The contribution of the ion of a given element to the effect has not been studied in detail. Emmenegger et al. (1968) have studied double sulphates of the Langbeinite structure, having the general formula $M_2^{I}M_2^{II}(SO_4)_3$. They concluded that the metallic ions contributed very little, the chief contribution being made by the acentric sulphate group. The exception was for the material $(NH_4)_2\ Mn_2\ (SO_4)_3$ in which the acentric ammonium group acted in an opposite sense to the sulphate group and a relatively small electro-optic effect was observed.

1.10 Linear Electro-Optic Materials

Tables of electro-optic coefficients can be found in the American Institute of Physics Handbook of Physics and Chemistry and in Physical Chemical Tables (1962). Further reviews have been published by Kaminow (1966),

Spencer et al. (1967). The properties of oxygen octahedron ferroelectrics has been summarised by Wemple (1969).

Table 1.1 gives a list of typical electro-optic materials as classified in section 1.4. The largest coefficient and the half wave voltage is given where the data has been published. A large electro-optic coefficient does not necessarily mean a small half wave voltage as this is a function of difference between coefficients.

1.11 The Tungsten Bronze Oxides

A review of the chemistry of the tungsten bronze oxides is given by A. D. Wadsley (1960). The structure is made up of oxygen octahedra arranged in rings to form five, four and three sided tunnels as shown in the unit cell, fig. 1.1. The pentavalent ions are located near the centre of the octahedra, the monovalent or divalent ions are located in the tunnel sites. Fig. 1.1 shows the tetragonal form; orthorhombic and hexagonal unit cells are also found. The general formula for the tungsten bronze structure is $(A1)_2\ (A2)_4\ (C)_4\ (B1)_2\ (B2)_8\ O_{30}$. A detailed structural analysis of the material $Ba_{0.27}Sr_{0.75}Nb_2O_{5.78}$ has been performed by Jamieson (1968) who also reviewed the structure of tungsten bronze ferroelectrics. A wide range of properties is found in the bronzes, depending on the degree of stoichiometry and on the ions present in the structure. When all the A and B sites are filled the materials are ferroelectric. Of particular interest for electro-optic applications are materials in which A is lead, barium, strontium, potassium, sodium or lithium and B is titanium, niobium or tantalum. Rubin et al. (1967) prepared and determined the electro-optic properties of a number of niobate materials containing various combinations of the divalent and monovalent ions. Little work has been published on the properties of the tungsten bronze type $(A)^{2+}_6\ (B1)^{4+}_2\ (B2)^{5+}_8\ O_{30}$. The structure of $Ba_6Ti_2Nb_6O_{30}$

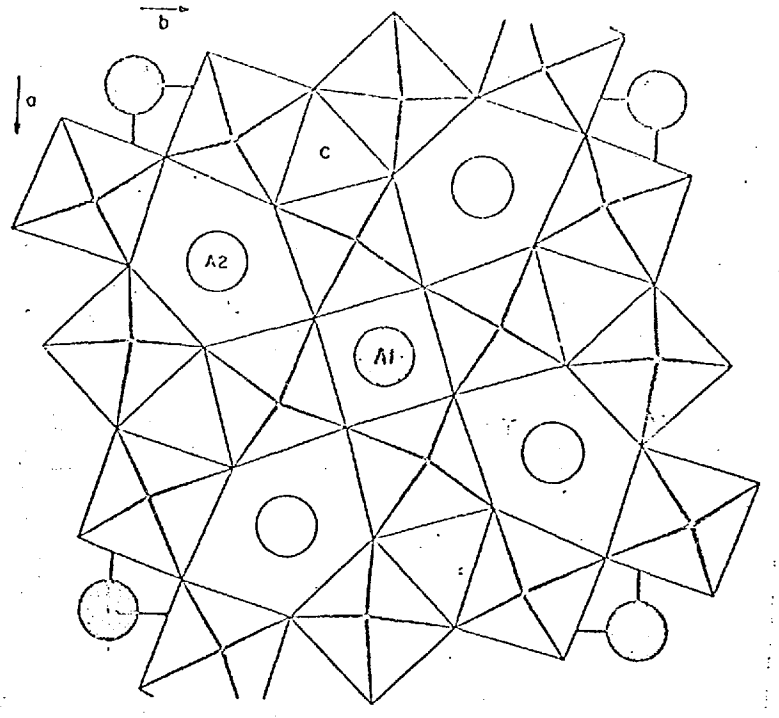

FIG. 1.1

TABLE 1.1

Material	Electro-optic Coefficient ($\times 10^8$cm/V)	Half Wave Voltage in Volts	References
AB Semiconductors			
CdS	$r_{51} = 1.2$		Kaminow (1966)
CuC-	$r_{41} = 2.0$		- do -
GaP	$r_{41} = 0.35$		- do -
ZnS	$r_{41} = 0.60$		- do -
KDP and isomorphs			
KH_2PO_4	$r_{63} = 32$	7500	- do -
$(NH_4)H_2PO_4$	$r_{61} = 25$	9600	- do -
KH_2AsO_4	$r_{63} = 39$	6200	- do -
Organic compounds			
Rochelle salt	$r_{41} = 6.0$		American Institute of
Tourmaline	$r_{22} = 0.1$		Physics Handbook
$C(CH_2OH)_4$	$r_{52} = 0.5$		
BO_6 Oxygen Octahedra			
Perovskite			
$BaTiO_3$	$r_{42} = 8.2$		Johnston (1965)
Illeminite type			
$LiNbO_3$	$r_{22} = 20$	2800	
Tungsten Bronze			
$Sr_{.75}Ba_{.25}Nb_2O_6$	$r_{33} = 10.1$	37	Lenzo (1967)
$BaNaNb_2O_6$	$r_{33} = 0.3$	1600	Geusic (1967)
$K_6Li_4Nb_{10}O_{30}$	$r_{33} = 0.84$	930	van Uitert (1967)
$Sr_2KNb_2O_{15}$	$r_{11} = 1.3$	400	Giess (1967)
Miscellaneous			
$K_2Mg_2(SO_4)_3$	$r_{41} = 0.3$		Ememmengger (1968)
$Bi_4(GeO_4)_3$	$r_{41} = 0.34$		Spencer (1967)

Electro - Optic Coefficients and Half - Wave Voltages of typical materials.

has been analysed by Stephenson (1965). The X-ray evidence suggested the material should be a ferroelectric.

1.12 Lead Tantalate $PbTa_2O_6$

The earliest investigations were made on ceramic discs prepared from the two oxides. Smolenski et al. (1954) demonstrated that the material was ferroelectric with a Curie point at 260°C. Francombe (1958) reported that lead tantalate was a tetragonal tungsten bronze ferroelectric with a Curie temperature of 150°C. Ismailizide (1959) reported the space group as the orthorhombic Cm2m in the ferroelectric phase which becomes the tetragonal P4/mbm above the Curie point. Ismailzide (1966) confirmed these results with a more accurate X-study and gave the Curie temperature as 265°C.

As described in section 1.13, Subbarao (1960) prepared single crystals of lead tantalate. They gave the lattice constants as a = 17.68, c = 7.754Å and b/a = 1.002. The polar axis was normal to the [001] axis and the spontaneous polarisation was 10×10^{-6} coul. cm^{-2}. They measured the natural birefringence along the three crystallographic axes. Their dielectric study on the single crystals indicated a Curie temperature of 265°C. Thus a Curie temperature of 265°C is independently confirmed and may be taken to be the most accurate value.

The sub-solidus phase diagram of the $PbO-Ta_2O_5$ system has been investigated by Subbarao (1961). He concluded that ferroelectric lead tantalate was a metastable phase formed only above 1140°C. The equilibrium room temperature form is rhombohedral and non-ferroelectric. The transition from orthorhombic to rhombohedral is extremely slow and can be only partially accomplished by heating the orthorhombic form at 900°C for 24 hours.

1.13 The Growth of Lead Tantalate Single Crystals

Lead tantalate crystals cannot readily be grown from the pure melt as lead oxide is very volatile above 1100°C, the melting point of lead tantalate being above 1500°C (Subbarao, (1961)). Crystals have been grown from solution in lead vanadate, $Ph_2V_2O_7$ by Subbarao (1960). The best crystals obtained measured 1 x 1 x 4 mm. They were elongated along the [001] axis and were frequently twinned. The ferroelectric phase could only be prepared from solutions initially heated above 1140°C.

Chemical vapour phase transport is unsuitable for such a refractory oxide as tantalum pentoxide due to its low vapour pressure and chemical activity. This leaves the possibility of using the hydrothermal technique. Hill (1966) found that for lead niobate, which has a very similar phase diagram to that of lead tantalate, had no stability field for the ferroelectric phase at any pressure below 25 atmospheres or at any temperature below 1150°C. A similar result may be expected for lead tantalate. Hence, high temperature solution is the only effective technique for preparation of lead tantalate crystals.

1.14 High Temperature Solution

Reviews of the high temperature solution technique have been published by Laudise (1963), White (I, 1965) and Roy (1968). Laudise discusses phase relationships of solute and solvent and illustrates the discussion with reference to the growth of barium titanate and yttrium iron garnet. White has given a more comprehensive review, and discusses the experimental techniques and apparatus, the criteria for the choice of solvents, methods of determining solubility, and finally, the crystal quality in terms of the growth process. Roy describes recent improvements in experimental techniques. All the reviewers state there is a great need for measurement of the solution's properties. Kohman (1963) has

reviewed the theory of growth of solution. Cobb (1967) has given theoretical requirements for the growth of large single crystals of alumina from a lanthanum fluoride solution by slow cooling and temperature gradient transport. He also measured the density and viscosity of the solution.

1.14.1 Nucleation

The theory of nucleation of crystals has been given by Strickland-Constable (1968). White (I, 1965) has remarked that the supersaturation for spontaneous nucleation is much greater than that required for stable growth. Crystals grown by spontaneous nucleation are characterised by cores of highly disordered dendritic type material. The best method of obtaining good crystal growth is to use a seed crystal (Kohman, 1963).

1.14.2 The rate of growth of the interface

The theory of crystal growth has been discussed by Strickland-Constable (1968). The conventional model of crystal growth is shown in figure2.3. There is an unstirred layer in contact with the crystal face in which there is a concentration gradient through which the crystal molecules diffuse. In the surface layers the molecules migrate until they are incorporated into the crystal. There are two rate determining processes, one is diffusion through the unstirred layer, the other is the incorporation of the molecule into the interface. The rate determining step for particle integration was thought to be the rate of production of a two-dimensional nucleus on an otherwise atomically flat surface, (Volmer (1931)), (Stranski (1928)), (Becker (1935)), but it predicted a much slower growth rate than the experimentally observed one. Frank (1949) suggested a screw dislocation emerging from the surface would provide a nucleus which would be perpetuated during growth. Burton, Cabera and Frank (1951) calculated the rate of growth of the interface for molecules integrated into the lattice at a kink in such a nucleus. They derived

a linear growth rate $v = \frac{c}{\sigma_1} \sigma^2$ at low supersaturations and $v = c\sigma$ at high supersaturations where c, σ, are constants and σ is the relative supersaturation. This treatment was extended by Benema (1965) to include surface diffusion.

Bryce (I, 1967) has considered non-diffusion limited solution growth. He derives six relationships between supersaturation and growth rate which are dependent on the nature of the surface. He considers three situation (1) where particles are incorporated at any point, (2) where they are attached to a nucleus on an otherwise flat surface, and (3) where there is a spiral dislocation. He considers these at high and low supersaturations. He further considers diffusion limited growth (Bryce II, 1967) and concludes that the growth rate $v = k_1 \sigma$ at high supersaturation and $v = k_2 \sigma^n$ at low supersaturations where k_1, k_2 ^{n}, are constants and n varies between 1 and 2 and is determined experimentally.

1.14.3. The rate of production of supersaturation

The rate at which supersaturation is produced in the solution is determined by the rate of slow cooling of the solution, the temperature gradient or the temperature of solution according to the technique chosen. In general, these conditions may be chosen before by the experimenter. Laudise (1963) has derived the linear growth rate, R, of a crystal face in slowly cooled solution as $R = \frac{M\beta}{A\rho} \frac{d\theta}{dt}$ where M is the mass of solution, A the surface area of the growing crystal face, P the density of the melt, β the temperature coefficient of solubility, and $\frac{d\theta}{dt}$ the cooling rate. Wood (1970) has derived the relation for the decrease in solution temperature with time for a linear growth rate a constant supersaturation as:

$$\Delta\theta_t = \alpha t^3$$

where $\Delta\theta_t = \theta_c - \theta_t$; θ_c is the saturation temperature and θ_t is the

solution temperature at time t.

α is a constant given by

$$\alpha = \frac{N}{nk} \frac{\rho}{27} f^3 \quad R^3$$

where N is the number of seed, n the number of litres of solution, k is the slope of the solubility curve, f^3 the habit factor and ρ the density of solution.

Both relationships require a knowledge of the solubility as a function of temperature. While (I, 1965) describes methods of determining solubility by quenching techniques. These experiments are somewhat tedious and can fail to give any consistent results. This was found to be so by Cobb (1967) who also used differential thermal analysis techniques without success. A simple and very effective method of determining solubility using a thermobalance technique has been reported by Elwell (1967).

Standard thermodynamic techniques can be used to derive an expression for the solubility of a given solute-solvent system (Kohman, 1963) provided all the thermodynamic variables are known. This is rarely the case, especially for new materials. Cobb (1969) has derived an expression for solubility which depends only on temperature of the solution and the melting point and heat of fusion of the solute in the pure state.

1.14.4. The Transport of solute through the bulk solution

The transport of heat and mass through the bulk of the solution to the crystal surface is a problem of fluid mechanics. Jakob (1953) reviews the problems of heat and mass flow in systems where there is a change of phase. There is an exact equivalence in the description between a system where there is an isothermal transport of mass and a system where there is a transport of heat at constant composition. Thus,

solutions of heat flow equations can be applied to equivalent problems in mass flow. Growth by slow cooling approximately to isothermal mass transport. Where heat and mass flow occur simultaneously the transport is defined by the equations

$$a = \frac{\alpha}{L} \cdot \left| N_{Gr}', N_{Pr}, N_{Sc} \right|$$

$$b = \frac{\delta}{L} \cdot \left| N_{Gr}', N_{Pr}, N_{Sc} \right|$$

where a, b are the coefficients of heat and mass transfer respectively,

is some function defined by the experimental conditions,

α is the thermal diffusivity, and

δ the mechanical diffusivity.

N_{Gr}', N_{Pr} and N_{Sc} are modified Grashof number, the Prandtl number and the Schmidt number. A glossary of these terms is given in Appendix A.

Carlson (1958) used the similarity between heat and mass flow to study the growth of crystals from aqueous solution. For an equal deposition of mass to occur over the crystal surface, neglecting surface diffusion, there must be a variation of concentration over the surface. For a given solution velocity there are points on the surface where the solute concentration falls below the equilibrium concentration and a 'starvation' veil results. Carlson calculated the length which a crystal face may grow at a given solution velocity without any veils forming.

1.14.5 Constitutional supercooling

Constitutional supercooling has been shown by Bardsley (1961) to cause instability in the growing interface of crystal grown from slightly impure melts. Hurle (1961) has derived a theory for this effect, the condition for stability being a negative gradient of supercooling ahead of the interface. Mullin (1963) derived from the diffusion equa-

tions the conditions under which an interface was stable. He agreed with Hurle's criteria, but with the further condition that a perturbation of the interface will not expand if the increase in surface energy is greater than the decrease in free energy due to the supercooling.

White (II, 1965) has described the conditions for constitutional supercooling in solution growth. Tiller (1968) has extended the theory of constitutional supercooling from melts to solutions. He derives a maximum growth rate for stable growth which is dependent on the temperature gradient at the interface and the decrease in the liquidus temperature caused by each component in the solution. This treatment neglected any effect due to the increasing surface energy of an interface perturbation. Brice (1969) has used the criteria that if the interface were instantaneously advanced a small distance then its growth rate would decrease and the interface would be stable. He derives a maximum growth rate which depends on the temperature gradient, the heat of crystallisation, and the change of the growth rate with temperature. Unfortunately, there is insufficient experimental evidence to test the theories of Brice and Tiller.

White (I, 1965) and Elwell (1970) consider that dissipating the heat of crystallisation through the crystal, rather than through the solution, increases the interface stability.

CHAPTER II

2. THE MEASUREMENT OF THE PROPERTIES OF SOLUTIONS OF LEAD TANTALATE

2.1 High Temperature Solution Techniques

The reviews in section 1.13 noted that the high temperature technique has been used to prepare crystals of many materials, but that in all but a very few cases very little systematic study has been made of the properties of the solutions used and the conditions required to prepare large crystals. The reviews were unanimous in deploring this lack of study and point out that the need for an investigation of the mechanisms involved in crystal growth technique and of the solution properties which determine these mechanisms. This need arises because there is little consistency in the results when the same crystal growth experiment is performed in different laboratories. This must be the case when the significant experimental parameters are unknown and hence unmeasurable. In order that the high temperature techniques can be used in large scale production of crystals for devices a reproduciblity in experimental results must be achieved and this can follow only from a measurement of the significant experimental parameters. In order to make this specification the solution properties that are to be measured must first be deduced. These properties can be found from the following consideration of the techniques used to grow crystals from solution.

An idealised phase diagram of a solvent system to be used for high temperature solution growth is shown in figure 2.1.

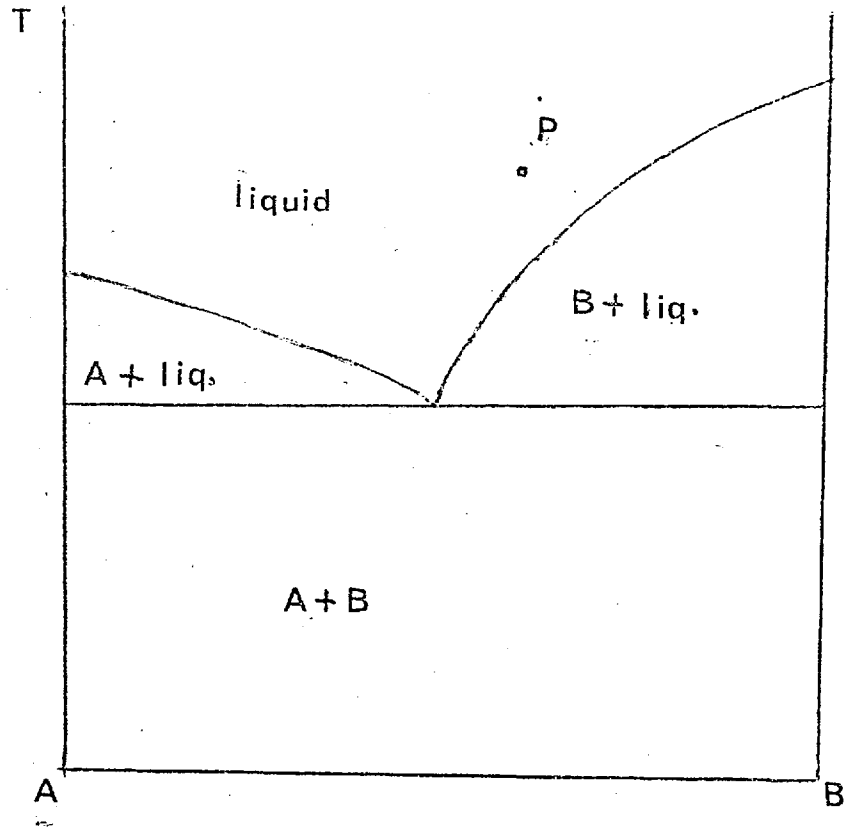

FIG. 2.1

Solid B is the desired phase to be crystallised and A is the solvent material. If B is incongruently melting, or has a destructive phase change between its melting point and room temperature, it cannot be grown as large single-crystals from the pure melt. The addition of component A to molten B is shown in figure 2.1. It effectively lowers the melting point of B so that solid B is in equilibrium with a melt over a range of temperature. Thus, by variation of composition or temperature B may be precipitated at a temperature below that of any undesirable phase change. Although the addition of component A creates additional growth problems over those encountered in growth from the pure melt, there are advantages in the high temperature solution technique: growth rates are much lower as are the temperature gradients in the crystal and environment, and consequently crystals can be obtained with much lower defect densities than by other techniques. This is of great importance when crystals are required for applications using high power light beams.

A number of different experimental configurations are used to prepare crystals from solution. If components A and B are mixed to give the composition N_B and are heated to a temperature T_1 to give the point P, the solution is a single phase liquid at P. If the solution temperature is decreased at constant composition, the slow cooling technique, the point P describing the solution moves parallel to the ordinate and when it reaches the phase boundary the solution becomes saturated. On further cooling solid B is precipitated, usually at a number of different nucleii, although a finite degree of supersaturation is observed before crystallisation commences. With further cooling, molecules or ions or complexes containing B are transported through the solution to the nucleii either by stirring, or by a combination of convection and diffusion, and are then incorporated into the molecule (after dissociation if molecular complexes are formed). Supersaturation may also be produced by evaporating the

solvent A, which is generally more volatile than the soluteB. In this case the point P moves parallel to the abscissa until supersaturation occurs.

Crystal growth may also be achieved by the temperature gradient technique (White, I, 1965). A temperature gradient is applied to the vessel such that the solution is coolest at the top. The vessel is charged so that at the base there is an excess solid material B. The solution can be divided into three zones; the hottest zone at the base in which the solution becomes saturated, the middle zone through which the saturated solution is transported by convection and diffusion, and the third, coolest zone at the surface where the solution becomes supersaturated and growth occurs onto a seed crystal. The reverse configuration may also be used where the more concentrated solution becomes denser. In this case the excess charge is held in a hot zone at the surface and the seed is in a cool zone at the base.

Whilst the production of supersaturation in some arbitrary manner will serve to precipitate the solute phase, a close control of the experimental conditions is necessary for large single crystals to be grown. Returning to the model of crystal growth by slow cooling it was noted that the first stage in crystal growth was the formation of nucleii; i.e. spontaneous nucleation. Obviously, for a given mass of solute precipitated larger crystals will result if fewer nucleii are formed. Tammann (1903, 1925) has shown that the rate of nucleation is a function of supersaturation of the form shown in figure 2.2

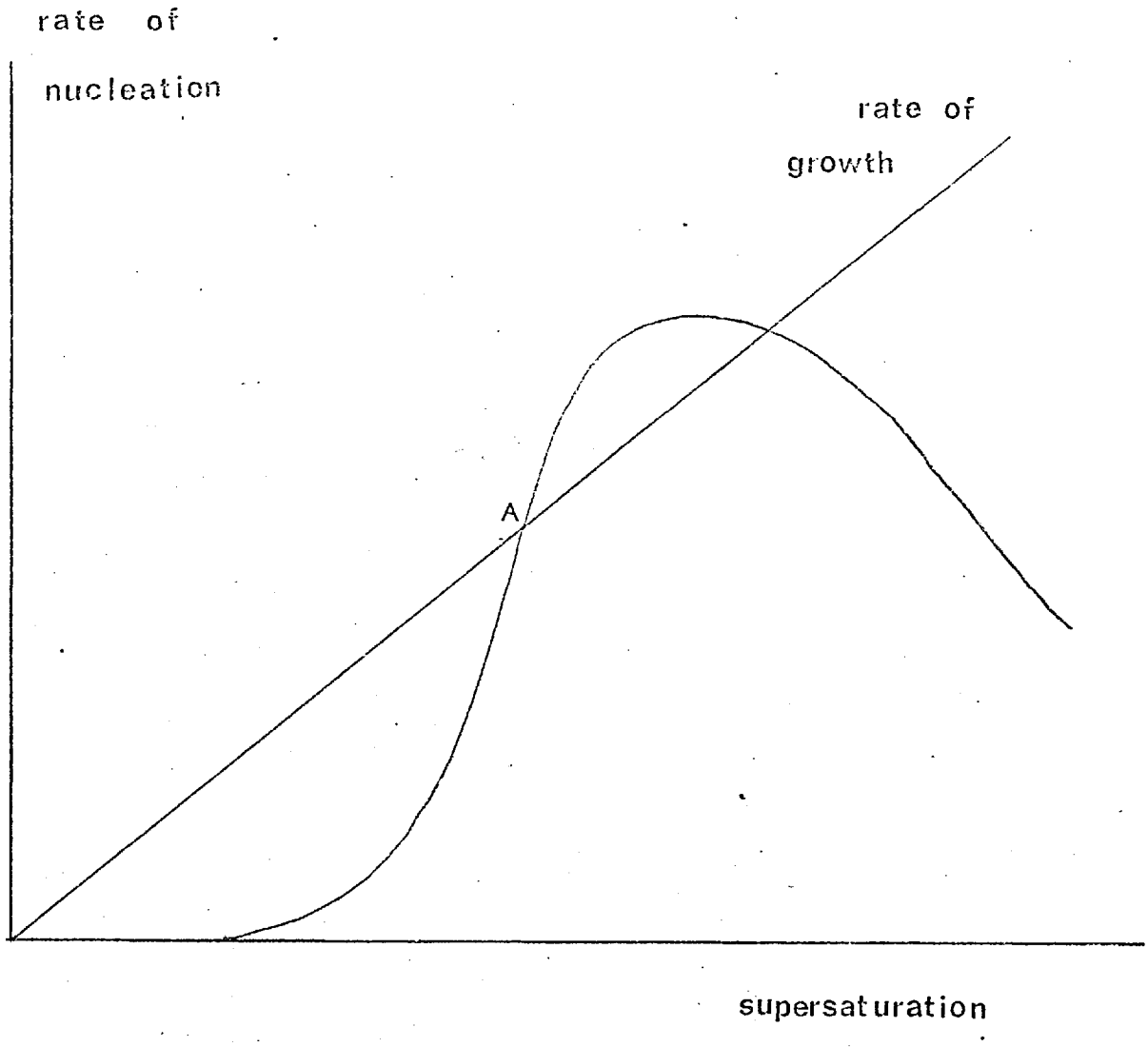

FIG. 2.2.

The straight line shows the rate of growth of a crystal as a function of supersaturation. Clearly, once an appreciable number of nucleii form at supersaturation A they are able to grow very rapidly and many crystals, each containing a core of dendritic material, result. However, if a seed crystal is inserted into the melt at supersaturations less than A, growth can proceed with no further nucleation and a large dendrite-free crystal results. Hence, wherever the phase diagram is accurately known, seeding of the solution rather than spontaneous nucleation is used.

Given that a seed crystal is used, the situation in steady crystal growth is depicted in figure 2.3.

Solute is brought through the bulk of solution by some mass transport process such as stirring or convection. The solute is then transported through the boundary layer (3) by diffusion only as determined by the concentration difference between the bulk and the interface. In the interface region the arriving solute molecules are redistributed by surface diffusion until they are incorporated into the crystal lattice. In addition to moving through the boundary layer into the crystal, there may be some chemical interaction between the solute and solvent due to the dissolution process. Each step (2), (3) or (4) may be the rate limiting process in the crystal's growth. Carlson (1958) has considered the rate of transport of solid to the crystal surface and the effect of diffusion

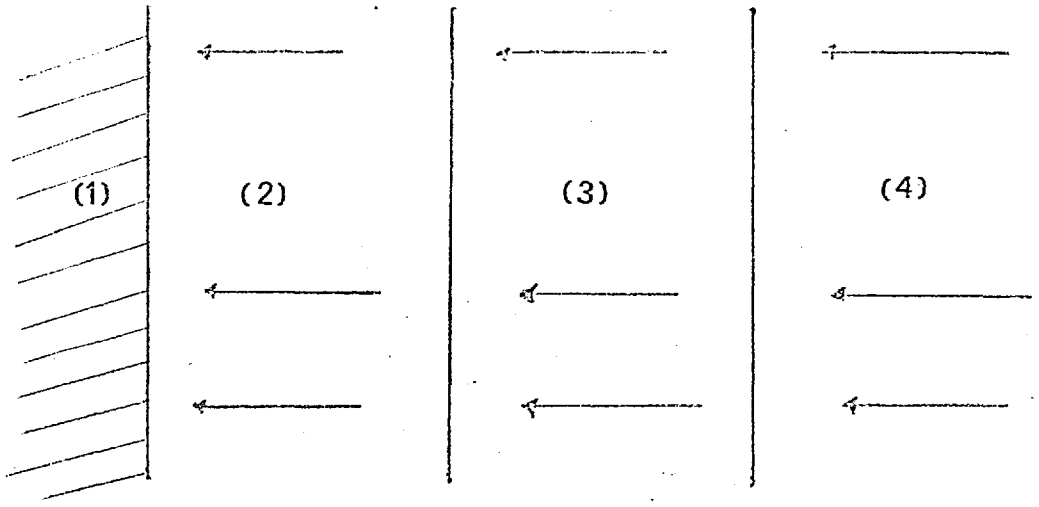

1 crystal

2 interface region

3 diffusional boundary layer

4 bulk

FIG 2.3.

through the boundary layer. He found that for a given velocity of solution flowing past a crystal plate the solution flow could only carry enough solute for the crystal to grow inclusion free to a certain maximum length x_s. This relationship between velocity and crystal size depends on the diffusivity of the solute in the solvent, the viscosity and density of the solution and the ratio of growth rate to the difference between the bulk and interface concentrations. As many high temperature solution growth experiments have been carried out using natural convection, that is a low solution velocity, to produce the solute transport, it would have been most informative if the experimenters had determined these parameters as their results could then be extrapolated for use in other experiments to grow the same crystal with different apparatus. No such measurements have been reported.

In solutions that are well stirred either stage (2) or (3) forms the limiting step. In aqueous solution these stages are investigated by measurement of growth rate as a function of supersaturation over a wide range of conditions and the mechanism of growth is deduced. This is not possible in high temperature solutions, since the measurement of solution concentration is made by visual study of a seed crystal at a given temperature in a solution and furthermore, very small temperature differences must be measured. While aqueous solutions are contained in glass vessels and very accurate temperature control is possible (better than $\pm 0.05^{\circ}C$) these measurements are relatively simple. High temperature solutions must be contained in platinum or similar inert metal crucibles due to their highly corrosive nature and the crucible must be heated in a furnace which can be controlled to a temperature at best only of $\pm 1^{\circ}C$. Hence direct visual measurement of small changes cannot be performed. The rate determining step can only be deduced from examination of the grown crystals, which are usually rods or plates or which exhibit rapid growth

at corners for diffusion limited growth.

Figure 2.3 indicates the stable growth of a crystal interface, but instability can arise from two sources. The first is due to the phenomenon of constitutional supercooling which was responsible for instability of interfaces in the growth of materials from impure melts (Hurle, 1961) and was further shown by White (II, 1965) to cause instability in solution growth. The two cases are shown in fig. 2.4 (a), (b).

In the melt case (2.4(a)) impurity atoms are rejected at the interface and accumulate in the adjacent melt, causing a depression of the melting point. This creates a region of supercooled melt ahead of the interface and any ridge on the interface will enter a region of increasingly supercooled solution which causes rapid growth of the ridge. Volumes of high impurity concentration melt are then trapped between ridges, thus forming troughs of impure material in the crystal. A similar phenomenon occurs in the solution case (2.4(b)). There is a concentration gradient at the interface due to the adsorption of solute into the crystal. Any ridge on the interface will see an increasingly supersaturated solution and will grow rapidly, creating inclusions in the crystal between ridges. The interface is in a metastable state and unless a perturbation occurs the growth will be stable. The perturbation may be caused by a fluctuation from the temperature control mechanism or the emergence of high

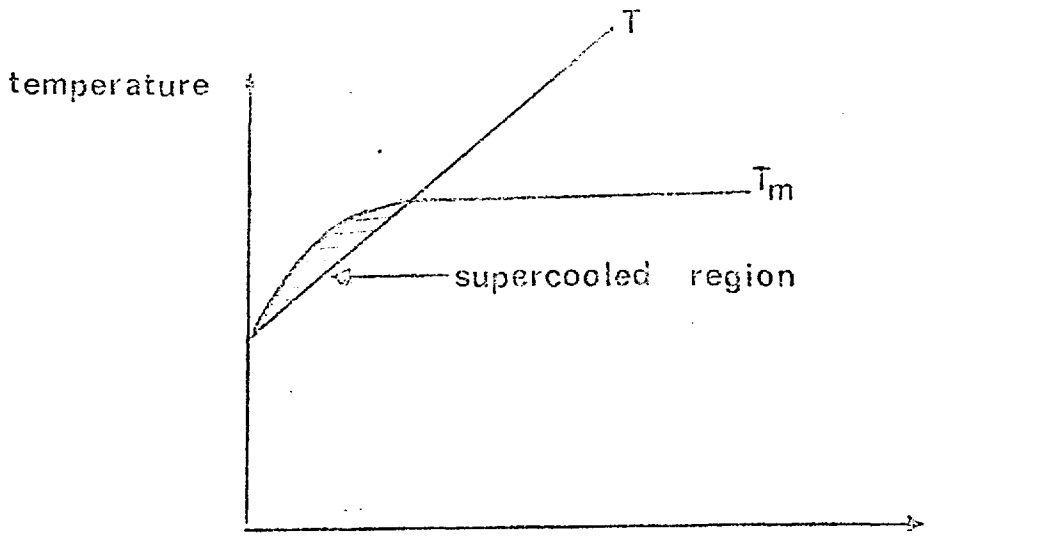
temperature
T
T_m
supercooled region
distance into melt

(a)

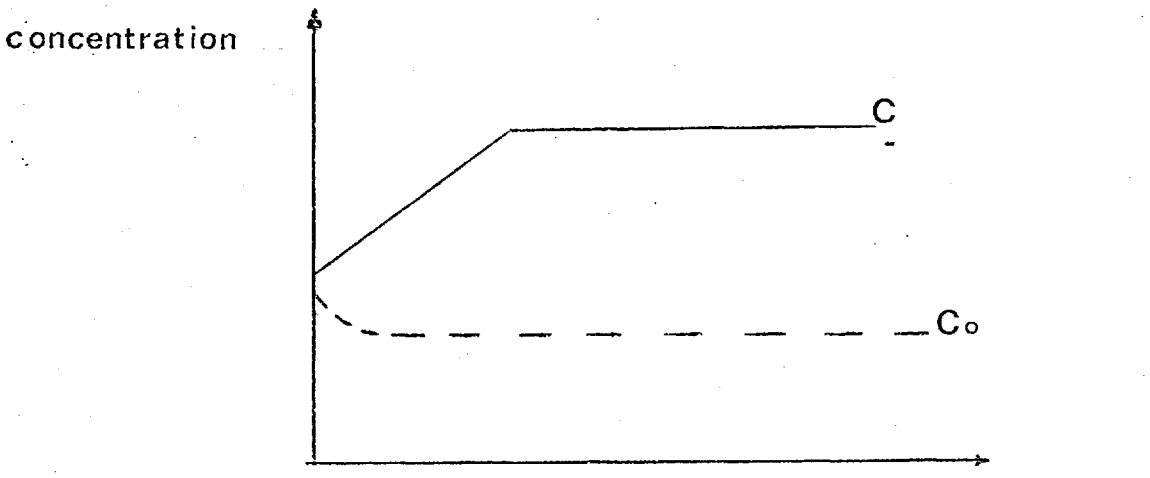
concentration
C
C_o
distance into solution

(b)

FIG. 2.4.

Miller index planes on the crystal due to twinning. The perturbation will not expand if its increase in surface energy is greater than the corresponding decrease in the free energy of the chemical forces causing crystallisation. Constitutional supersaturation is, therefore, inherent in crystal growth in diffusion limited systems, but does not produce instability where the surface free energy of the crystal in the solute solvent system is high.

The second case of instability is the local heating of the interface by the heat of crystallisation liberated there. This is illustrated in fig. 2.4(b) by the slight increase in the equilibrium concentration bear the interface. This further enhances the effect of the constitutional supersaturation already present. Thus, the heating of the interface is a perturbation likely to cause unstable growth. Its magnitude may be calculated if the heat of crystallisation, thermal conductivies of solution and crystal and the specific heat of the solution are known. A similar cause of instability may be temperature fluctuations in the solution as a direct result of natural convection.

To conclude, an adequate description of the growth of single crystals from solution depends upon the measurement of certain parameters which determine the rate at which molecules are incorporated into the crystal and of other parameters which determine the stability of the interface during growth. From the above discussion of the crystal growth there are a number of physical properties to be determined. Firstly, the dimensionless numbers which specify the fluid motion in the solution; these are functions of the density, viscosity, expansivity, thermal conductivity, thermal capacity of the solution, the diffusivity of the solute and geometrical factors such as the temperature gradient in the solution and the size of the crucible. Further parameters which are needed to determine the conditions for stability of the interface are the heat of crystallisation, the surface energy of the crystal and the rate

of growth as a function of supersaturation.

In order to determine the initial conditions of temperature and composition of the melt for crystal growing experiments and for the experimental determination of the above solution properties, the solubility must be known as a function of temperature. No systematic investigation of all these variables has been carried out and at the present time, due to the difficulties in containing the melt in suitable measuring apparatus, the surface energy of the crystal in solution cannot be measured. However, the remaining necessary properties have been measured as described below and their relative importance in the growth of crystals of lead tantalate is discussed in Chapter 3.

2.2 The Choice of a Solvent for Lead Tantalate

The criteria for a good solvent have been given by White (I, 1965) as:-

1. Reasonably high solubility of the solute
2. Will not react irreversibly with the solute
3. Low melting point, high boiling point, low vapour pressure.
4. Low viscosity
5. Low toxicity
6. High solubility in water or other common solvent
7. Contains common ion with the solute or ions of such size as not to readily enter the solute crystal lattice.

There is no one universally good solvent, but a number of useful ones are known and experiments must be performed to find out how suitable they are for a given solute. Using the thermobalance technique (described in 2.3) a number of common solvents were tried and the first phase to crystallise from solution was identified by X-ray powder diffraction tech-

niques as described in 2.3. The results are given in Table 2.1 in which the figures in column four refer to figure 2.5.

Table 2.1

The Phase Crystallising from from various solvents.

Solvent	Phase Crystallising	Structure	X-ray Photograph
PbF_2	$Pb_2Ta_2O_7$	Pyrochlore	(i)
PbB_2O_4	$Pb_2Ta_2O_7$	Pyrochlore	(ii)
Bi_2O_3-B_2O_3	$PbTa_2O_6$	Orthorhombic	(iii)
PbV_2O_6	$PbTa_2O_6$	Orthorhombic	(iv)
$Pb_2V_2O_7$	$PbTa_2O_6$	Orthorhombic	(v)

As lead fluoride and lead borate reacted with the solute no further use was made of these solvents. The variation of solubility with temperature was measured using the thermobalance technique for the remaining three solvents which precipitated the desired phase.

2.3 The Determination of Solubility by the The Thermobalance Technique

Elwell (1967) first described the determination of the crystallisation temperature of a high temperature solution using a thermobalance. A platinum wire was suspended from a chemical balance and immersed to a depth of a few millimetres into a solution contained in a platinum crucible supported in a furnace. The weight of the wire was monitored regularly as the solution was cooled. The wire acted as a nucleating site when supersaturation occurred; solute was deposited on the wire and a consequent increase in weight was observed. The temperature at which a weight change occurred was called the crystallisation temperature and this is assumed to be the temperature at which the solution is saturated, only a very small degree of supersaturation being

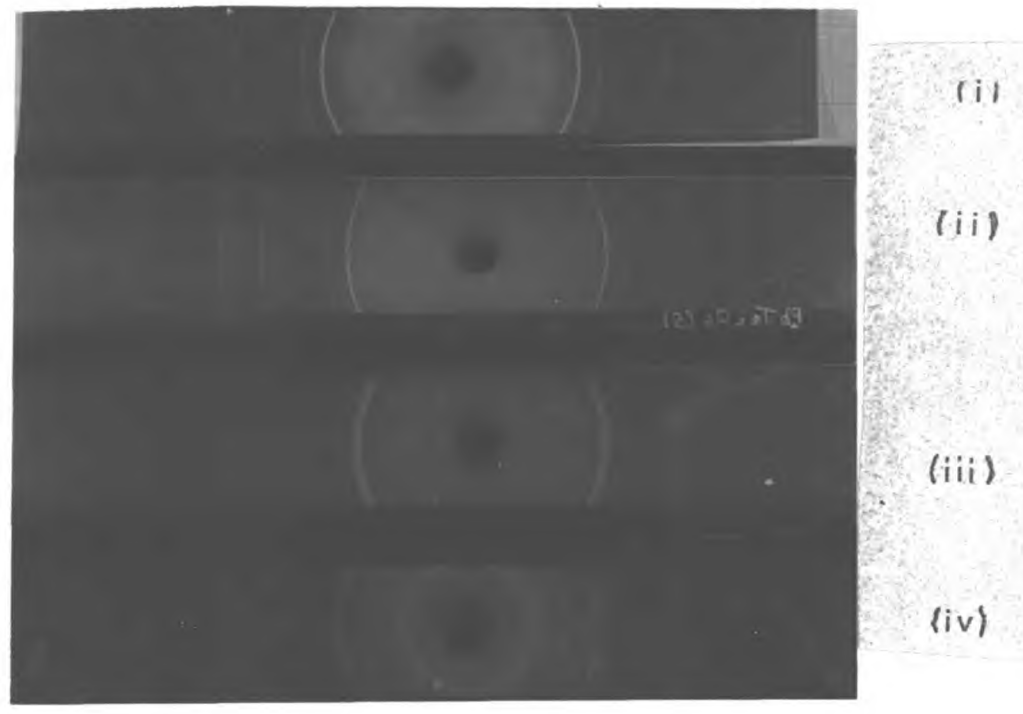

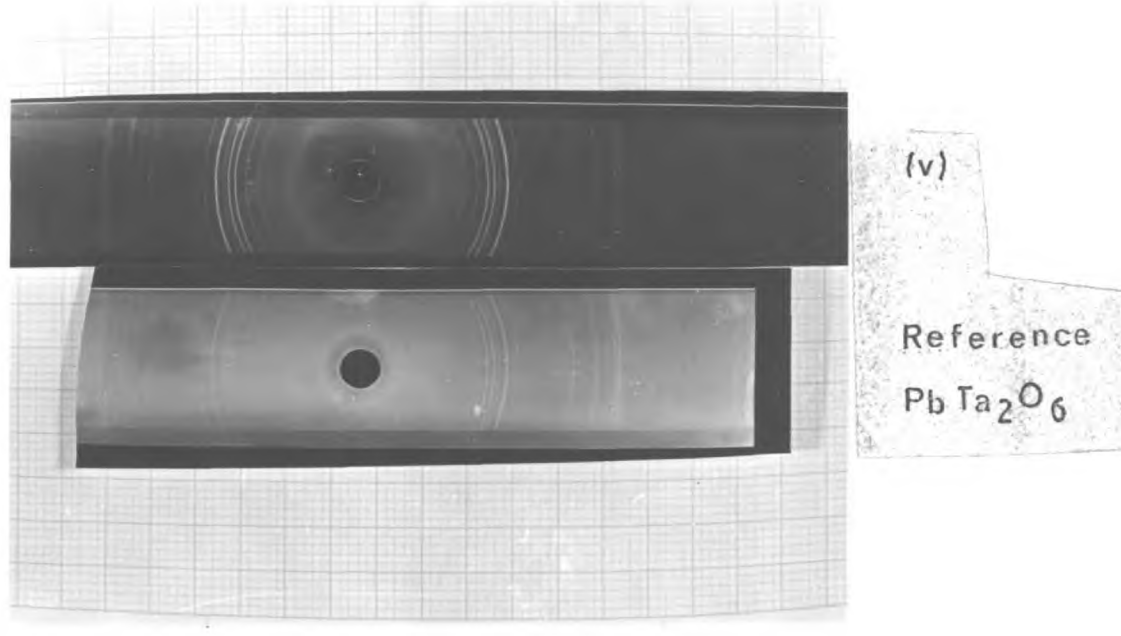

FIG. 2.5

required for crystallisation to be detected. The concentration of the solution may be varied and a series of crystallisation temperatures are obtained. As these are effectively the saturation temperatures for given solution concentrations, the solubility-temperature curve is obtained. Hence the solubility as a function of temperature is measured.

The apparatus used is shown in fig. 2.6. The furnace consisted of a recrystallised alumina tube, three inches internal diameter and eighteen inches long, mounted vertically. Kanthal A1 wire was tightly wound around the tube, and cemented into place, as the heating element. For later measurements on vanadate fluxes silicon carbide furnace rods were used due to the high failure rate of the Kanthal windings. For temperature control a Eurotherm PID/SCR25 controller was used in conjunction with a platinum/platinum - 13% rhodium thermocouple. A similar thermocouple was inserted into the mouth of the furnace tube to monitor the solution temperature. A temperature control to within $\pm 1^{\circ}C$ was obtained. The furnace was insulated with Morgan MI28 bricks and was mounted on a steel frame designed to support the microbalance measuring head. The solution was contained in a 30ml platinum crucible supported on an alumina cylinder inside the furnace. The temperature gradient across the crucible was approximately $1^{\circ}C$ per cm.

A C. I. Electronics, mark II, model C, microbalance was used, the head of which was enclosed in a pyrex glass mounting which was positioned above the furnace. The balance head is shown in figure 2.7. In this instrument balance arm is mounted on a galvanometer type movement and acts as a shutter between two photo-diodes which are symmetrically placed above and below the balance position. When the arm is displaced a differential current is produced by the photodiodes which is amplified and fed into the galvanometer and a restoring force is applied. Hence, a closed servo-loop is established in which a static torque on the moving arm is directly

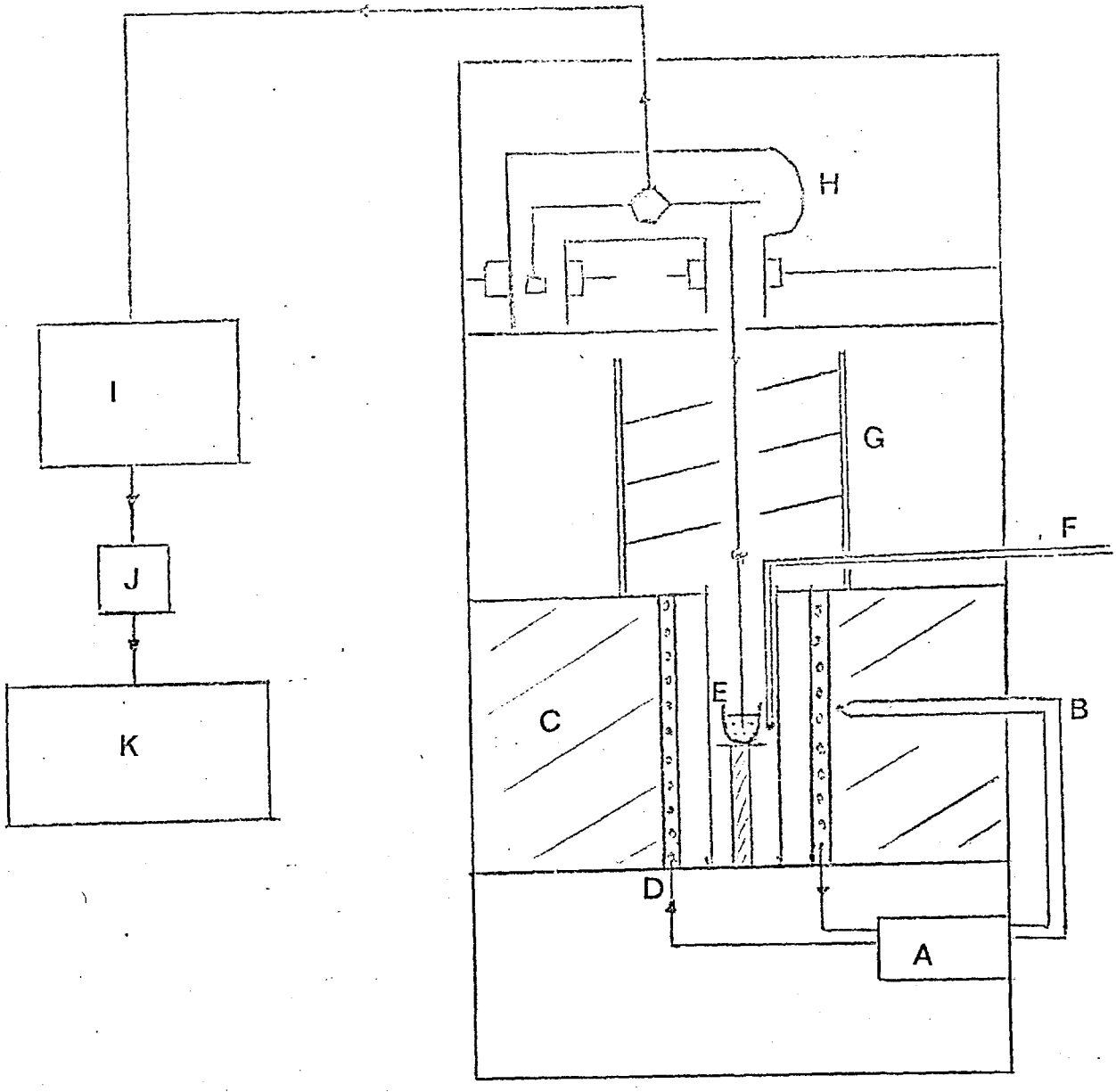

A controller
B thermocouple
C insulation
D heating element
E crucible
F thermocouple
G baffles
H balance head
I balance control
J matching unit
K recorder

FIG. 2.6

FIG. 2.7

proportional to an electric current. This current can be read off on a scale on the instrument case or can be fed into the input of a chart recorder. The right hand end of the balance arm is used for weighing and a counter-weight may be applied to the left hand end. The full scale measurement is 100 mg, but using counterweights, weights of up to 1.5 g may be weighed without loss of accuracy. A matching unit is necessary between the balance and the recorder to filter out the fluctuating a.c. components of the servo mechanism. A C. I. Electronics Universal Matching Unit was used. A fine gain adjustment control was fitted to allow calibration of the chart recorder, a Smith's Servoscribe Potentiometric recorder. The usual ranges used were 0 to 100 mg on the balance and 0 to 100 mV on the recorder.

The balance was calibrated before each solubility determination. Scale pans were attached to each end of the balance arm and the coarse medium and fine zero adjustments were used to give a zero reading for each balance range. Standard weights were placed in the right hand pan and the reading was adjusted using the calibration potentiometer. The chart recorder was also calibrated using the balance output. The balance head worked accurately at ambient temperatures up to 50°C. It was protected from direct furnace heating by a series of aluminium baffles and an insulating plate.

The suspension from the balance arm to the melt was made of platinum wires, 0.8 mm diameter and about 10 cm long, ending in hooks. These suspension wires rapidly damped out any oscillation and were easily threaded through the apparatus. The length of suspension was chosen so that the end wire was immersed 3 mm into the melt.

The following procedure was used in the determination. The starting materials were finely mixed in powder form and loaded into the crucible, which was then heated at 1000°C. After complete melting of the

powder, the crucible was removed and placed in the thermobalance furnace. The required length of suspension wire was measured, the baffles put in position and the suspension wires attached to the balance, which was counterweighted to give a reading in mid-scale. The furnace was switched on and the solution was left for 16 hours at a temperature 100°C above the expected crystallisation temperature. This was found by a process of trial and error for each new solvent. The balance and recorder were then switched on and the temperature was reduced in 10°C intervals by resetting the temperature controller. A period of 30 minutes was allowed for the solution to come to equilibrium before a further decrease was made. The chart could be read to an accuracy of ±0.1 mV and a kink in the weight-time curve was readily observed at the crystallisation temperature which was read from the monitoring thermocouple with a potentiometer. The crystallisation temperature could be determined to an accuracy of ±3°C. This uncertainty arose due to the time required for the solution to come to thermal equilibrium. When an increase in weight was observed the balance and recorder were switched off and the solution was further cooled. The suspension wire was then removed and the material which was precipitated was examined using the X-ray powder diffraction technique.

2.4 The Solubility Determination for Bismuth Borate and Lead Vanadate

The procedure described above was followed. The starting materials used were the oxides of lead, bismuth, boron, vanadium and tantalum. They were of Analytical Reagent quality, supplied by B.D.H. Chemicals Ltd. A typical charge weighed 50g. For bismuth borate the solvent oxides were in the proportion 0.55 Bi_2O_3 to 0.45 B_2O_3. Two compositions of lead vanadate were used, $PbO:V_2O_5$ and $2PbO:V_2O_5$. In each case a weight loss of 0.25% of the total solution mass was experienced due to evaporation of PbO.

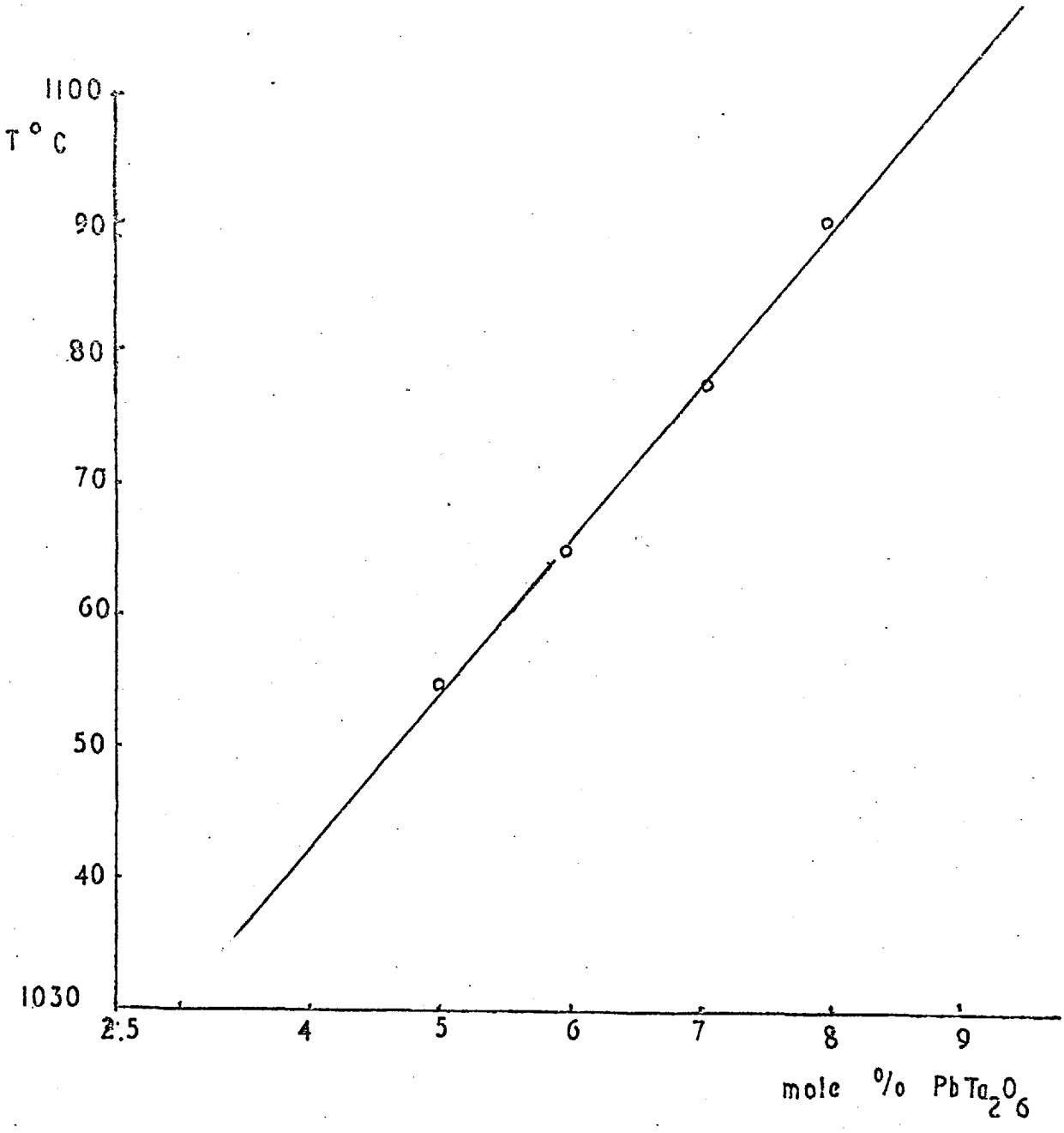

FIG.2.8. THE CRYSTALLISATION TEMPERATURE OF A SOLUTION OF $PbTa_2O_6$ IN Bi_2O_3— B_2O_3 Vs. CONCENTRATION

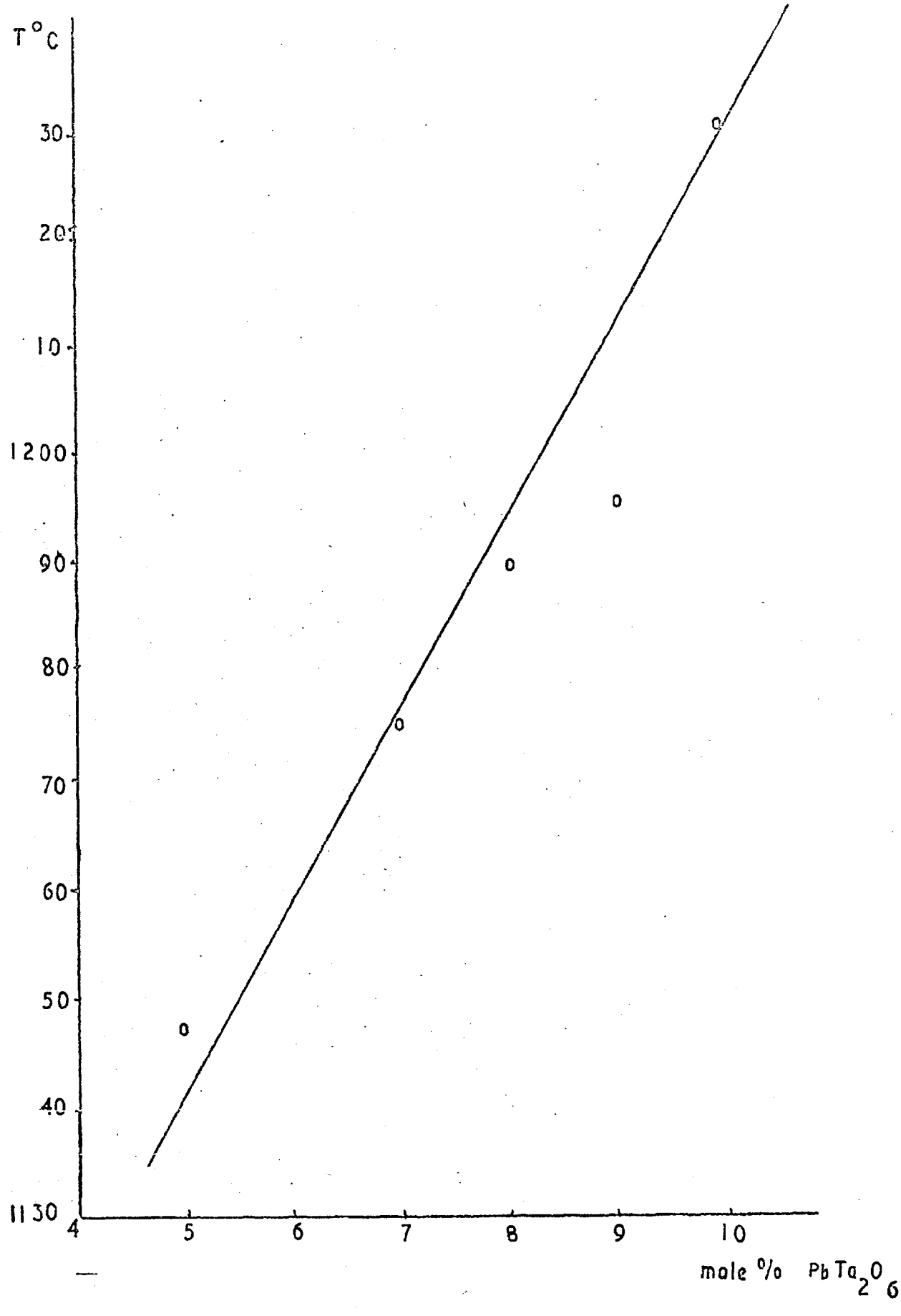

FIG. 2.9 THE CRYSTALLISATION TEMPERATURE OF A SOLUTION OF $PbTa_2O_6$ IN $Pb_2V_2O_7$ Vs. CONCENTRATION.

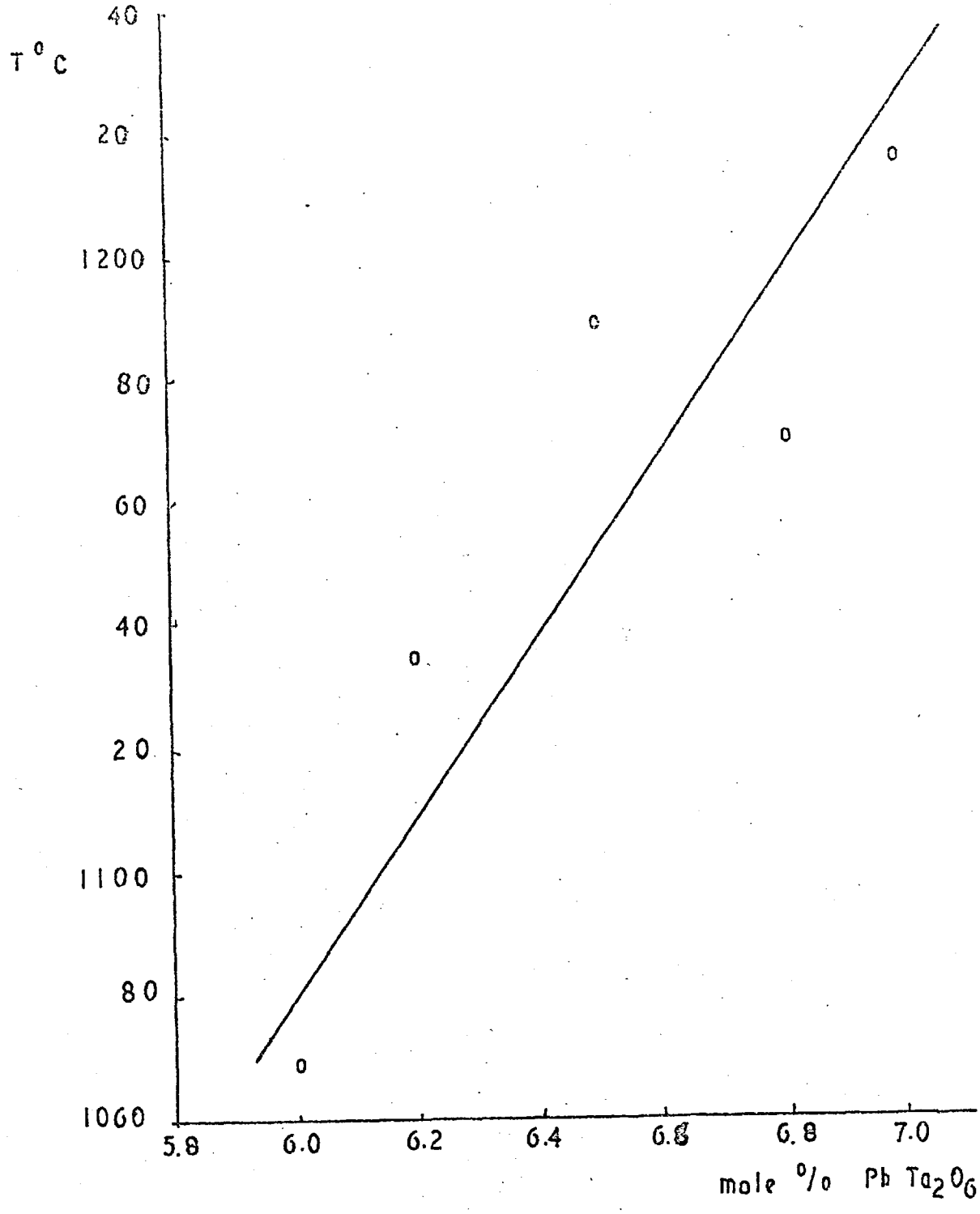

FIG. 2.10 THE CRYSTALLISATION TEMPERATURE OF A SOLUTION OF $PbTa_2O_6$ IN PbV_2O_6 Vs. CONCENTRATION.

A standard reference X-ray powder photograph of the ferroelectric orthorhombic form of lead tantalate was taken using a ceramic disc of lead oxide and tantalum pentoxide finely mixed in 1:1 proportions, pressed and fired at 1180°C. The spacings of the lines agreed with those of Subbarao (1960). The X-ray photographs obtained from the material grown in the thermobalance were then compared with this standard. In each case the phase crystallising was ferroelectric, orthorhombic lead tantalate.

The graph of crystallisation temperature against concentration for each solvent is given in figures 2.8, 2.9 and 2.10. These results are also plotted as the log of the mole fraction of solute against the reciprocal of absolute temperature in figure 2.19 and a discussion of the significance of these results is given in 2.11.

2.5 The Determination of Density and the Coefficient of Expansion of Solutions of Lead Tantalate in Lead Vanadate

A review of the methods of determining the density of liquids at high temperatures has been given by White (J. L. 1959). A robust technique using simple apparatus must be used with high temperature solutions. White suggests that the simplest method is the two bob Archimedean method.

In measuring the upthrust on an immersed body a correction has to be made for the effect of surface tension on the suspension to the bob. This may be eliminated if two bobs of identical suspension but differing volumes are used. If U is the measured difference between the weight in air and the weight in liquid, ρ is the density of the liquid, V the volume of the bob and S the surface tension force, then

$$U = \rho V + S$$

Using subscripts 1 and 2 for the smaller and larger bob respectively, then

$$U_1 = \rho V_1 + S$$

$$U_2 = \rho V_2 + S$$

and

$$\rho = \frac{U_2 - U_1}{V_2 - V_1}$$

If the density is measured a function of temperature then the coefficient of cubical expansion β may be found from the slope of the density temperature curve as

$$\beta = \frac{\rho_T - \rho_o}{\rho_o (T - T_o)}$$

where T is the temperature and ρ_T and ρ_o the density of the liquid at T and T_o respectively.

2.5.1 Apparatus and Experimental Procedure

Two platinum bobs were made by welding platinum wire into a ball using an oxy-hydrogen torch. The platinum wire was 99.9% pure metal supplied by Johnson Matthey Chemicals Ltd. The two bobs were of differing volume, but had similar suspension wires (fig. 2 .11). The bobs were weighed in air and their volumes calculated using the density data for Platinum (American Institute of Physics Handbook of Physics and Chemistry p.2-19). Correction has to be made for the volume expansion of the bob at the temperature of the solution, using the coefficient of linear expansion given in tables (ibid p.4-52). The furnace and balance previously described were used. In addition, at the high temperatures used the solution lost PbO by volatization and an air-cooled copper coil was placed immediately above the furnace mouth to act as a site for condensation of the vapour rather than the suspension wires.

The crucible was charged as for the solubility determination. The length of suspension required to completely immerse the bob was found and the bob was then weighed in air. The crucible was placed in the furnace and the suspension wires fitted. The furnace was brought to a temperature above the crystallisation temperature of the solution and held

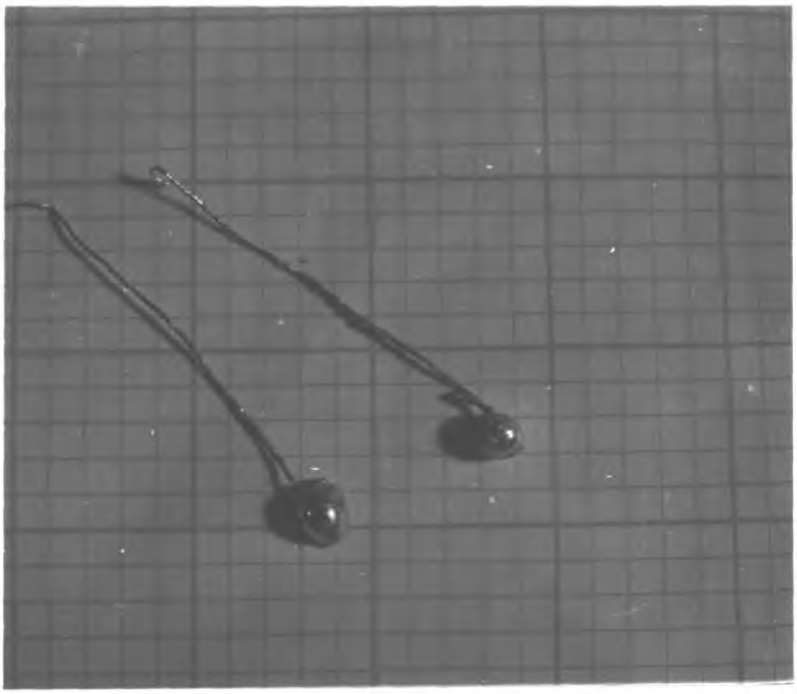

FIG. 2.11.

at that temperature for 16 hours. The balance and recorder were switched on and the weight of the bob recorded at a number of temperatures. The same procedure was used for the second bob.

2.5.2. Results of Density Determinations

Determinations of the density of the two pure solvents PbV_2O_6 and $Pb_2V_2O_7$ were made over a wide range of temperatures to permit an accurate estimate of the coefficient of expansion to be made. The density as a function of temperature is plotted in figures 2.12 and 2.13 for $Pb_1V_2O_6$ and $Pb_2V_2O_7$ respectively.

The density as a function of concentration of lead tantalate in the two solutes was measured and is shown in figure 2.14 and 2.15 for PbV_2O_6 and $Pb_2V_2O_7$ respectively. The error in the results is estimated at ±2%. This was deduced by using the measured density to calculate the surface tension force. This is approximately constant over a small temperature range and hence any variation in its calculated value must be due to the error in measuring the density. The error due to changes in the composition of the melt was negligible, since the loss of PbO was less than 1% of the charge which produces a compositional error of less than 0.01%. The coefficient of expansion for PbV_2O_6 was $(2.21 \pm 0.4) \times 10^{-4}$ and for $Pb_2V_2O_7$ was $(3.5 \pm 0.6) \times 10^{-4}\ C^{-1}$. This compares well with the published figures for the coefficients of expansion of molten salts as shown in Table 2.2. The figures quoted are taken from Janz (1967).

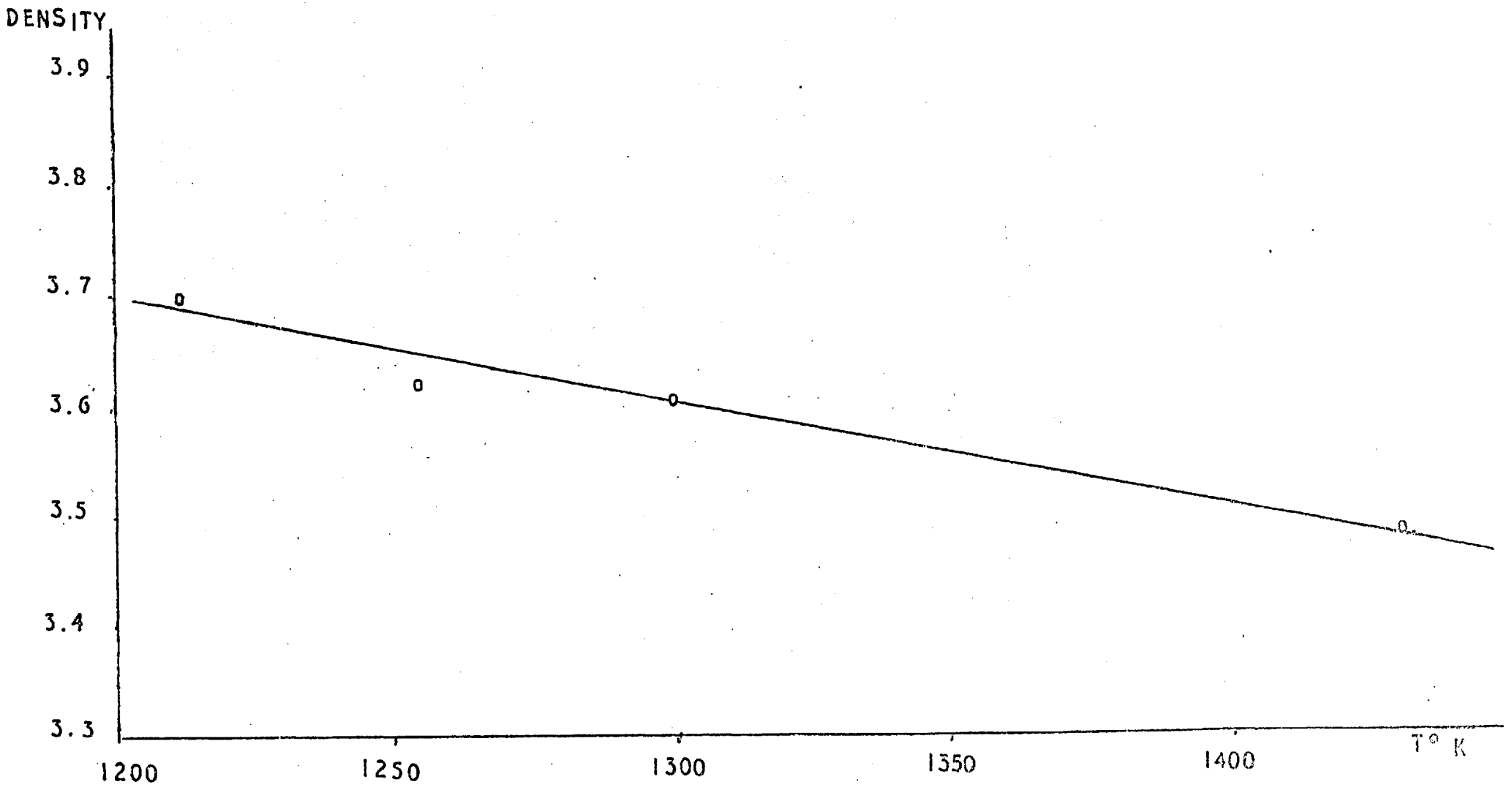

FIG-2.12 THE DENSITY OF MOLTEN PbV_2O_6 Vs. TEMPERATURE

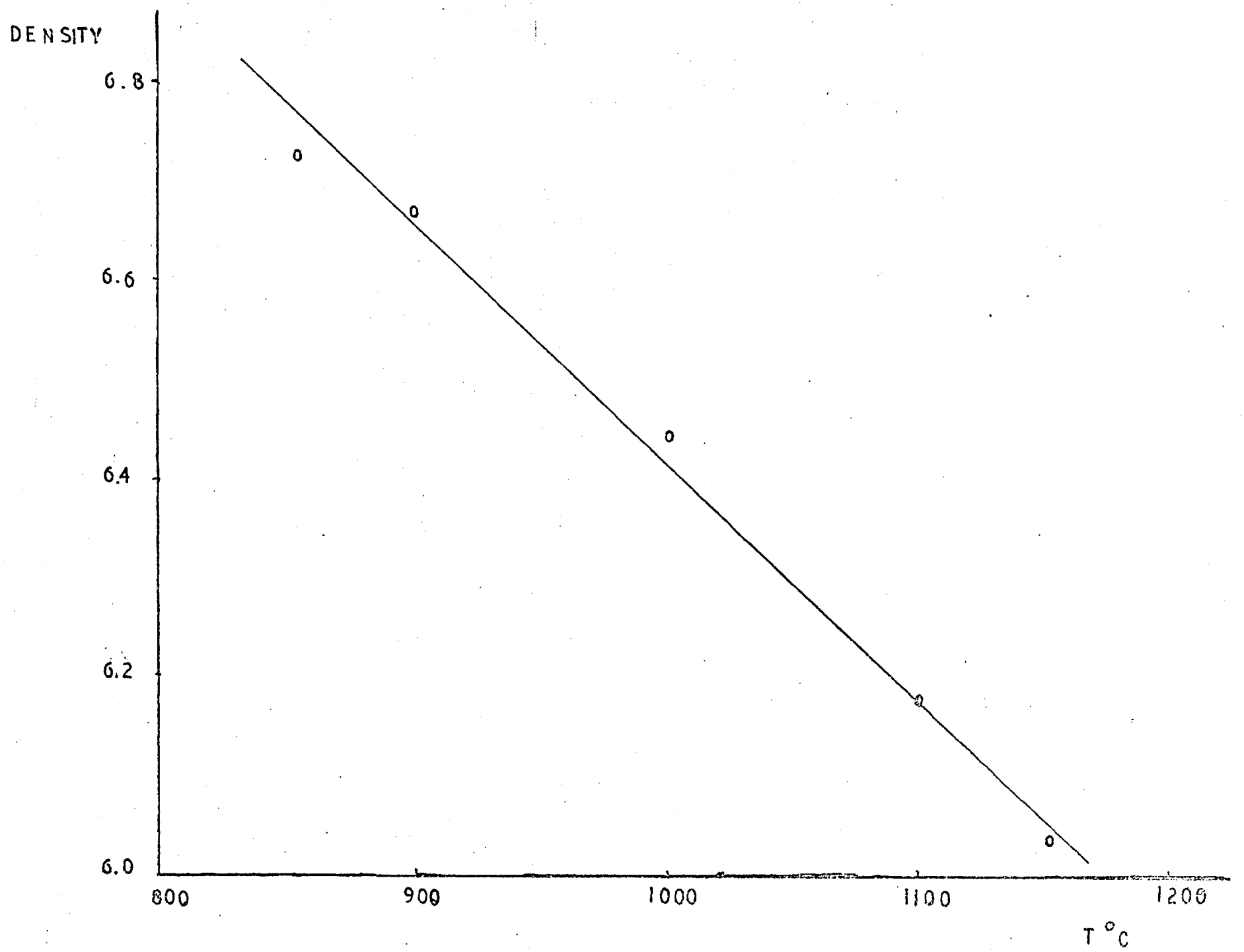

FIG. 2.13 THE DENSITY OF $Pb_2V_2O_7$ Vs. TEMPERATURE

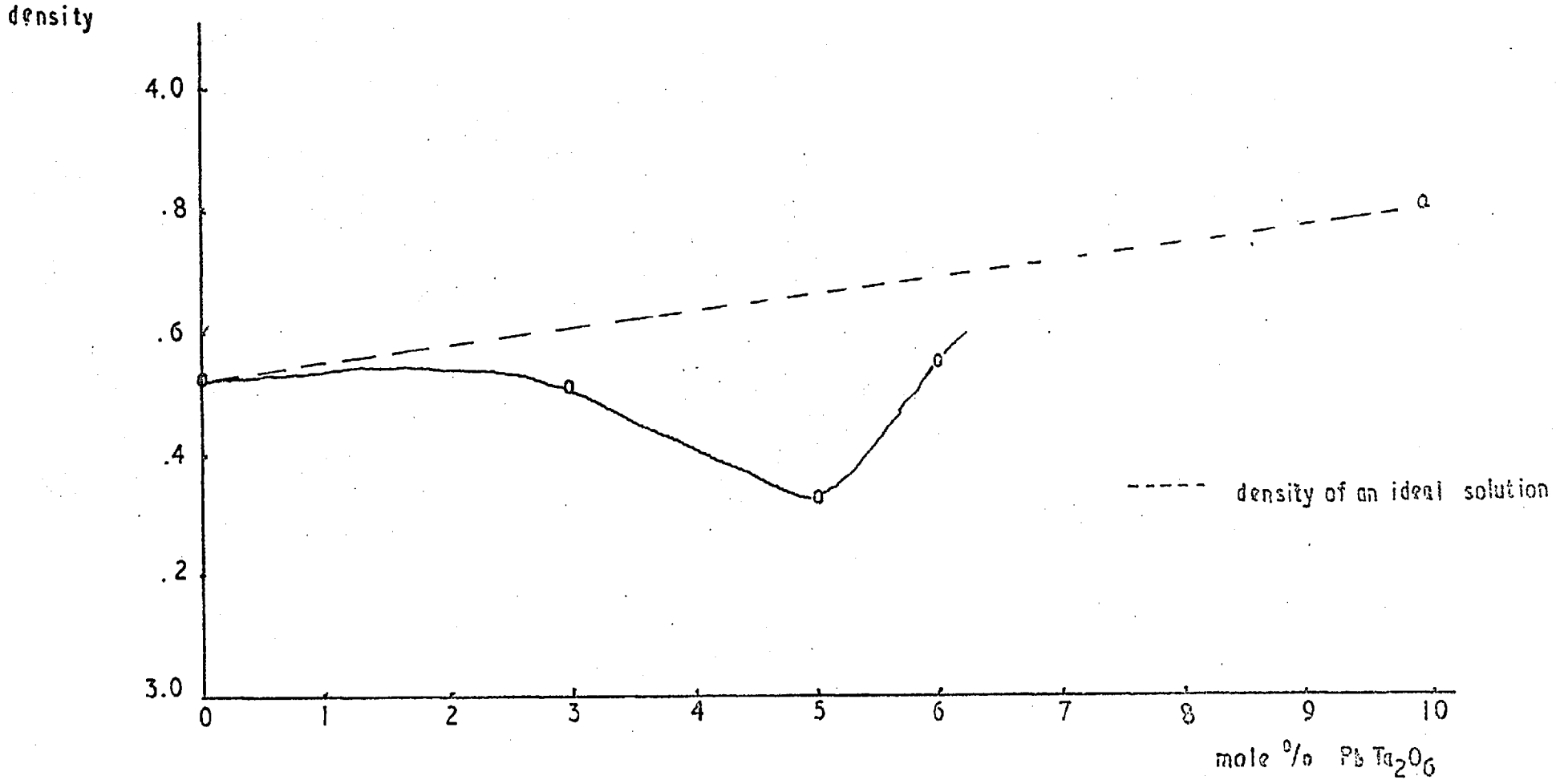

FIG. 2.14. THE DENSITY OF A SOLUTION OF $PbTa_2O_6$ IN PbV_2O_6 AT 1160 °C Vs. CONCENTRATION.

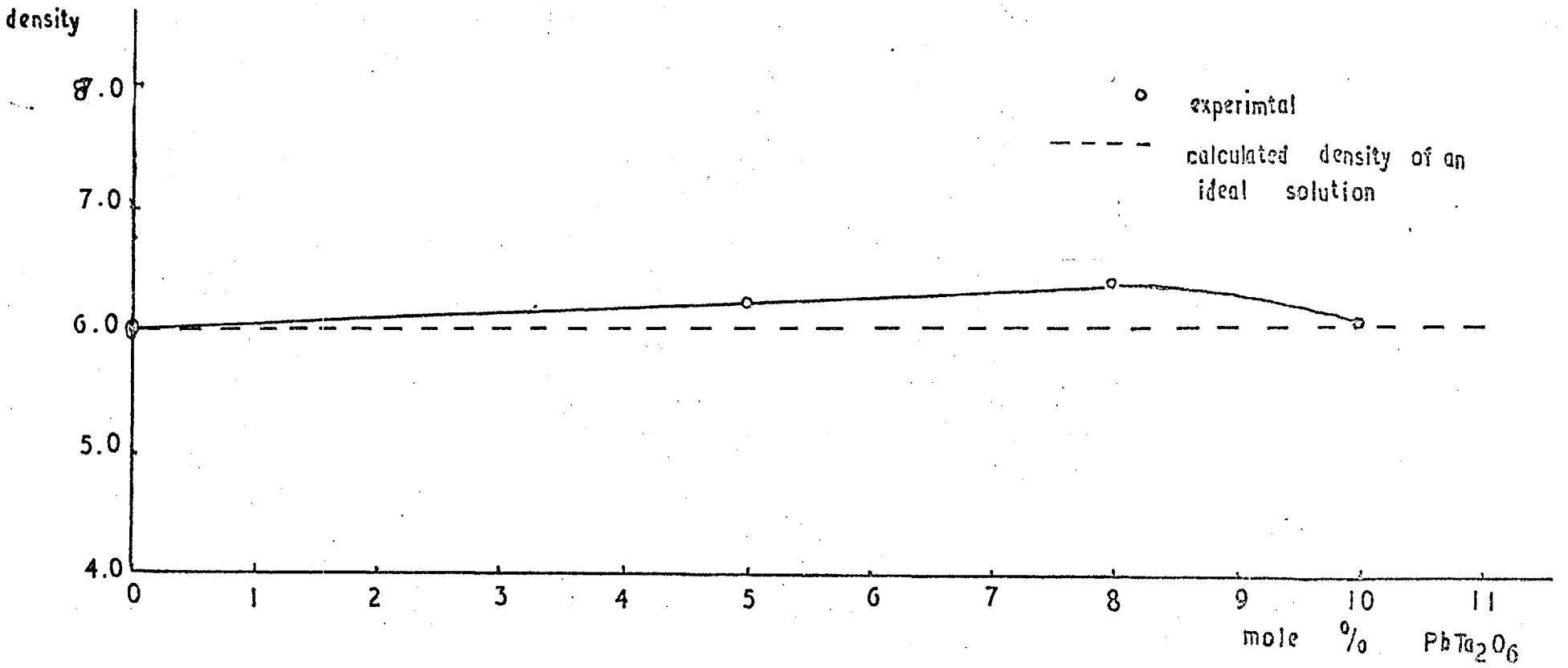

FIG 2.15 THE DENSITY OF A SOLUTION OF $PbTa_2O_6$ IN $Pb_2V_2O_7$ AT 1230 °C

Vs. CONCENTRATION

Table 2.2

The coefficient of expansion of lead vanadate and other salts.

Material	Coefficient of expansion $C^{-1} \times 10^4$
$Pb_2V_2O_7$	3.5
PbV_2O_6	2.21
NaCl	3.5
KCl	4.5
$PbCl_2$	4.10
Li_2CO_3	2.20
AgBr	1.88

2.6. The Determination of Viscosity of a Solution of Lead Tantalate in Lead Vanadate ($Pb_2V_2O_7$)

Mackenzie (1959) has reviewed the methods of determining viscosity in liquids at high temperatures. The simplest method which has also been used by Cobb (1967) is the oscillating bob technique. A bob immersed in the melt is set into rotational oscillation and the viscosity is calculated from the damping of these oscillations by the following formula.

$$\lambda - \lambda_o = C_1(\eta\rho)^{\frac{1}{2}} + C_2(\eta) + C_3(\eta\rho)$$

where λ is the logarithmic decrement, that is the amplitude of two consecutive oscillations, η is the dynamic viscosity and ρ is the density of the melt. C_1, C_2, C_3 are geometrical constants dependent on the shape of the bob and the clearances within the melt.

This formula was derived by Fawsitt (1908) and was found to be valid for a wide range of liquids with viscosities up to 0.4 poise. The constants C_1, C_2, C_3 must be found by calibration with three known liquids; water, alcohol and benzene were used.

2.6.1. Apparatus and Procedure to Measure Viscosity

The bob was made of platinum foil wound into a solid cylinder and welded in place. The bob support is made of a platinum rhodium wire brazed to a molybdenum foil strip. The strip was bent into a loop and the loop threaded over a rod held in an adjustable clamp which could be used to lower the bob into the melt.

The apparatus used is shown in figure 2.16. The oscillations were observed using an optical lever; a mirror was mounted on the molybdenum foil to reflect the light source onto the scale. The furnace used was described above (2.4).

To calibrate the bob a 120 ml platinum crucible was filled two-thirds full with distilled water and placed in the furnace. The bob was immersed in the melt and set into oscillation by giving the mirror a small deflection. The amplitude of the oscillations were then observed. The logarithmic decrement was calculated from the initial amplitude and the amplitude five ascillations later. Consecutive amplitudes could not be accurately measured due to the rapid oscillation of the bob. The procedure was repeated using absolute alcohol, benzene, and with an empty crucible to determine λ_o

The crucible was then filled with an eight mole per cent mixture of lead tantalate in lead vanadate ($Pb_2V_2O_7$) and premelted. Further charge was added until the crucible was two-thirds full. The crucible was placed in the furnace and brought to a temperature above the crystallisation temperature and maintained for 16 hours to allow complete solution. The bob was then immersed in the solution and the logarithmic decrement measured at a number of temperatures.

2.6.2. Results of Viscosity Measurements

The following density and viscosity data (Kay(1959)) were used to calibrate the bob at $20^{o}C$

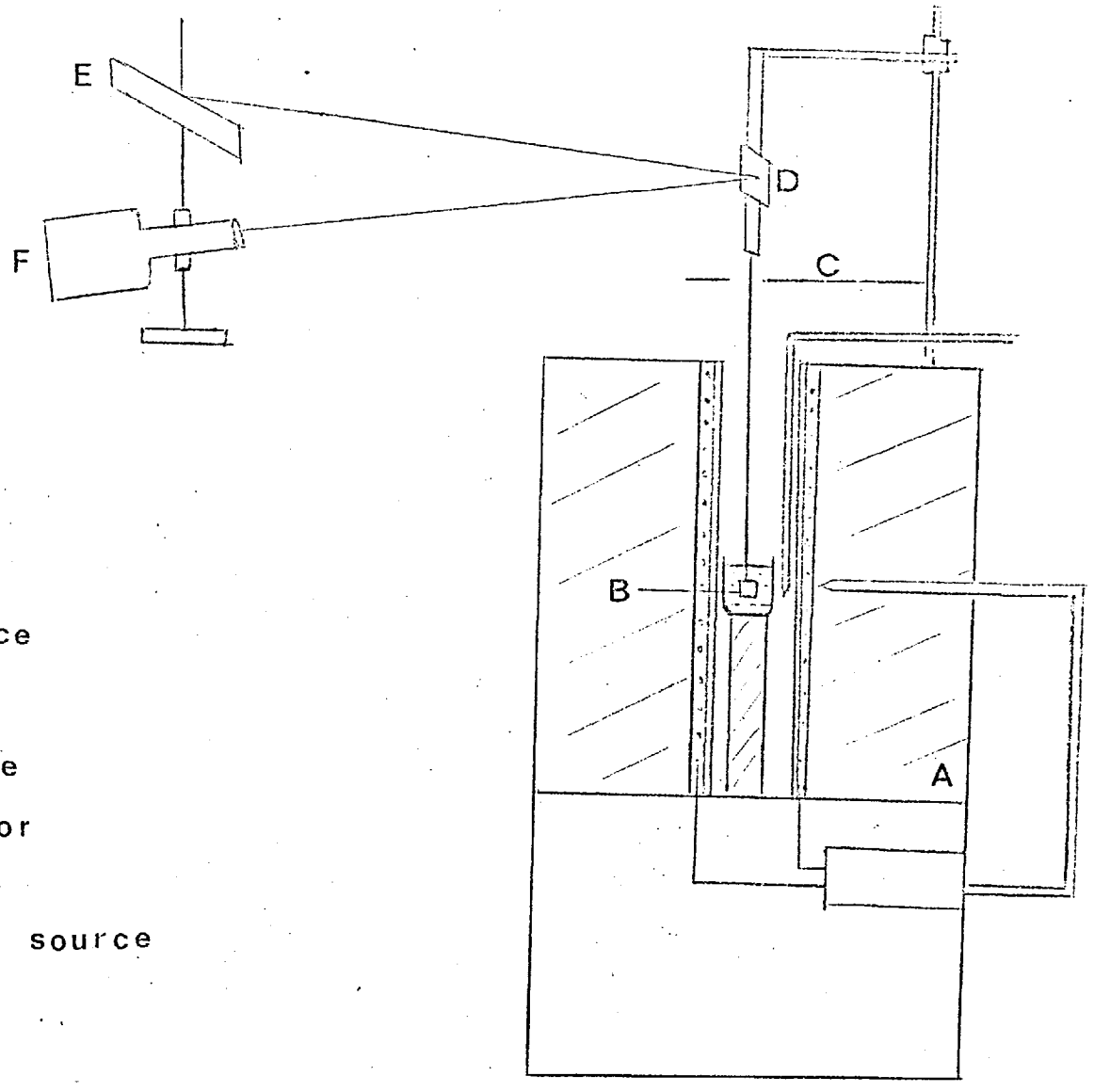

A furnace

B bob

C baffle

D mirror

E scale

F light source

FIG. 2.16

	Density	Viscosity in Centi-poise
Water	1.000	1.0020
Benzene	0.8787	0.647
Alcohol	0.918	1.197

The logarithmic decrements, the average of twelve measurements, for calibration were 0.0259, 0.0279, 0.0196 and 0.0035 for water, alcohol, benzene and air respectively. This gave the value of the constants as:

$$C_1 = 0.158$$

$$C_2 = 0.662$$

$$C_3 = -0.0038$$

The mean logarithmic decrements of the solution as a function of temperature are given in Table 2.3 and were used to give the stated dynamic viscosities.

The density of the solution was taken from the data in section 2.5.2. The dynamic viscosity as a function of temperature is plotted in figures 2.17.

Table 2.3

The logarithmic decrement and dynamic viscosity of an eight mole per cent solution of lead tantalate in $Pb_2V_2O_7$

Temperature in ^{o}C	Mean logarithmic decrement	Dynamic Viscosity in Centipoise
1,184	0.0772	2.23
1,214	0.0761	2.13
1,218	0.737	2.02
1,230	0.0742	2.06
1,257	0.0744	2.09

The measurements of λ are accurate to $\pm$ 0.5%; however, this small error leads to a large error in the calibration constants, giving an error in the viscosity of $\pm$ 5%.

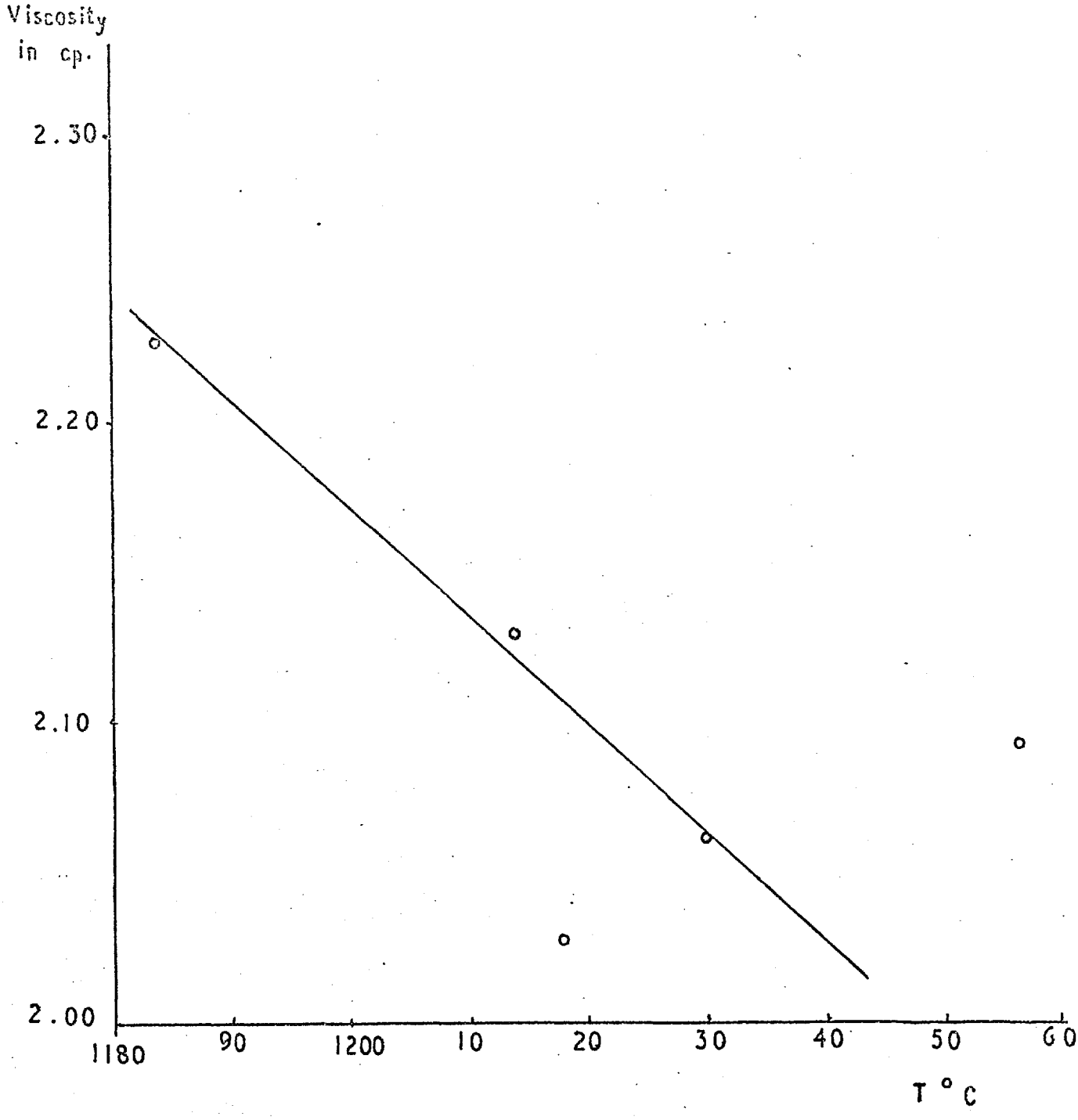

FIG. 2.17 THE DYNAMIC VISCOSITY OF AN 8 ml %.

SOLUTION OF $PbTa_2O_6$ IN $Pb_2V_2O_7$ Vs. TEMPERATURE

The value of 2.23 centipoise for dynamic viscosity is less than that observed by Cobb (1967) for a lanthanum fluoride- alumina solution (8 centipoise) but agrees with the generalisation of Bloom (1967) that molten salts have viscosities comparable with that of water.

2.7 The Measurement of the Diffusion Constant of Lead Tantalate in Solution

The experimental evidence discussed in 2.11 indicates that lead tantalate is not ionised in solution. Thus electrical methods are unsuitable for measuring the diffusion coefficient. Other methods of measuring diffusivity are described by Chen (1959) using radioactive tracing elements. These techniques involve highly specialised apparatus and rely upon quenching the solution. The disadvantages in quenching experiments have been discussed above (1.14.3)

A simple technique for measuring the diffusion coefficient which to the author's knowledge has not previously been reported, for high temperature solutions, has been used. A small crystal was suspended in the solution and its weight loss as a function of time recorded. The experiment was repeated for a range of values of undersaturation of the solution. Nernsts' Equation (Levich, 1963) describes the rate of isothermal mass transfer by diffusion, Q, from a dissolving crystal as

$$Q = \frac{AD}{\delta} (C_s - C_o) \qquad (2.7.1.)$$

where A is the area of the crystal, D is the diffusion coefficient, C_s and C_o are the concentration of the solution at the interface and in the bulk of solution, δ is the thickness of the mass boundary layer. Nernst assumed that C_s was the saturation concentration at the solution temperature. The value of δ for a plate immersed in a turbulent liquid moving with a relative velocity V is $\delta = \delta_o / N_{sc}^{\frac{1}{4}}$, where $\delta_o = 4.64 \left(\frac{\upsilon L}{V}\right)^{\frac{1}{2}}$, the thickness of the momentum boundary layer (Knudsen, 1958) N_{sc} is the dimensionless

Schmidt number defined as $N_{sc} = \frac{\upsilon}{D}$

where υ is the kinematic viscosity and L, a characteristic dimension of the crystal. Hence

$$\delta = 4.64 \left(\frac{V}{L}\right)^{\frac{1}{2}} \upsilon^{\frac{1}{4}} D^{\frac{1}{4}} \qquad \ldots(2.7.2.)$$

2.7.1. Experimental procedure

The thermobalance equipment described above was used. The crucible was charged with the appropriate mixture of the starting oxides and placed in the furnace after premelting. A small crystal of lead tantalate, prepared as described in Chapter 3, was mounted at the end of the platinum suspension wires. The length of the suspension and the counterweight were chosen so that with the balance switched off the balance arm was raised and the crystal suspended just above the solution. When the solution had been brought to temperature and complete solution achieved, a small weight was added to the crystal suspension and thus made the crystal arm heavier than the counterweight arm. Consequently the crystal arm swung downwards, immersing the crystal in the melt. This was found to be the most efficient method of inserting the crystal into the melt. The weight loss was measured until the crystal was totally dissolved. The experiment was repeated at different temperatures which corresponded to varying degrees of undersaturation of the solution.

2.7.2. Results and calculation of the diffusion coefficient

The weight loss indicated on the chart had to be corrected for the upthrust on the crystal due to the density difference between the crystal and solution. Thus, if the weight loss on the chart was Qm, then the true weight loss Qr was

$$Qm/(1 - \rho_s/\rho_c)$$

where ρ_s and ρ_c are the densities of solution and crystal.

It is noted in Chapter 3 that the crystals are elongated in the [001] direction and it is probable that dissolution of the crystal occurs

preferentially in that direction. Thus, the area of the crystal A in equation 2.7.1. is that of the [001] faces of the crystal. As all the crystals used were very nearly of the same length, that is 4.0 mm, the area was, therefore, proportional to the mass of the crystal used.

$$\therefore \quad A = km$$

where k is a constant and m is the crystal mass. For a 1 x 1 x 4 mm crystal, then $A = 0.02\ cm^2$, and if $\rho_c = 7.17$, then $k = 0.6969$. The value of ρ_c was calculated from the X-ray diffraction data given by Subbarao (1960).

If the mass of the crystal indicated on the chart was m_1 and the real mass was m_r, then $m_r = m_1/(1 - \rho_s/\rho_c)$

Therefore: $$\frac{Q_r}{A} = \frac{Q_r}{km_r} = \frac{Q_m}{km_1}$$

but: $$\frac{Q_r}{A} = \frac{D}{\delta}(C_s - C_o)$$

therefore: $$\frac{Q_m}{m_1} = \frac{kD}{\delta}(C_s - C_o).$$

Hence a graph of rate of weight loss divided by the mass of crystal (using the figures from the chart) against unsaturation should be a straight line with slope $\frac{kD}{\delta}$. This graph is plotted in figure 2.18. The values of C_s were obtained by measuring the temperature of solution with the monitoring thermocouple and finding the saturation concentration from figure 2.9. The plot is a straight line with a slope $2.428 \times 10^{-4}\ sec^{-1}$.

$$\therefore \quad \frac{k}{4.64} D^{2/3} \upsilon^{-\frac{1}{4}} \left(\frac{V}{L}\right)^{\frac{1}{2}} = 2.428 \times 10^{-4}.$$

Using L = 4mm, $\upsilon = \frac{\eta}{\rho}$, where $\eta = 2.4 \times 10^{-2}$ centipoise, $\rho = 6.22$, V = 9.0 cm sec, a typical figure for the velocity of a liquid flowing under free concection in a turbulent manner, as derived in section 3.3. Hence the value of D is $D = 1.137 \times 10^{-6}\ cm^2\ sec^{-1}$.

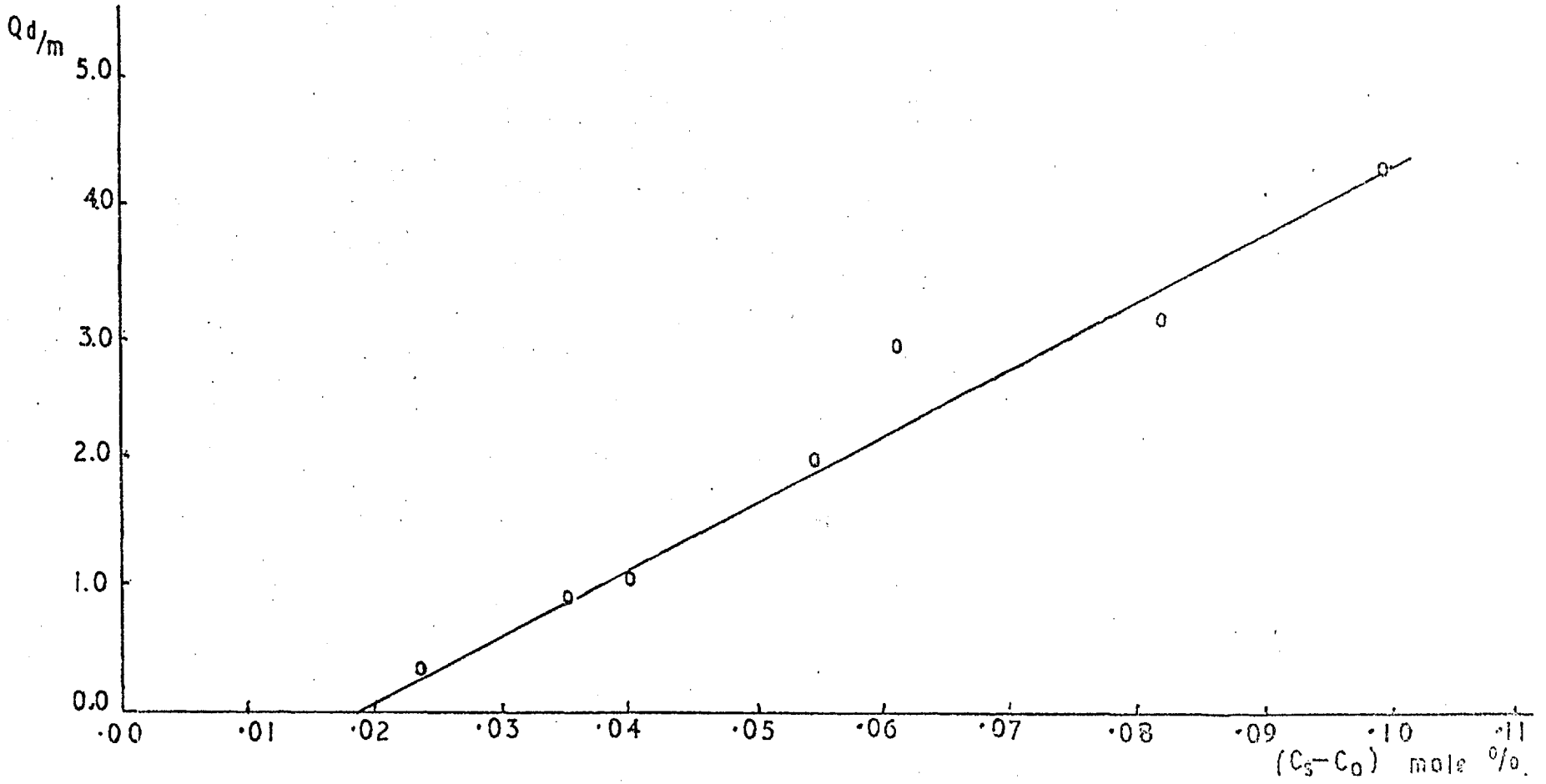

FIG. 2.18. THE WEIGHT LOSS PER UNIT AREA Vs. UNDERSATURATION.

This is a factor of ten less than that observed for diffusivities of ionic salts in aqueous solution. However, a lower value might be expected due to the large size of the diffusing lead tantalate molecule and due to the higher dynamic viscosity of the solution, since diffusivity is inversely proportional to dynamic viscosity (Tyrell, 1961).

In Figure 2.18, the curve does not pass through the origin which might be expected from the theory. However, if a certain supersaturation is required for surface diffusion and particle incorporation into the lattice the supersaturation across the boundary layer becomes $C^1 - Co$ where C^1 is the concentration at the interface. Then $C\infty - C^1$ is the supersaturation required for surface diffusion and equals the intercept on the × axis in figure 2.18.

2.8 Heat of Crystallisation of Lead Tantalate

In an ideal solution the molar concentration K is related to the heat of crystallisation by the following relationship

$$\ln N = \frac{\Delta H_c}{RT}$$

where ΔH_c is the heat of crystallisation, R is the gas constant and T is the absolute temperature. In section 2.11.3. it is shown that lead tantalate dissolved in $Pb_2V_2O_7$ is nearly an ideal solution. In fig. 2.19, log N has been plotted against the reciprocal of absolute temperature. The slope is 2.35×10^4 and therefore the heat of crystallisation is 11.8 ± 3.0 K cal/mole.

2.9 Specific Heat of Lead Tantalate in Lead Vanadate Solution

Specific heats of solutions may be measured by standard D.T.A. techniques. The rate at which the solution cools is compared with the rate of cooling of a similar crucible containing aluminium oxide. If the heat capacities were the same no temperature difference would result. In fact there is usually a difference. A curve is therefore obtained in the differential temperature against time. The area under this curve is

related to the heat evolved by the relation

$$\Delta H = \frac{\psi}{m} \int_{T_1}^{T_2} \theta dT \quad \text{(Hahn, 1963)}$$

where ΔH is the heat evolved, m the mass of material, T_1 and T_2 the initial and final temperature, θ is the differential temperature and ψ is a constant of the apparatus to be determined by calibration.

Two identical platinum crucibles were charged, one with 4 grm of alumina and the other with 20 grm of sodium chloride. They were placed in a furnace which could be slow cooled at 100 deg C/hr and their temperatures were monitored with platinum - platinum 13% rhodium thermocouples connected in opposition to a potentiometric recorder. The furnace temperature was raised to well above the melting point of sodium chloride and the furnace was then slowly cooled. The differential temperature was then recorded on the chart. The initial and final temperatures were recorded and the area under the curve measured. Using a value of Cp for sodium chloride of 16.0 cal/deg mole (Janz 1967) the value of the constant ψ was found to be 6.57×10^3.

The crucible was then cleaned and charged with 62 grm of an 8 mole % solution of lead tantalate in $Pb_2V_2O_7$ and the experiment was repeated. The heat capacity of the solution was found to be 9.3×10^{-2} cal/g^{-1} C, alternatively as 58.2 ± 5 cal/deg C^{-1} mole.

2.10 Thermal Conductivity of Lead Tantalate Solutions

Tyrell (1961) has reviewed the methods of measuring thermal conductivities of liquids. The basic requirement in each technique is that a volume of liquid in which no convection takes place, should be contained in a cell formed with at least four walls of thermally insulating material. These requirements make the measurement of the thermal conductivity of high temperature solvents extremely difficult, as the solvent can only be

contained in noble metal crucibles which are not thermal insulators and are not easily formed in complex and easily demountable apparatus. The requirement that there should be no convection places the constraint for a lead vanadate solution according to 3.3, that the total temperature variation through 1 cm of solution should not exceed $1^{o}C$, which is less than the accuracy with which it may be measured. Thus, the equipment to measure thermal conductivity requires an inert high temperature impervious thermally insulating material that has not yet been developed and a temperature control better than that which is normally achieved in crystal growth experiments. For these reasons it is necessary to take an average value of thermal conductivity from the literature. A study of the table of thermal conductivities given by Janz (1961) leads to an average value of 4.0 cal cm^{-1} sec^{-1} C^{-1}./ This is sufficiently accurate for ensuing calculations, which only require an order of magnitude accuracy.

measured on materials which do not present the difficulties above.

2.11 The Comparison Between Experiment and Theory for the Values of the Solubility of Lead Tantalate in Solution

2.11.1. The theoretical relationship of solubility with temperature

Whilst it is possible to predict the solubility from theoretical considerations, the data necessary to compute a solubility value at a given temperature is rarely available, especially for "new" materials. As noted in 1.14 Cobb (1969) has derived a formula for solubility which depends on the heat of fusion ΔH^{F}, melting point T_m, the change in heat capacity on melting of the pure solute, ΔCp, and the temperature of the solution T. The relationship is

$$\ln K = \left(\frac{T_m}{T} - 1\right)\left(\frac{\Delta H_m}{RT_m} - \frac{\Delta Cp}{R}\right) + \frac{\Delta Cp}{R} \ln \frac{T_m}{T} \qquad \text{...(eqn. 2.11.1)}$$

where ln K is the equilibrium constant. Equation 2.11.1 is derived in Appendix B.

$$\ln (K) = \ln \frac{\gamma N}{a_o}$$

where γ is the activity coefficient and N the mole fraction of solute, a_o is the activity of the solute in the pure reference state and is by definition unity; for the derivation of 2.11.1 this reference is taken as pure molten solute at temperature T. If the solute is fully ionised the ionic fraction X_i and an ionic activity coefficient a_i must be used instead of the molar fraction. For an oxide solute RxOy the ionic fraction is of the cation

$$X_R \left(\frac{2y}{x}\right)^{+} = \frac{\frac{2x}{y} A}{\frac{2x}{y} A + \text{sum of the other cations times their charge}}$$

and similarly for the anions. Where all the molecules present are fully dissociated oxides the ionic fraction of the oxygen ions is unity.

In an ideal solution $\gamma = 1$ and $\ln (K) = \ln (N)$.

Where the solution is regular $\gamma \neq 1$ and there is a heat of mixing term $\Delta H^M = RT \ln \gamma$, which in general is not known for a new material.

Equation 2.11.1. has not been tested experimentally. However, if proved to be valid it should be valuable in giving an estimate of the solubility from very little experimental measurement.

2.11.2. The theoretical estimate of solubility

None of the values of the constants in equation 2.11.1 is to be found in the literature for lead tantalate and so approximations must be made. To determine the heat of fusion ΔH_M, molten lead oxide and molten tantalum pentoxide are assumed to form a solution in one another, this solution being molten lead tantalate. Consider the following reaction at the melting point of lead tantalate.

$$PbTa_2O_6(S) \rightleftharpoons PbO(S) + Ta_2O_5(S) \rightleftharpoons PbO(\ell) + Ta_2O_5(\ell) \rightleftharpoons PbTa_2O_6(\ell)$$

(A)

This is equivalent to

$$PbTa_2O_6(S) \rightleftharpoons PbTa_2O_6(\ell) \qquad (B)$$

The heat of reaction for reaction (B) which is ΔH_M, by Hess's law equals the total heat of reaction for reaction (A).

$$\therefore \quad \Delta H_M = \Delta H_d + (\Delta H_M)_{PbO} + (\Delta H_M)_{Ta_2O_5} + \Delta H_s$$

ΔH_d is the heat of dissociation of solid lead tantalate into its component oxides, $(\Delta H_M)_{PbO}$ and $(\Delta H_M)_{Ta_2O_5}$ are the heats of fusion of the respective oxides, and ΔH_S is the heat of mixing liquid oxides. Assume that $\Delta Hd = -\Delta H_S$ and therefore

$$\Delta H_M = (\Delta H_M)_{PbO} + (\Delta H_M)_{Ta_2O_5} \qquad .. 2.11.2(1)$$

where $(\Delta H_M)_{PbO}$ and $(\Delta H_M)_{Ta_2O_5}$ are measured at the melting point of lead tantalate, Tm, which has not been reported. It was measured using a hot stage microscope as described in section 5.4, single crystals of lead tantalate were used and a melting point of 1700 ± 20°C determined. The error was due to the loss of lead oxide from the crystals and due to the failure of the thermocouple, since 1700°C was very close to its maximum working temperature.

The heat of fusion of lead oxide is 6.3 K Cal $mole^{-1}$ at 886°C (Kubochewski, 1956). No value of the heat of fusion of tantalum pentoxide could be found. However, Kubachewski (1956) suggests that chemically similar compounds have similar heats of fusion. The heat of fusion of the very similar niobium pentoxide is 30.0 Kcal per mole, and this figure was used for the heat of fusion of tantalum pentoxide at 1890°C. These heats of fusion must be given at 1700°C. The heat of fusion is related to temperature by the equation

$$(\Delta H)_{T_2} = (\Delta H)_{T_1} + \int_{T}^{T_2} \Delta C_p dT \qquad .. 2.11.2(11)$$

where ΔCp is the difference in heat capacity between liquid and solid. An average value of ΔCp is used as given by Cobb (1969) ie. $\Delta Cp = 1.0$ cal deg^{-1} g $atom^{-1}$. Using the above values in equations 2.11.2 (i) and (ii) one obtains $\Delta H_M = 36.7$ K Cal/$mole^{-1}$ at 1700°C. Thus, using the values of ΔH_M, Tm and ΔCp the value of log (K) can be calculated as a function of absolute temperature. In fig. 2.19 the graph of log (K) against the reciprocal of absolute temperature has been plotted. The error in the measurement of the melting point is significant and the consequent error in log (K) is shown.

2.11.3 Analysis of the experimental data

The solubility was measured in 2.4 by finding the temperature at which a solution of certain concentration becomes saturated. In order to compare the experimental results with the theoretical one of section 2.11.2, the concentration of solution must be expressed in the form log (K). If the solute is fully ionized, then $(K)_I = a_1 X_{Pb}^{2+} + a_2 2X_{Ta}5+$, where a_1 and a_2 are the activities of the ions in solution, $X_{Pb}2+$ and $X_{Ta}5+$ are the ionic fractions of the lead and tantalum ions in the melt. In calculating $(K)_I$ it is assumed that the solution is ideal and, therefore, a_1 and a_2 are equal to unity. The results given in section 2.5 are used to calculate $(K)_I$ and log $(K)_I$ is plotted against the reciprocal of absolute temperature in figure 2.19 for each solvent. A different value of K is obtained if it is assumed that the solute is undissociated in the melt. If the equilibrium in this case is $(K)_{II}$, then $K_{II} = \gamma N$, where γ is the activity coefficient and N is the mole fraction of solute. The solution is assumed to be ideal and $\gamma = 1$. The log $(K)_{II}$ is plotted against the reciprocal of temperature in figure 2.19 for each solvent.

2.11.3 Discussion of the correlation between the experimental and calculated results

In fig. 2.19, while all of the K_I curves show only a poor correlation with the theoretical curve, the K_{II} curves do show some correlation. The K_{II} curve for bismuth borate lies parallel to the

theoretical curve, but is displaced from it. This deviation can be explained if the regular solution model were used in deducing the theoretical curve rather than the ideal solution molecule. A factor of log γ must be added to the theoretical value of log K to include the heat of mixing term not present in the ideal case. Measuring the difference between experimental and theoretical curves for lead tantalate in bismuth borate leads to a value for the heat of mixing of 31.5 K cal $mole^{-1}$. This is rather large and indicates some chemical reaction between solute and solvent. Further support for this interaction is provided by the fact (3.2)that single crystals of lead tantalate grown from this solvent contain a high percentage of bismuth in solid solution.

The K_{II} curve for the solvent PbV_2O_6 is of interest since there is little change in solubility with temperature. Since dissociation into ions decreases solubility, and as the temperature increases so the degree of ionisation of lead tantalate becomes greater ; the overall solubility remains unchanged. To confirm this the depression in the freezing point of pure PbV_2O_7 was measured as a function of lead tantalate added. The slope of the curve obtained is proportional to the number of species of molecules or ions other than those of PbV_2O_6, present in the melt. Owing to the comparatively large experimental error incurred by the use of simple equipment, the results were not precise enough to give conclusive evidence of ionisation. It is likely that there is some irreversible interaction between solute and solvent as crystals grown from this solvent contain a significant proportion of vanadium (0.6 mole %).

The K_{II} curve for the solvent $Pb_2V_2O_7$ is parallel to the theoretical one and nearly equal in magnitude. Thus, the solution is nearly ideal and the crystals grown from this solvent contain only traces of vanadium. Consequently, the density of the solution should increase linearly with increasing concentration of solute at constant temperature.

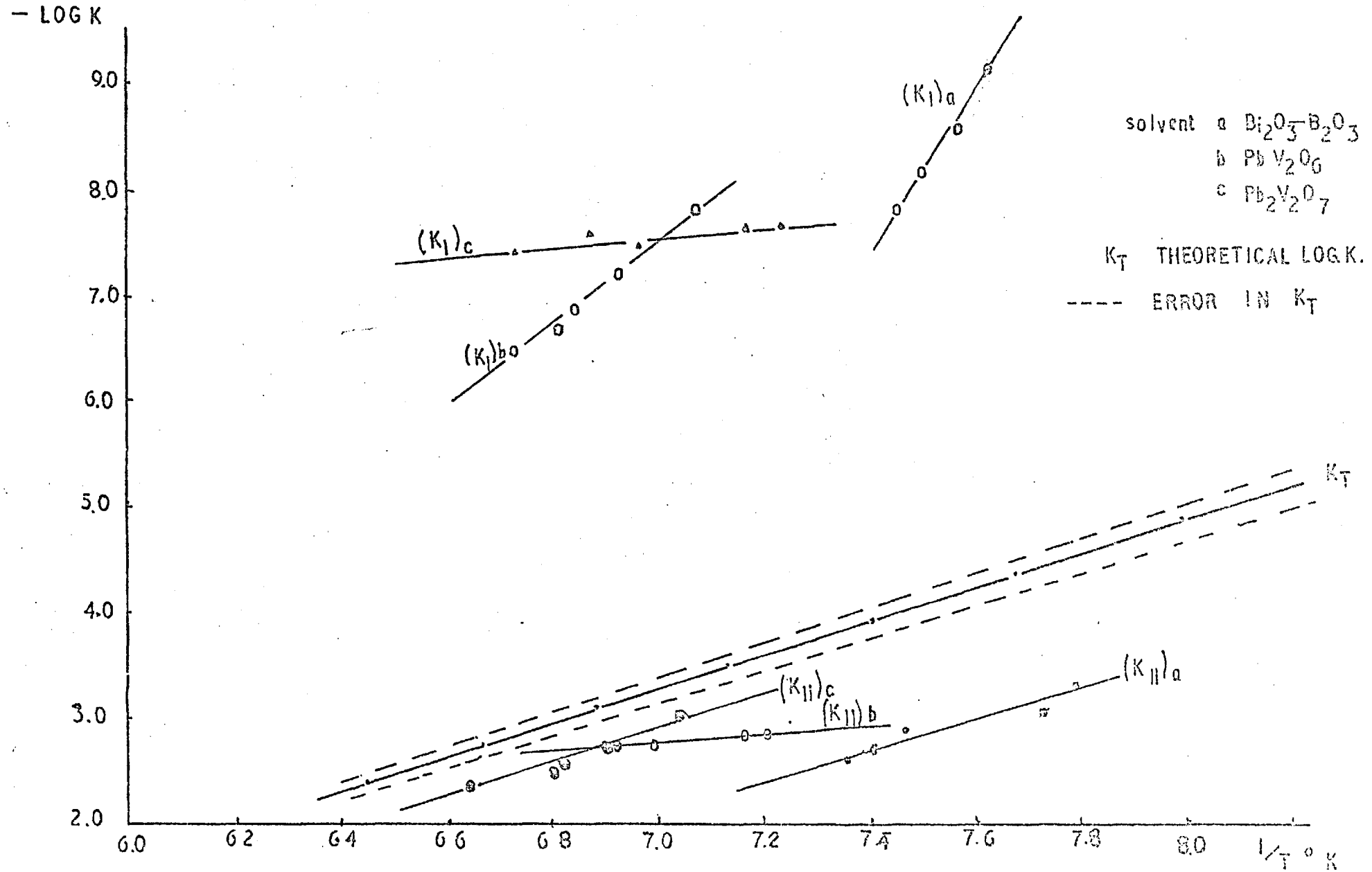

FIG 2.19. LOG K Vs. THE RECIPROCAL OF TEMPERATURE FOR VARIOUS SOLVENTS

The graph of density against concentration is given in fig. 2.15 and the hypothetical density of an ideal solution is also drawn. However, the density data is not sufficiently accurate, nor is there information over a sufficiently wide composition range to confirm the ideal nature of the solution.

The most important conclusion that may be drawn is that lead tantalate exists in the solution as a molecule rather than as ions. Therefore, a description of the crystal growth of lead tantalate must consider the diffusion of entire lead tantalate molecules.

CHAPTER III

3. THE GROWTH OF SINGLE CRYSTALS OF LEAD TANTALATE

3.1 Introduction

In this chapter the experimental growth of single crystals of lead tantalate from solution in $Pb_2V_2O_7$ is described. The rate limiting process is deduced from the experimental evidence and probable causes of instability of the interface during growth are discussed.

3.2 The Growth of Lead Tantalate Single Crystals

The three solvents, Bi_2O_3-B_2O_3, PbV_2O_6 and $Pb_2V_2O_7$ were used in the experiments which were performed using both the slow cooling technique and the temperature gradient transport technique which have been described in section 2.1. The slow cooling technique was used initially for each solvent as this technique is simpler than the temperature gradient transport technique. When the slow cooling technique was found to be inadequate because it was impossible to cool the solution at a sufficiently slow rate, the temperature gradient technique was employed because its advantages are that growth occurs at constant temperature, hence with less thermal strain in the crystal, and slower growth rates are possible. The same furnace and temperature control equipment was used in all experiments and is shown in figure 3.1.

The furnace consisted of a vertical recrystallised alumina tube four inches in diameter, heated with six silicon carbide crusilite rods (Morgan Electroheat Ltd) and insulated with Morganite M128 refractory bricks. The temperature was controlled by a Eurotherm PID SCR 25 controller using a platinum-platinum 13% rhodium thermocouple located inside the alumina tube. A similar thermocouple was used to monitor the crucible temperature and to determine the vertical temperature gradient in the

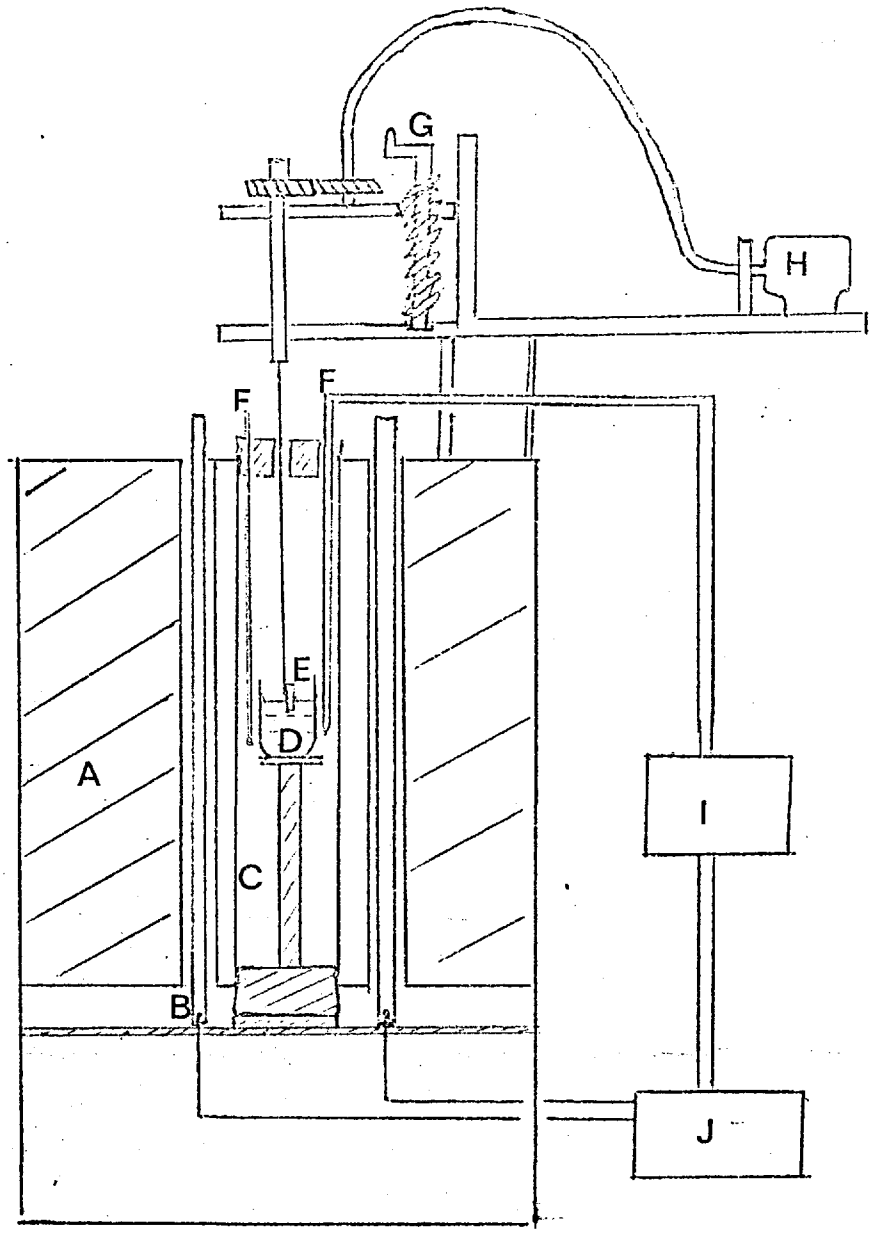

A	insulation	F	control + monitor thermocouples
B	heating element	G	height of seed control
C	alumina tube	H	rotation motor
D	crucible	I	programmer
E	seed crystal	J	temperature controller

FIG. 3.1

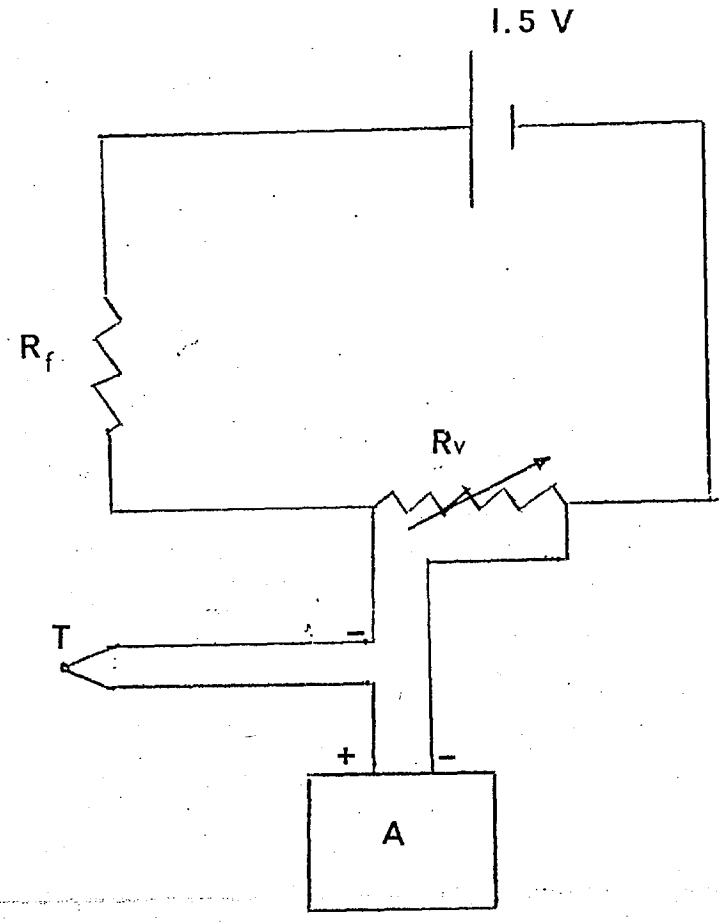

A temperature controller

R_f fixed resistance

R_v helical potentiometer

T thermocouple

FIG. 3.2

furnace. A temperature programming unit was included in the temperature control circuit as shown in figure 3.2. A small positive d.c. voltage, equivalent to a temperature increase, from the potentiometer was added to the control thermocouple signal and consequently less power was supplied by the SCR unit to the furnace so that the furnace temperature decreased by an amount exactly determined by the additional d.c. voltage. The potentiometer was of helical type and the variable voltage output was determined by the position of a central spindle which could be rotated by an electric motor via a variable gearbox to give a continuously increasing or decreasing signal to the controller. The voltage across the potentiometer was supplied by a 1·5 Volt battery which provided adequate stability at the low current used during the length of a run. The rate of cooling was determined by the choice of the fixed resistance R_f and by the rate of rotation of the spindle as set by the gearbox output drive, which could be increased in discrete steps from 0.0003 to 10 r.p.m. The minimum rate of cooling that could be used was $0.5^{\circ}C\ hr^{-1}$ because the temperature control was only stable to within limits of $\pm\ 0.2^{\circ}C$.

The crucible was mounted on an alumina pedestal which rested on a firebrick, which closed the lower end of the furnace tube. The upper end was similarly closed with a firebrick through which holes had been drilled to admit the thermocouples and the seed support. The seed crystal was tied with fine platinum wire to a platinum-rhodium rod 1 mm in diameter which in turn was fixed into a stainless steel rod. The whole seed support could be rotated and raised or lowered. The rotation was provided by a geared synchronous motor at a set speed of 4.5 r.p.m.

In slow cooling experiments the crucible was charged with the oxides constituents (all were supplied by B.D.H. Chemicals Ltd.) as shown in table 3.1 and placed in the furnace, which was then raised to the crystallisation temperature of the solution. The solution was maintained

at this temperature for sixteen hours to allow complete solution to occur and then the seed crystal was inserted so that only the crystal and no part of the support was in the melt. Seed crystals were obtained initially by spontaneous nucleation onto the seed support rod. The slow cool programmer was then switched on and the crystal was then allowed to grow while the temperature was lowered through 40°C. Cooling rates of 0.5, 1.5 and 4.0°C hour^{-1} were used with and without rotation of the seed. The typical results obtained are shown in table 3.1.

Table 3.1

Composition and cooling rates of various solutions used to grow lead tantalate single crystals

3.1(a) Solvent 55 mole % Bi_2O_3 - 45 moles % B_2O_3.

Concentration of solution in moles %	Charge	Slow Cooling rate	Product
5	Bi_2O_3 324g	4.0°C hr^{-1}	Many small, needle-
	B_2O_3 39g	1.5°C hr^{-1}	like crystals up to
	PbO 14.3g		4mm in length
	Ta_2O_5 29.1g		
	total 405.4g		
3.1(b) Solvent PbV_2O_6			
6	PbO 223.2g	4.0, 1.5,	
	V_2O_5 171.6g	0.5°C hr^{-1}	Opaque crystalline
	Ta_2O_5 26.2g		mass 1 x 1 x 1 cm.
	total 421.0g		
3.1(c) Solvent Pb_2V_2O7			
8	PbO 300g	4.0, 1.5,	Crystals 1 x 1 x 1 cm
	V_2O_5 116g	0.5°C hr^{-1}	containing
	Ta_2O_5 25g		inclusions
	total 441g		

As indicated in table 3.1(a) for the solvent Bismuth Borate growth did not occur on the seed, but many small, needle-like crystals grew up to 4mm long and less than 0.5 x 0.5 mm in cross section. The crystals were frequently cracked and contained many inclusions. So that slower growth rates could be used the temperature gradient transport technique was used, but no improvement in crystal quality was obtained. There was no investigation to determine the optimum conditions for growth by temperature gradient transport as Bismuth Borate was found to be unsuitable for the following reasons. A crystal was examined with a transmission polarising microscope, the light being parallel to the [001] direction, which had been identified by X-ray rotation photograph technique as the elongated dimension of the grown crystals. The crystal was seen to contain many antiparallel domains (fig. 3.3). Further electron microprobe analysis of the crystals showed that Bismuth was present in solid solution in the crystals in concentrations up to 10% by weight. This impurity, which possibly causes the fine domain structure by fixing domain walls, renders the crystals unsuitable for electro-optic measurement, since the domain structure scatters light out of the crystal and any variation in impurity content would cause irreproducibility in measurements of the electro-optic constant.

In the growth experiments by slow cooling of the PbV_2O_6 solution, controlled nucleation was achieved. Crystals measuring 1 x 1 x 1cm were formed on the seed and possessed facet-like faces, although they were frequently cracked and contained many inclusions. The crystals were a dark brown colour and were opaque. Electron microprobe analysis indicated a vanadium concentration of up to 0.6% by weight in the grown crystals. As the dark brown colour is characteristic of vanadium compounds and as oxygen firing failed to reduce the colour, this vanadium impurity probably caused the crystals to be opaque and hence this solvent is unsuitable for

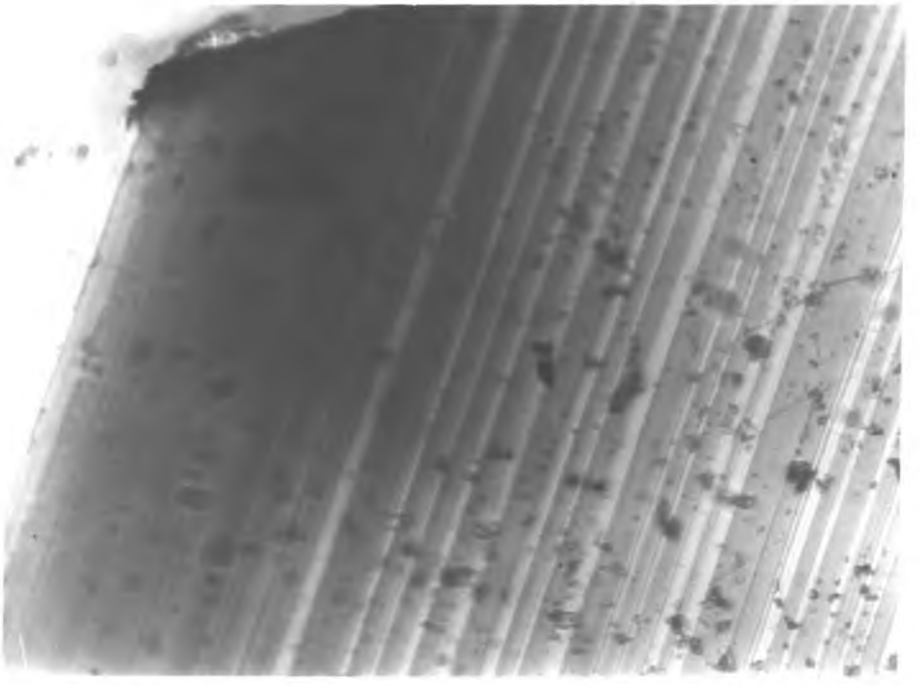

X 320

FIG. 3.3.

the growth of lead tantalate for electro-optic measurements.

By slowly cooling the $Pb_2V_2O_7$ solution controlled nucleation was achieved and the seed crystal grew to 1 x 1 x½cm in size. However, as can be seen in figure 3.4, the crystal contained many solvent inclusions. Upon prolonged treatment in dilute nitric acid some large crystals broke up into many smaller, transparent crystals, of which some were plates measuring 4 x 2 x 1 mm and were free of inclusions. A number of slow cooling rates were used as shown in table 3.1 and the seed crystal was rotated during growth, but no significant increase in crystal quality was observed.

In addition to linear cooling rates, a cooling rate which followed the t^3 law (section 1.14.3) was used to eliminate any rapid dendritic type growth when the seed is first lowered into the melt. Using the relation that $\Delta\theta = \alpha t^3$, where $\Delta\theta$, α and t are defined in 1.14.3, and where $\alpha = 6.6 \times 10^{-4}$ using the values of the ρ and k given in figs. 2.15 and 2.9, a temperature programme was used as shown in figure 3.5 with a series of linear cooling steps to approximate to the t^3 dependence of temperature on time. This experiment did not improve the crystal quality, although no other nucleation sites were formed in the crucible, all the growth occurring on the seed.

As slower growth rates generally give better interface stability (1.14.5) the temperature gradient transport technique was used with the solvent $Pb_2V_2O_7$. The charges and temperature gradients that were used are shown in table 3.2. Poor quality crystals grown by the slow cooling technique were used as the source material at the crucible base, and were encased in platinum foil to inhibit dissolution. A number of temperature gradients could be applied to the crucible by varying its height in the furnace. The crucible was placed so that the base was hotter than the top, the furnace temperature gradient being determined during each growth experiment using the monitoring thermocouple; the usual depth of solution

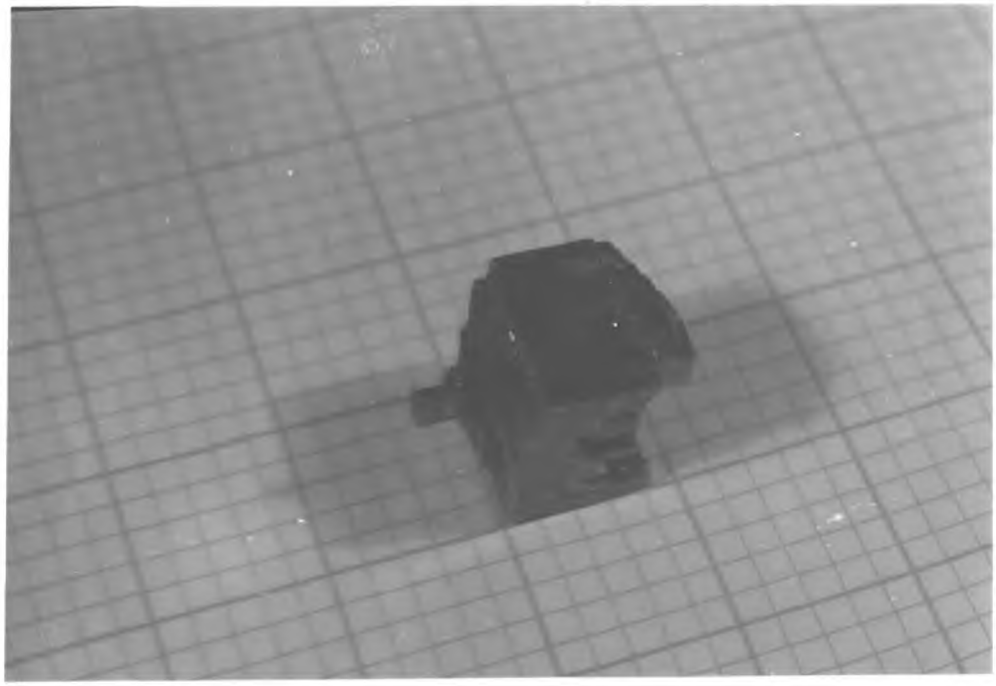

1 DIV. = 2mm.

FIG. 3.4.

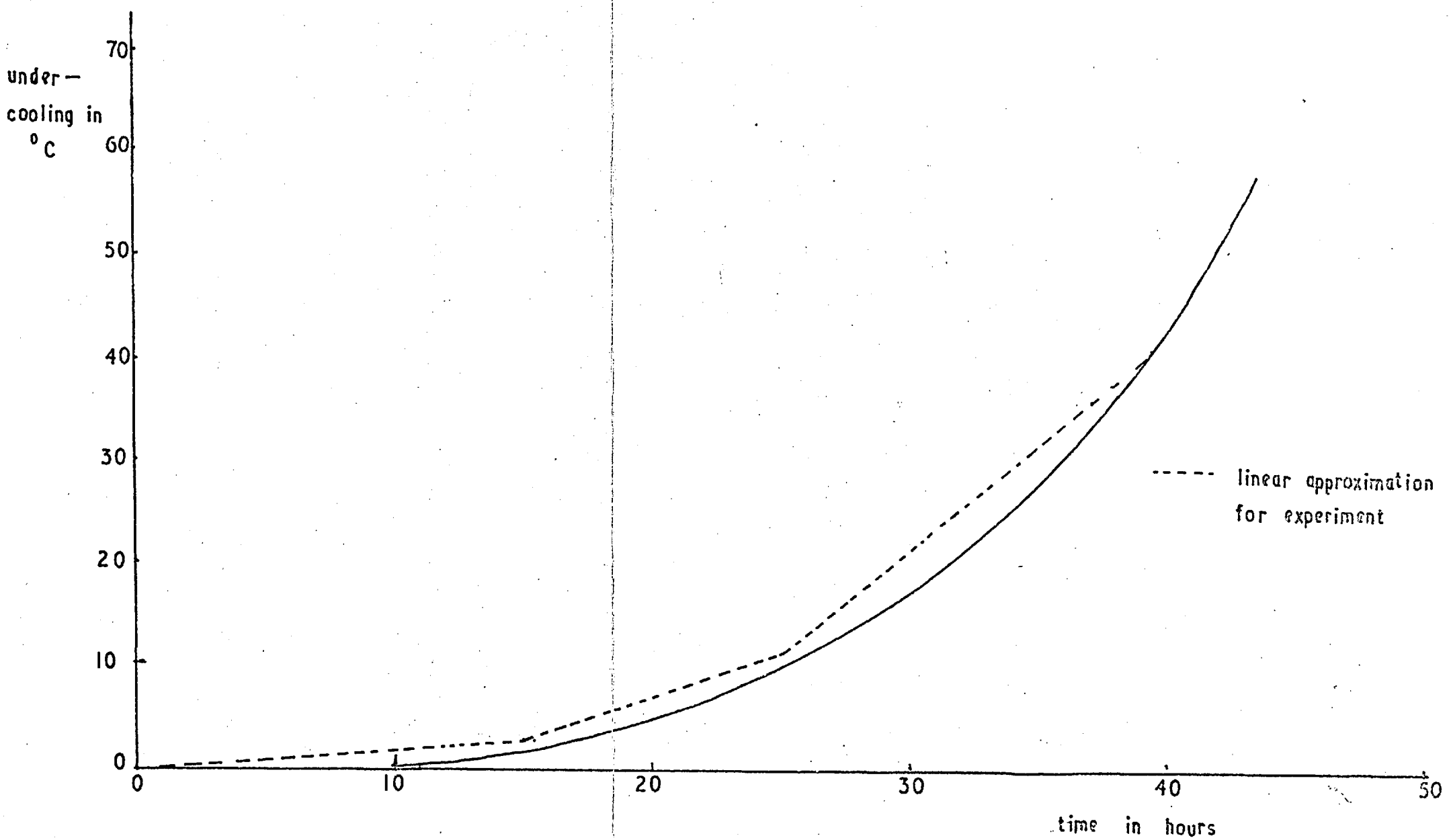

FIG. 3.5 THE DECREASE IN SOLUTION TEMPERATURE Vs. TIME.

was 4 cm. The crucible was charged by placing the platinum encased crystals into the crucible and then adding the rest of the charge as given in the amounts given in table 3.2. The crucible was heated to the crystallisation temperature of the solution and the seed was inserted after a sixteen hour soak period. No rotation of the seed was used as an adequate growth rate was observed without rotation. The grown crystal was removed after a few days. Crystals very similar to those produced by slow cooling were obtained. The variations of the applied temperature gradient had no appreciable effect on the crystal quality.

Table 3.2

The conditions used in the growth of lead tantalate from $Pb_2V_2O_7$ solution by the temperature gradient transport technique.

Solution concentration	Mass of source material	Additional charge in g		Mass of crystal in g	Duration of run in hours	Temperature gradient $^{o}C\ cm^{-1}$
8 mole %	20g	PbO	450	13.0	144	5
		V_2O_5	174	8.0	120	4
		Ta_2O_5	37.5	1.0	112	3
		total	661.5			

After treatment with dilute nitric acid the large crystalline masses usually broke up into many smaller crystals (fig. 3.6) which were plates or rods. The rod-like crystals were most common and typically measured 1 x 1 x 4 mm, the facets being mutually perpendicular. An X-ray rotation photograph (fig. 3.7) taken by rotating the crystal about its longest axis showed this axis to be the [001] axis, using the lattice parameters given by Subbarao (1960) to index the photograph. A Laué back reflection photograph (fig. 3.8) taken of the crystal face parallel to the [001] axis. Clearly, two mirror planes can be seen, demonstrating that the crystal facet is of an (100) type. Hence, the grown crystals are

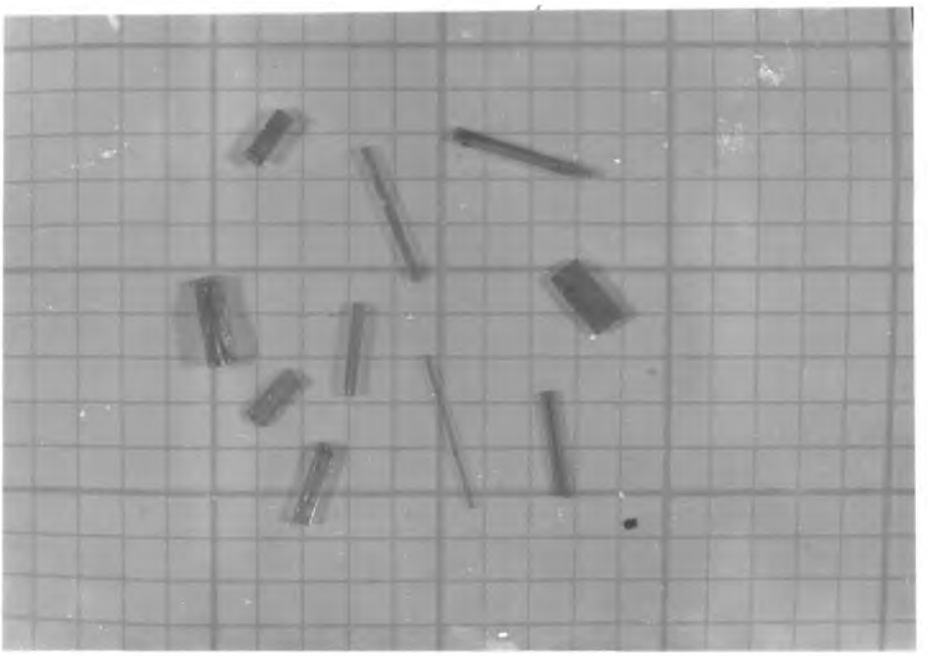

1 DIV. = 2mm.

FIG. 3.6

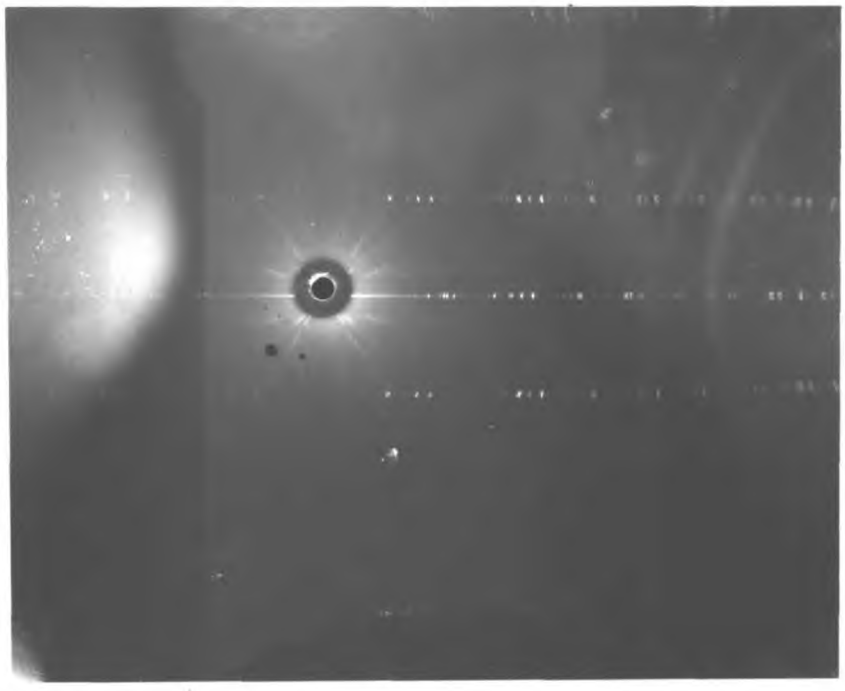

FIG. 3.7.

FIG. 3.8

bound by <100> faces and are elongated in the [001] direction.

To confirm that the phase crystallising from solution was ferroelectric and to estimate the stoichiometry of the crystal, measurement was made of the dielectric constant of the crystal as a function of temperature. An inclusion-free crystal plate measuring 0.7 x 1.0 x 5.0 mm was chosen and gold electrodes were evaporated onto the 5.0 x 0.7 mm faces. The crystal was placed between aluminium electrodes, which also had been coated with gold to ensure good electrical contact, and which were connected to a Wayne Kerr capacitance bridge. The electrode assembly to which a nickle chrome-nickle alumel thermocouple was attached was placed in a furnace. The capacitance was then measured as a function of temperature and from the capacitance measurement the dielectric constant was calculated. The plot of dielectric constant against temperature is shown in fig. 3.9 and a Curie-Weis plot of the reciprocal of dielectric constant against absolute temperature is shown in fig. 3.10. The dielectric anomaly shown in figure 3.9 is typical of a ferroelectric transition and the Curie-Weis plot gives the Curie transition temperature of 260°C. This agrees well with the value 265°C as reported by Subbarao (1960) and Ismailizide (1966) within the experimental error of ± 5°C. Thus, the crystals were ferroelectric with an average composition very close to the ideal $PbTa_2O_6$.

The crystals were pale yellow in colour and as oxygen defficiency causes colouration of tungsten bronzes (Levinstein (1967)) crystals were fired in oxygen at 1000°C for sixteen hours. No change in the colour was observed and it is, therefore, possible that the colour is due to traces of vanadium in the crystal. Electron microprobe analysis revealed the vanadium content of the crystals to be below the limit of detection, that is less than 0.2% by weight. This limit is relatively high and there is sufficient vanadium below this limit to cause the colouration.

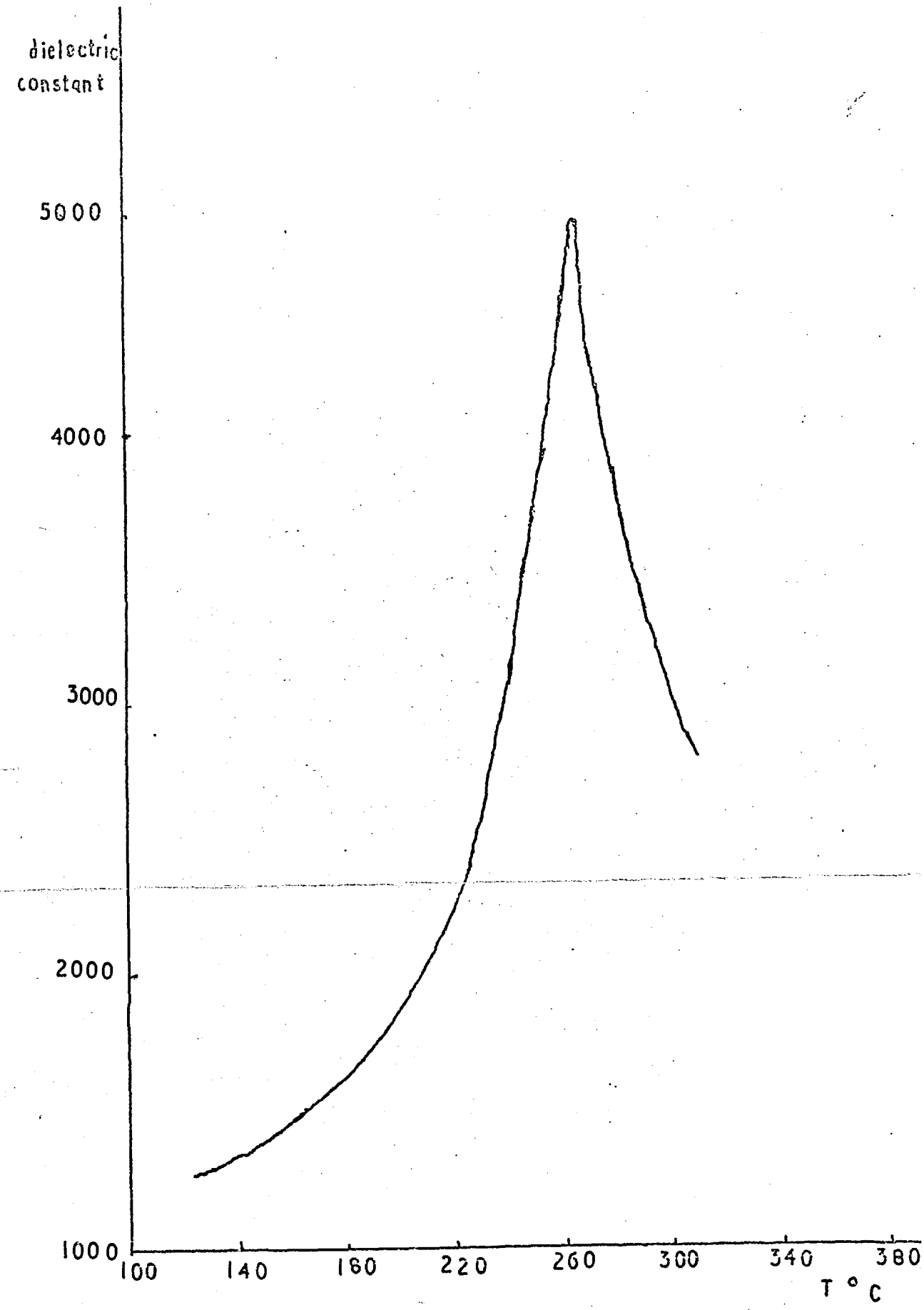

FIG 3.9 THE DIELECTRIC CONSTANT OF $PbTa_2O_6$

Vs. TEMPERATURE

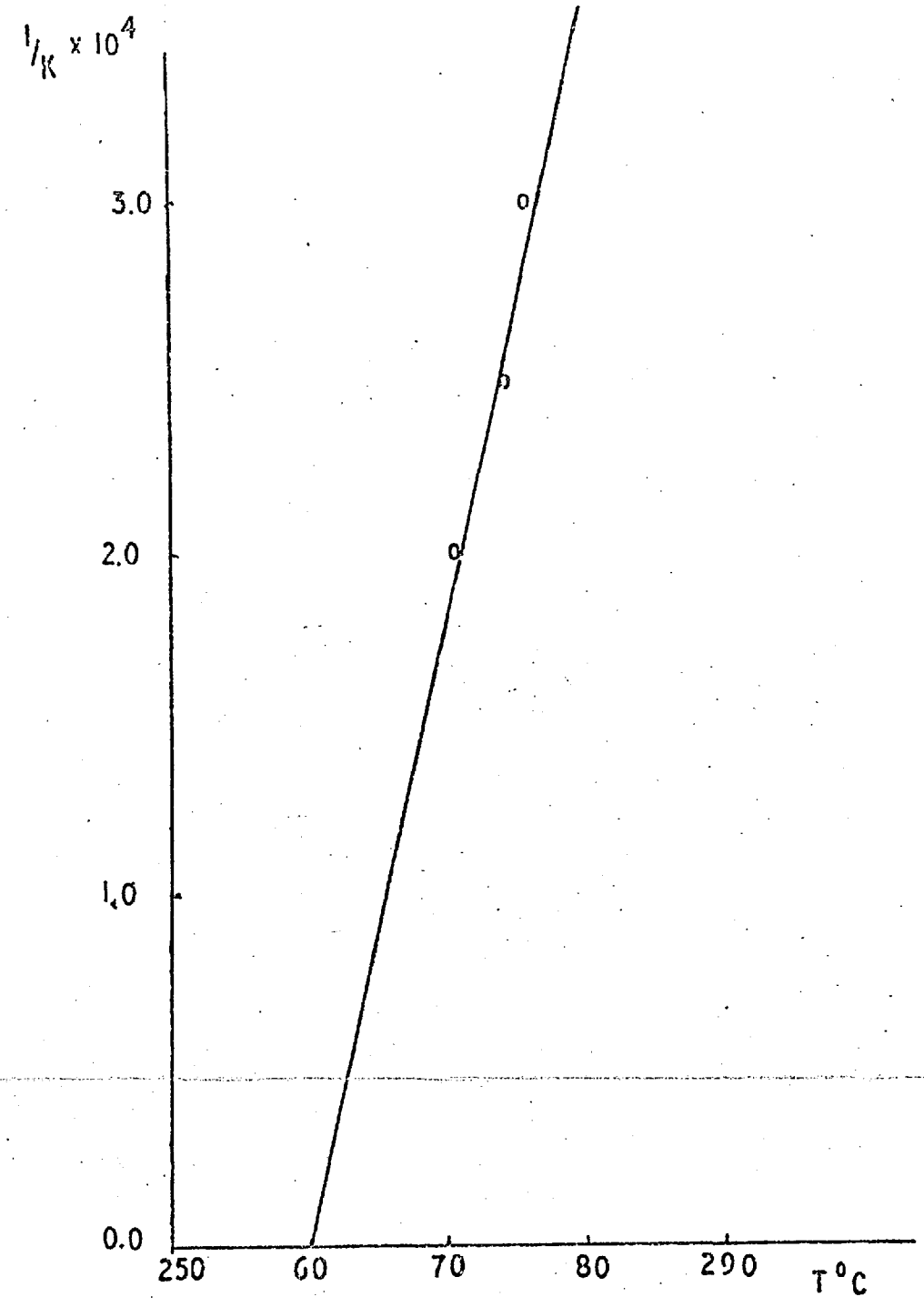

FIG. 3.10. THE GRAPH OF THE RECIPROCAL OF THE DIELECTRIC CONSTANT OF $PbTa_2O_6$ Vs. TEMPERATURE

When viewed using transmitted light, using a polarising microscope, the crystal appeared strain free and ferroelectric domains were observed only at the very edge of a crystal. The polar direction was normal to the surface of the largest area in the plate like crystals grown. This is consistent with the X-ray analysis result that the crystal faces are (100) type.

In summary, crystals may be grown from the solvent $Pb_2V_2O_7$ which are of good optical quality and of sufficient size for measurement of their electro-optic coefficients.

3.3 A Model For The Growth Of Lead Tantalate Single Crystals From a Solution in $Pb_2V_2O_7$

An adequate description of the growth of lead tantalate single crystals must specify the rate limiting process, the cause of instability of the interface and should indicate how the experimental conditions may be changed in order to improve the quality of the grown crystal.

There are three possible rate limiting processes in crystal growth as discussed in section 2.1; these are the transport of solute through the bulk of solution, diffusion through the boundary layer and, finally, surface diffusion and incorporation into the crystal lattice. The rate of stirring in the melt determines which process is the rate limiting one, as is illustrated in fig. 3.11, which shows the rate of growth of yttrium iron garnet as a function of the rate of stirring of the solution. (Laudise, 1963)

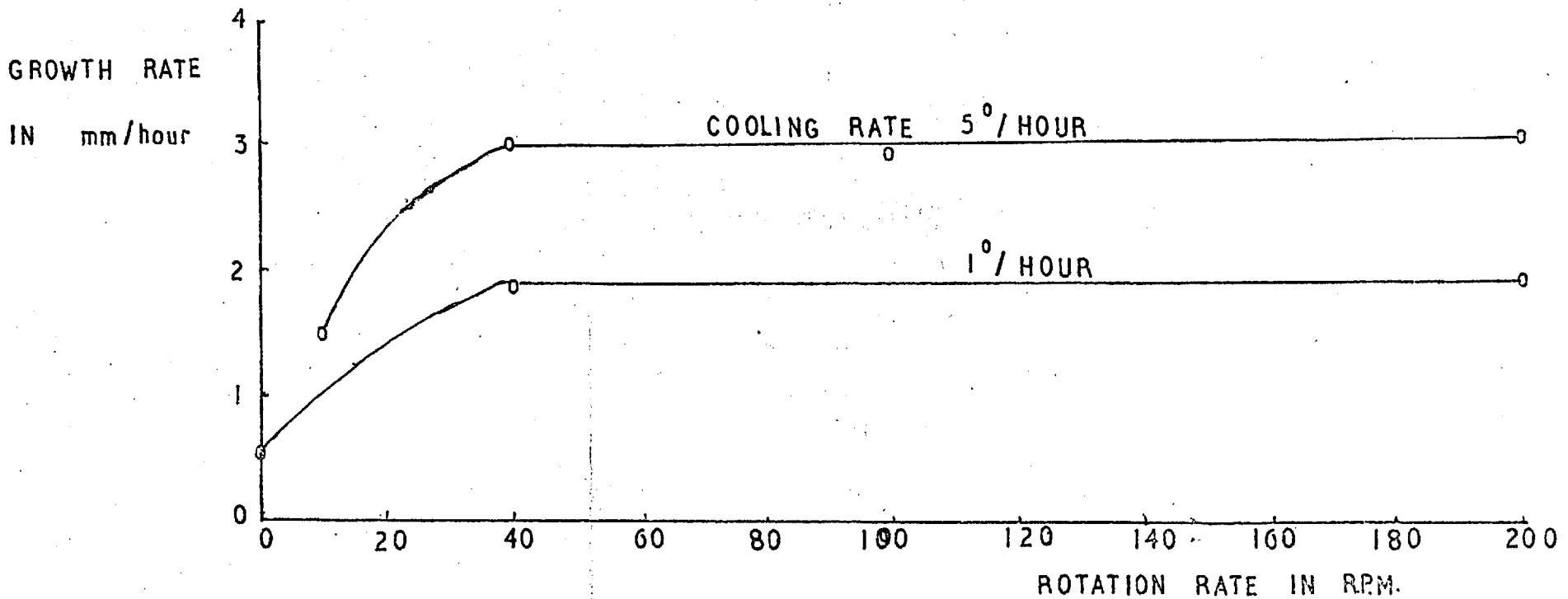
GROWTH RATE
IN mm/hour
4
3
2
1
0
COOLING RATE 5°/HOUR
1°/HOUR
0
20
40
60
80
100
120
140
160
180
200
ROTATION RATE IN R.P.M.

FIG. 3.11.

At high stirring rates the growth rate is independent of the stirring and the growth rate is determined by the surface diffusion on molecules (or ions) on the crystal interface. At lower stirring rates diffusion through the boundary layer is the limiting step. At very low stirring rates the growth rate is nearly independent of the cooling rate and corresponds to crystal growth limited by transport of solute to the crystal through the bulk of solution. In the growth of lead tantalate the only stirring in the melt was effected by free convection, which is a relatively slow when compared with mechanical stirring, and consequently the first consideration must be given to transport of solute process and the diffusion through the boundary layer.

It must first be established that convection occurs in the crucible. The criteria for the onset of convection in a liquid zone heated at the base is given by the inequality $N_{Pr}N_{Gr} > 2000$ (Tyrell, 1961) where N_{Pr} is the Prandtl number and N_{Gr} is the Grashof number. Their full definitions are found in the glossary in Appendix A, and their values for an 8 mole % solution of lead tantalate in $Pb_2V_2O_7$ is calculated in Appendix A as $N_{Pr} = 0.513$ and $N_{Gr} = 19 \times 10^6$. Hence, $N_{Gr}.N_{Pr} = 10 \times 10^6$. For products $N_{Pr}.N_{Gr}$ in the range $2000 < N_{Pr}.N_{Gr} < 45{,}000$ the liquid forms a number of cells and within each cell elements of liquid move in a circulatory motion as illustrated in fig. 3.12(a). If $N_{Pr}.N_{Gr} > 45{,}000$, the cellular structure breaks down (3.12(b)) and a generally turbulent flow results (Tyrell, 1961) and this is the case for the lead tantalate solution.

A turbulent liquid is characterised by a Reynolds Number $N_{Re} = 10^4$ (Levich, 1963) where $N_{Re} = \frac{VL}{\nu}$ as defined in Appendix B. Using $L = 4$ cm and $\nu = 3.48 \times 10^{-3}$ poise the velocity of a fluid element is $V = 9.0$ cm sec^{-1}. This is only an approximate calculation as there is no established theory for calculating the velocity of a fluid under free

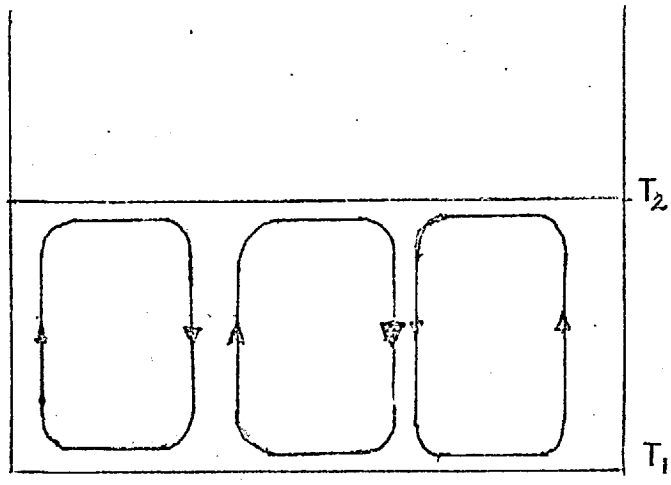

(a)

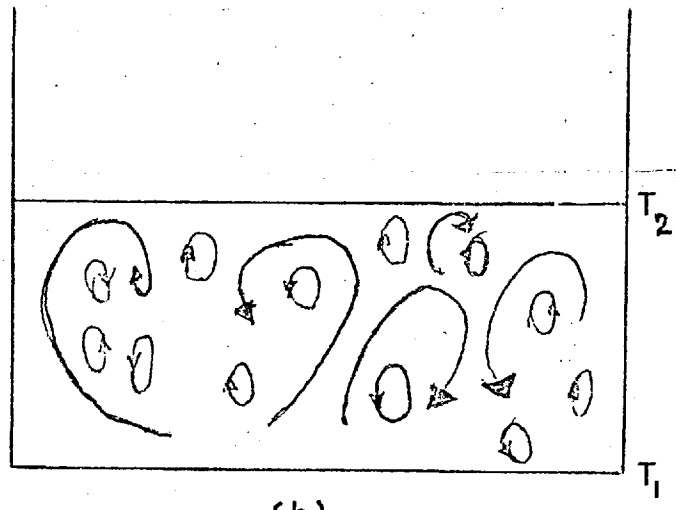

(b)

$T_2 > T_1$

FIG. 3. 12.

convection and contained in a crucible nor is there any published experimental evidence on which an estimate can be made. The uncertainty of V is the chief source of error in a fluid mechanical description of crystal growth. As there is no net translation of the solution in the crucible, the velocity V is the average velocity of an element of fluid within an eddy of the turbulent flow and it is taken as the velocity of the liquid relative to a crystal plate placed in the solution.

The diffusion of a solute in a moving solution is described by equation 3.1.

$$vx \frac{\partial c}{\partial x} + vy \frac{\partial c}{\partial y} + vz \frac{\partial c}{\partial z} = D\left(\frac{\partial^2 c}{\partial x^2} + \frac{\partial^2 c}{\partial y^2} + \frac{\partial^2 c}{\partial z^2}\right) \quad \ldots 3.1$$

where c is the concentration of an element in a position x,y,z and possessing a velocity with components vx, vy, vx. This equation can be reduced to a dimensionless form by dividing through by $CoVL^2$ where V is a characteristic velocity of the fluid, L a characteristic dimension of the fluid and Co is the bulk concentration. The equation becomes

$$Vx \frac{\partial C}{\partial X} + Vy \frac{C}{\partial Y} + Vz \frac{\partial C}{\partial Z} = \frac{D}{VL}\left(\frac{\partial^2 C}{\partial X^2} + \frac{\partial^2 C}{\partial Y^2} + \frac{\partial^2 C}{\partial Z^2}\right) \quad \ldots 3.2$$

where $Vx = \frac{v_x}{V}$, etc. $C = \frac{c}{C_o}$, $x = \frac{x}{L}$ etc.

$\frac{VL}{D}$ is dimensionless and is defined as the Péclet number N_{Pe}.

Rewriting equation 3.2 to include the Péclet number as

$$Vx \frac{\partial C}{\partial x} + Vy \frac{\partial C}{\partial x} + Vz \frac{\partial C}{\partial z} = \frac{1}{N_{Pe}}\left(\frac{\partial^2 C}{\partial X^2} + \frac{\partial^2 C}{\partial Y^2} + \frac{\partial^2 c}{\partial Z^2}\right) \quad \ldots 3.3$$

it may be seen that the Péclet number determines the importance of the fluid motion relative to the pure diffusional change in changing the solute concentration at a given point. For if N_{Pe} is small, the right-hand side of equation 3.3, the pure diffusion terms, are large compared with the left-hand side, the fluid motion terms, and pure diffusion is the

most significant process. The distribution of solute and its rate of change can then be found by solution of the diffusion equation with the relevant boundary conditions. If, however, N_{Pe} is large, the right-hand side of equation 3.3 tends to zero and the fluid motion determines the solute distribution and its rate of change. There is no sharp boundary between the two extreme mechanisms and no critical value of N_{Pe} has been given for the transition. However, for $N_{Pe} > 10^3$ (Levich, 1963) the fluid motion will certainly be dominant. For an 8 mole % solution of lead tantalate, $V = 9.0$ cm sec^{-1}, $D = 1.13 \times 10^{-6}$ cm^2 sec^{-1} and $L = 4$ cm, thus $N_{Pe} = 3.2 \times 10^7$, which is so large that only fluid motion terms are significant.

The fluid motion in the bulk of solution is extremely turbulent as indicated by the high value of the $N_{Pr} \cdot N_{Gr}$ product. Since the fluid motion determines the concentration distribution, the concentration in the bulk of solution will be uniform, turbulent flow being very effective in mixing individual fluid elements (Levich 1963) of differing concentration. Transport of solute is not the limiting process because as the solution is cooled the rapid turbulent mixing ensures the uniformity of concentration.

The situation for crystal growth of lead tantalate is, therefore, depicted in 3.13.

The bulk of solution is at uniform concentration, which falls to a value near the equilibrium concentration Co at the interface through the mass boundary layer δ. For systems with a high Schmidt number the mass

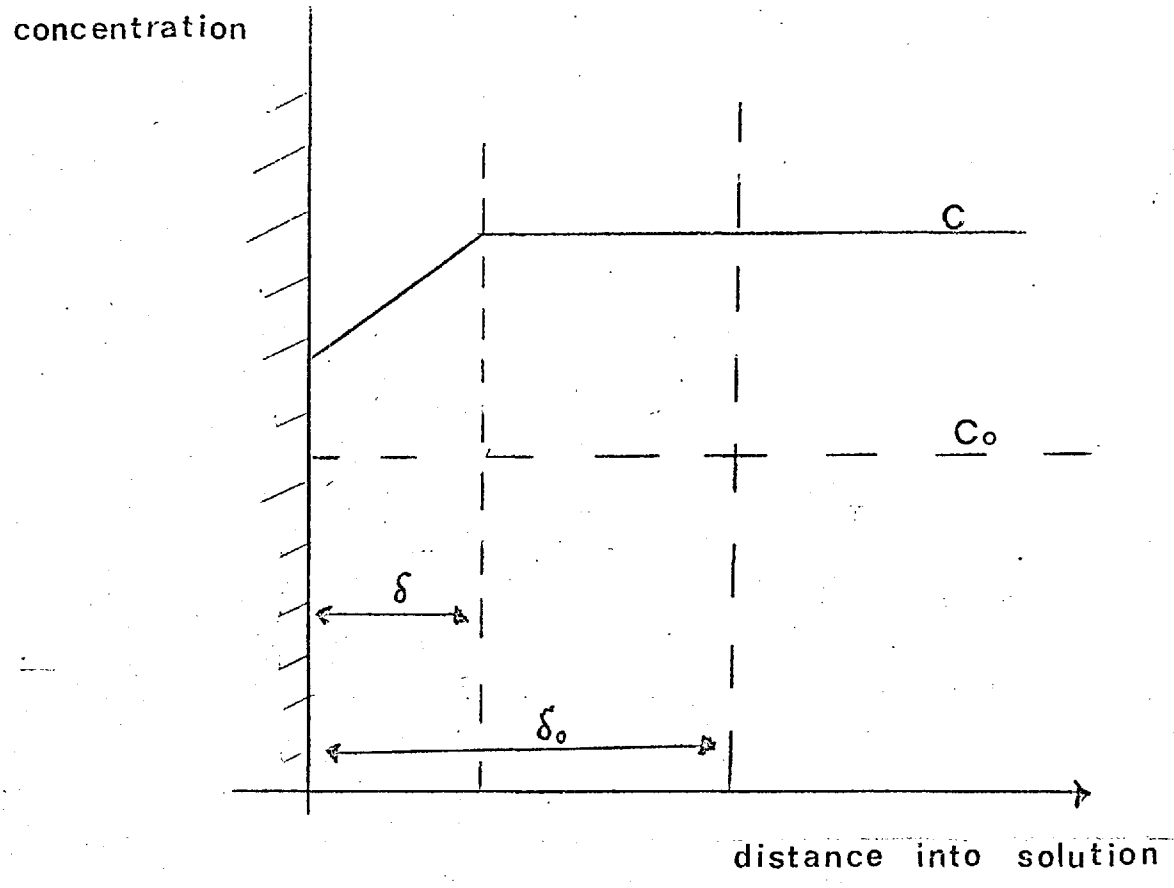

FIG. 3.13

boundary layer (alternatively called the diffusion boundary layer) δ_o lies within the momentum boundary layer δ. The crystal growth occurs as the supersaturated solution of the bulk flows past the crystal with velocity V and solute diffuses through the mass boundary layer into the crystal. The thickness of the boundary layer, and hence the rate of diffusion, is determined by the velocity of the solution past the plate. At low solution velocity the layer thickness is large and the growth is diffusion limited. That diffusion limited growth takes place may be deduced from the maximum size of crystal that can be grown free from inclusions. This is calculated in the following way.

Carlson (1958) has shown that a crystal plate grows in a turbulent flow of solution at a rate per unit area of

$$Qd = \frac{1}{3} N_{Sc}^{\frac{1}{3}} D (C_\infty - C)\left(\frac{V}{\nu x}\right)^{\frac{1}{2}} \quad \ldots \quad 3.4$$

where C_∞ the bulk solute concentration, C the concentration at the interface, and x, the distance downstream on the crystal, D the diffusion coefficient and ν the kinematic viscosity. This assumes that the concentration is constant over the crystal plate and leads to an uneven rate of growth over the crystal as shown by the form of Qd in figure 3.14.

An irregular wedge shaped crystal will result which is inconsistent with the observation that crystals grow with flat faces. Carlson showed that this difficulty is removed is the concentration is allowed to vary over the crystal plate in the form

$$C = C_\infty - bx^{\frac{1}{2}} \quad \ldots \quad 3.5$$

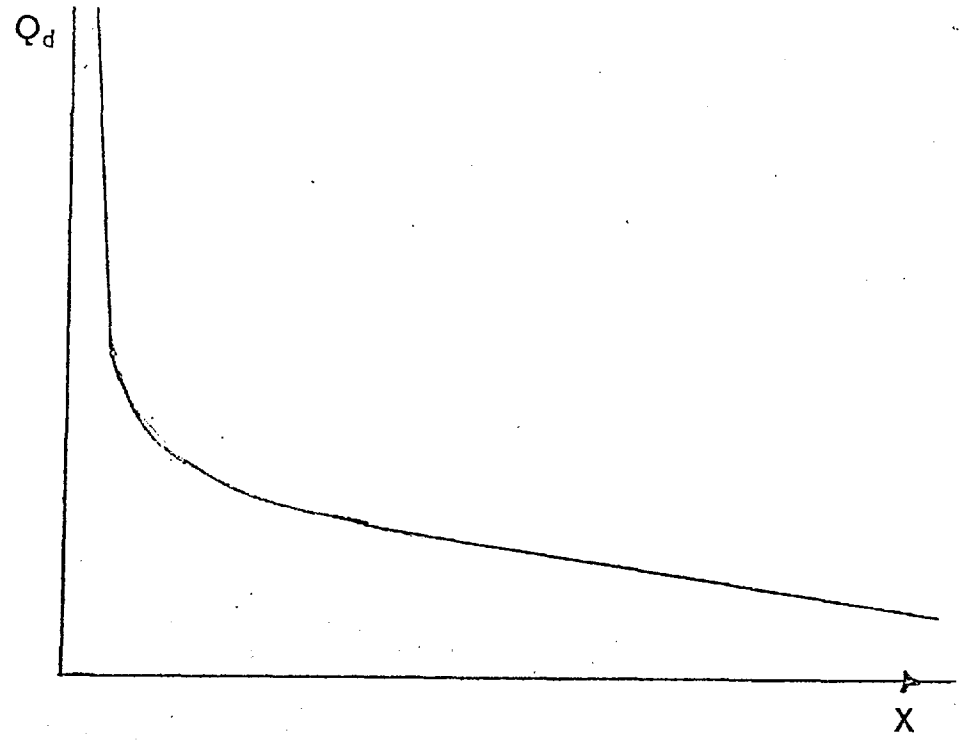

FIG. 3.14.

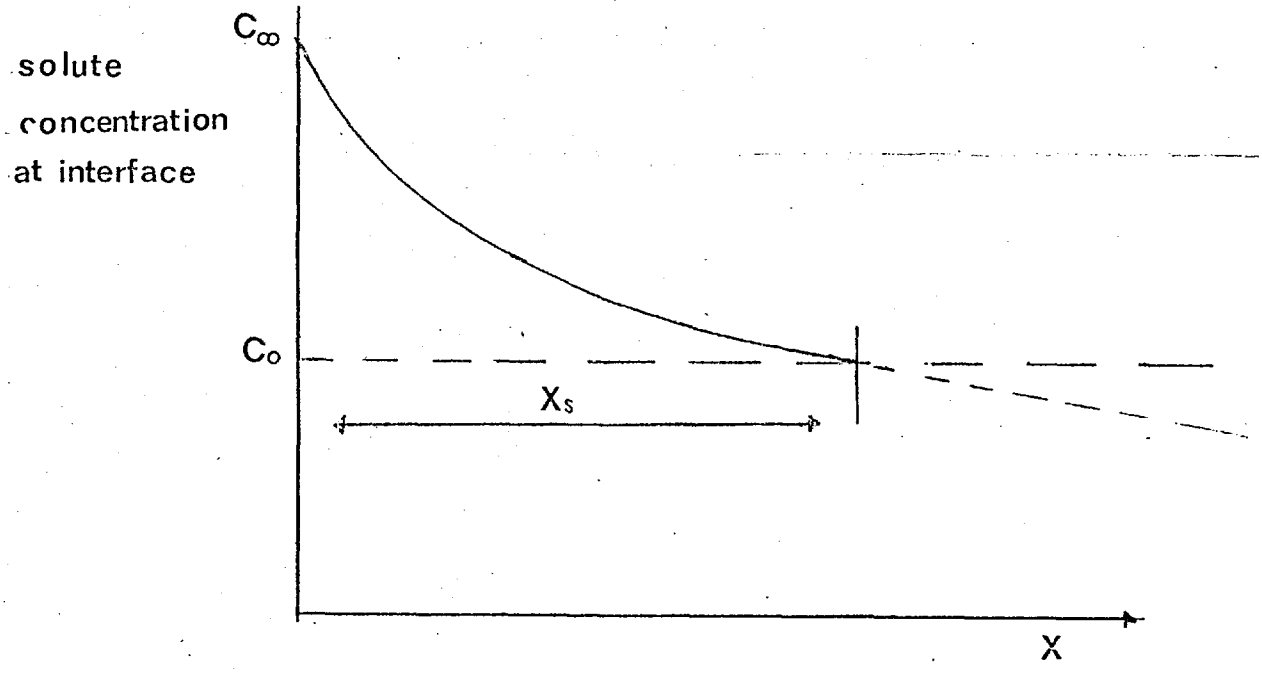

FIG. 3.15.

where b is a constant. By a treatment analogous to that of Page (1931) the rate of growth becomes uniform over the plate and

$$Qd = 0.463\ Db\ N_{Sc}^{\frac{1}{3}} \left(\frac{V}{L}\right)^{\frac{1}{2}} \qquad \ldots\ 3.6$$

However, the concentration now varies over the plate in the form shown in figure 3.14.

At some point x_s along the crystal the concentration falls to that of the equilibrium concentration C_o and growth is no longer possible at lengths of crystal greater than x_s. Putting $x = x_s$ and $C = C_o$ in equation 3.5 and substituting for b in equation 3.6, the length of crystal that may be grown is x_s

$$x_s = \frac{0.214\ VD}{N_{Sc}^{\frac{1}{3}} \left(Qd/C\infty - Co\right)^2} \qquad \ldots\ 3.7$$

The value of x_s may now be evaluated. V, D and N_{Sc} have been measured for an 8 mole % solution of lead tantalate and are given in Appendix A. The value of $Qd/C\infty - Co$ is found from the slope in figure 2.18, which is the plot of loss of weight of crystal against supersaturation. Although figure 2.18 was drawn using dissolution data it may also be used for the crystal growth situation since in diffusion limited growth the chemical reactions involved are not limiting processes. Using

$Qd/C\infty - Co = 3.48 \times 10^{-4}$, $N_{Sc} = 3.06 \times 10^{3}$, $V = 9.0$ cm sec^{-1}, $D = 1.137 \times 10^{-6}$ cm^2 sec^{-1}. in equation 3.7 one obtains $x_s = 1.2$ cms..

It should, therefore, be possible to grow cubes of material

1.2 x 1.2 x 1.2 cm free from inclusions. However, it was observed that crystals rarely grew bigger than 4 x 2 x 1 mm inclusion free and typical crystals measured 4 x 1 x 1 mm. The growth rate in the [001] direction is therefore four times that for growth in the [010] and [100] directions when inclusion free crystals are grown. Crystals were grown measuring 1 x 1 x 1 cm, but contained many inclusions which were in troughs parallel to the [001] direction. This indicates an abnormal growth due to interface instability in the [010] and [100] directions that is twice that for normal inclusion free growth. Hence, a value of $2Q_d/C_\infty - C_o$ must be used to calculate the length of crystal that can be grown inclusion free at the abnormal rate, giving x_s = 0.3 cm. Thus, the maximum size of inclusion free crystal that may be grown measures 1.2 x 0.3 x 0.3 cm. While the largest inclusion free crystal grown measured 4 x 2 x 1 mm, crystals were found up to 1 cm long, although generally less than 0.5 x 0.5 mm in cross section. Other crystals were found with dimensions up to 0.3 cm in the [010] and [100] directions, but none were found to be larger than this.

To summarise, the growth of lead tantalate from solution using only free convection is diffusion limited as demonstrated by the correlation between the size of inclusion free crystal grown and that expected by a theory based on diffusion limited growth. There is an instability in the growth of the interface which results in a decrease in the size of inclusion free crystal that may be grown. Before further discussion of this instability the mechanism of diffusion limited growth should be confirmed by reference to the temperature gradient transport technique and by reference to the effect of rotation on the quality of the grown crystal.

If the growth rate is determined by diffusion through the mass boundary layer, then equation 3.6 can be used to predict the rate of growth of a crystal by temperature gradient transport. Source material is

dissolved in the base hot zone and is carried by the turbulent flow to the region of the crystal interface where the solution is depleted of solvent by the diffusion into the growing crystal. The rate of growth will be determined by the velocity of the solution which determines the thickness of the mass boundary layer. There is a concentration gradient in the solution, therefore, there is also a density gradient associated with it and this gradient acts in addition to the one caused by the temperature gradient driving convection. This gives rise to a different velocity of solution V' to that in the case of slow cooling. Assuming that the velocity due to thermal convection V_c and the velocity due to the density difference, V_d, are additive, then $V' = V_d + V_c$ ... 3.8

V_c is taken as $V_c = 9.0$ cm sec^{-1} as in the slow cooling case.

The calculation of V_d is as follows. Consider a spherical element of fluid radius r. Then the viscous drag on the element is $6\pi r\delta V_d$ and the upthrust on the element is $\frac{4\pi r^3}{3} \Delta\rho\bar{av}$ where $\Delta\rho av$ is the average density difference between the element and the rest of the solution and is caused by the concentration gradient only. Assuming that if the solution is in thermal equilibrium at all points then the concentration gradient is directly proportional to the temperature gradient. The density difference between an 8 mole % solution and 10 mole % solution is $\Delta\rho = 0.14$ per mole (fig. 2.15). This is equivalent in solution to a density difference of $\Delta\rho = 0.004$ C. Therefore, if $\Delta\theta$ is the temperature difference across the solution, then $\Delta\rho av = \frac{0.004\Delta\theta}{2}$. Equating the upthrust to the viscous drag on the element one obtains $V_d = r^2/4\ \Delta\theta$ using $\eta = 2.2$ cp. As the flow is turbulent, r must be less than 0.1 cm and $V_d < 0.25$ cm/sec for $\Delta\theta \doteq 20$ and the maximum temperature difference used. This is insignificant compared with V_c and $V' = V_c = 9.0$ cm sec^{-1}.

It is now possible to evaluate $Qd = 0.463\ b\ N_{Sc}^{\frac{1}{3}} \left(\frac{V}{\sqrt{r}}\right)^{\frac{1}{2}}$ (3.6)

using $b = 1.146 \times 10^{-3}$ which was calculated from equation 3.5, using

x_s = 1.2 cm and $C_s - C_o$ = 0.18 from figure 2.18; the other constants in equation (3.6) are known. Hence, it is found that Qd = 0.37×10^{-7} g cm^2 sec^{-1}, independent of the temperature gradient. Table 3.2 records the results of experiments to grow lead tantalate by the temperature gradient transport technique using a number of temperature gradients. The figures given in table 3.2 are used to give an experimental value of Qd for each temperature gradient and the results are given in table 3.3. Qd is calculated by assuming the rate of deposition of mass on the seed to be constant in time and using the final area of the crystal to calculate the mass flux per unit area per unit time into the crystal, since this corresponds nearest to a steady state condition. As the grown crystal contained many inclusions it grew with an abnormally fast growth rate, which must be divided by a factor of four to give the normal growth rate for an inclusion free crystal.

Table 3.3

The theoretical and experimental growth rates of lead tantalate from solution by the temperature gradient technique.

Temperature Gradient C cm^{-1}	Qd experimental (abnormal)	Qd (corrected)	Qd (theoretical)
5	0.313×10^{-5}	7.8×10^{-7}	0.37×10^{-7}
4	0.309×10^{-6}	7.7×10^{-7}	0.37×10^{-7}
3	1.195×10^{-7}	0.3×10^{-7}	0.37×10^{-7}

All Qd are in units of g cm^{-2} sec^{-1}.

It is noted that there is good agreement between experiment and theory for growth under a temperature gradient of 3 C cm^{-1}. The discrepancy between the other results and the theory is probably due to the error in estimating the area of the crystal. The crystals grown at temperature gradients of 5 C cm^{-1} are 4 C cm^{-1} were much larger than the 3 C cm^{-1} one and did not possess good crystal facets, and it is probable that the area

of these crystals was underestimated due to the break down of the interface to give many smaller facets, particularly on the (001) face. Thus, after allowing for experimental error, the temperature gradient transport technique results confirm that diffusion limited growth occurs.

As diffusion limited growth occurs, it is to be expected that rotating the seed crystal would decrease the boundary layer thickness and lead to more stable growth. This was not observed at the rotation rate used because the decrease in the boundary layer was too small. That this is so has been calculated in the following way. A body rotating in a semi-infinite liquid with an angular velocity w induces a velocity component in the liquid of $0.89\sqrt{\nu w}$ (3.9) at distances greater than the momentum boundary layer, where ν is the kinematic viscosity of the liquid and this velocity is directed towards the crystal (Levich 1963). This rotational component V_r is assumed to be additive to the velocity due to convection V_c. Thus, the velocity of the liquid becomes

$$V_\ell = V_c + V_r \qquad \ldots \quad 3.10.$$

For an 8 mole % solution of lead tantalate $V = 3.48 \times 10^{-3}$ and $w = 0.15\pi$ rad sec^{-1} rotation used thus from equation 3.9. $V_r = 0.032$ cm sec^{-1}. Using $V_c = 9.0$ cm^{-1} as previously, then $V_\ell = 9.032$ cm sec^{-1}. Substituting for V_ℓ in equation 3.7 a new value x_s^1 for the length of the crystal than can be grown is obtained such that $x_s^1 = 1.003\, x_s$, where x_s is the maximum length of crystal that can be grown without rotation. Thus, the use of low rotation rates produces very little increase in crystal quality, but the use of higher rates of rotation could result in better quality crystals. From equation 3.9 and 3.10 a rotation rate of 10^5 r.p.m. would have to be used to produce $x_s^1 = 2x_s$, which is roughly the desired increase in quality. This calculation is invalid, since equation 3.9 is only true if the liquid is semi-infinite and the liquid in the crucible only approximates to this at low rotation rates. As the rotation rate increases

the diffusion boundary layer diminishes and the surface diffusion controls the growth, but the transition stirring rate can only be found experimentally.

It has been demonstrated above that if the growth is diffusion limited a crystal may only be grown to a certain size. As there is an instability in the growth, crystals can only be grown to a size 1.2 x 0.3 x 0.3 cm. The diffusion limited growth process does not itself cause inclusions in the crystal, but constitutional supersaturation is present and will produce inclusions if a perturbation of the surface occurs, given that surface free energy considerations do not cause the perturbation to decay.

The first possible perturbation of the surface can be caused by local heating due to the heat of crystallisation being liberated, which may produce a very small area of the interface of sufficiently high supersaturation for a secondary nucleii to form and grow rapidly. This effect may now be calculated for a crystal measuring 1 x 1 x 1.2 cm of mass 9.8 g grown on cooling a solution through 40°C at a linear cooling rate 1.7 C per hour. The growth rate is Qd = 1·71 x 10^{-4} g sec^{-1} and the heat liberated per second is $Q_T = \frac{Qd}{M} \Delta H$ where ΔH is the heat of crystallisation per mole of solute and M is the gram molecular weight of the solute. From 2.8, ΔH = 11.8 K cal $mole^{-1}$ and therefore Q_T = 3.04 x 10^{-5} cals. If the conditions are initially isothermal Q_T will be conducted away through the crystal in amount Q_1 and through the solution in amount Q_2. Then $Q_T = Q_1 + Q_2$ ... 3.10.

Let K_1, K_2 $\left(\frac{dT}{dx}\right)_1$, $\left(\frac{dT}{dx}\right)_2$ be the thermal conductivities and temperature gradients in crystal and solution respectively. Assuming that the heat conducted through each is proportional to the thermal conductivity of that medium then

$$\frac{Q_1}{Q_2} = \frac{k_1}{k_2} \qquad \ldots 3.11$$

$$Q_1 = k_1\left(\frac{dT}{dx}\right)_1 \quad \text{and} \quad Q_2 = k_2\left(\frac{dT}{dx}\right)_2 \qquad \ldots \quad 3.12$$

Simplifying 3.10, 3.11 and 3.12 yields $\left(\frac{dT}{dx}\right)_1 = \frac{Q_T}{(k_1 + k_2)}$

and using $k_1 = 2.5 \times 10^{-2}$ cal cm^{-1} sec^{-1} C^{-1} typical for that of an ionic crystal and $k_2 = 4.0 \times 10^{-3}$ cal cm^{-1} sec^{-1} C^{-1} $\left(\frac{dT}{dx}\right)_2 = 1 \times 10^{-3}$ C cm^{-1}.

This temperature gradient will only exist in the thermal boundary layer for which the thickness is

$$\Delta x = \frac{\delta o}{N_{\rho r}^{\frac{1}{4}}} = 4.64 \left(\frac{L}{V\nu}\right)^{\frac{1}{2}} N_{\rho r}^{\frac{1}{4}}$$

All terms are defined in appendix A. Hence, for an 8 mole % solution $\Delta x = 3.41 \times 10^{-2}$ and therefore $\Delta T = 3 \times 10^{-5}$C at the surface where $\Delta T = Ti - To$, Ti being the temperature of the interface and To being the initial isothermal temperature. This temperature produces a change in concentration (from fig. 2.9) of $\Delta Co = 0.0002$ mole in the equilibrium concentration at the interface. The required concentration difference to drive the surface diffusion is 0.018 moles (from fig. 2.18). Therefore, the effect of interface heating is negligible and dissipation of heat does not form a source of instability.

The source of instability is probably a two-dimensional nucleus or a plane of high Miller indices appearing on the surface. Considering a (010) plane shown in figure 3.16(a) the distribution of supersaturation over the surface is shown.

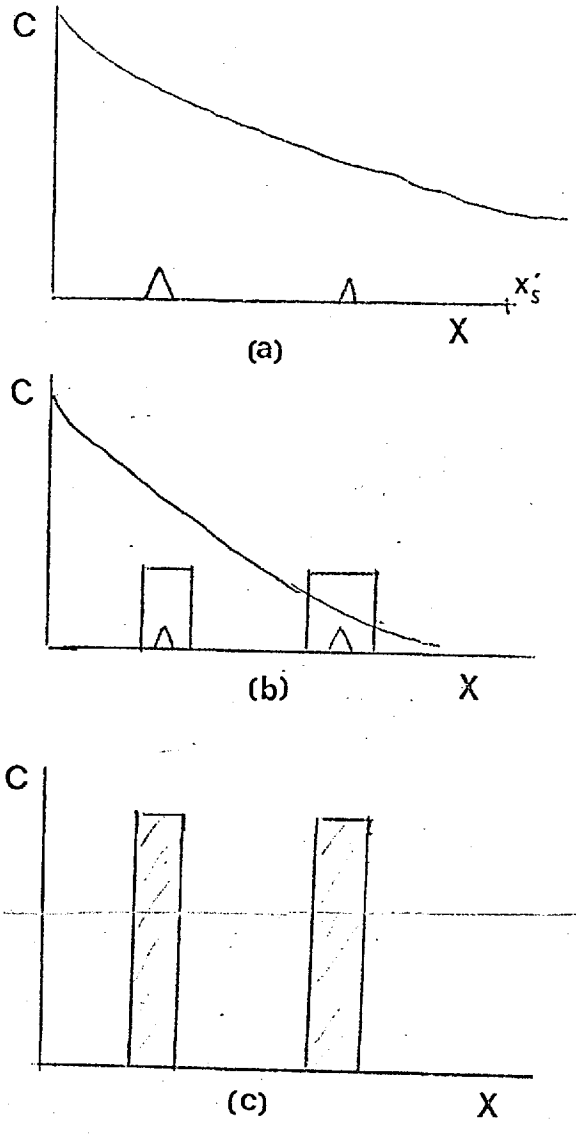

FIG. 3.16.

Suppose that a number of perturbations occur on the surface, they will grow rapidly depleting the solution in the boundary layer of solute. The solution flow can only supply enough solute to the boundary layer for one perturbation to grow 3 mm long parallel to the flow. As there are many perturbations depleting the solute, they will not grow to 3 mm long, but will grow rapidly outwards from the interface enclosing approximately a volume of solvent between them. The distance between the rapidly growing ridges will be about equal to x_s divided by the number of perturbations. The normal growth of the crystals in the [001] direction is sufficiently fast that the perturbation grows normally in that direction. A similar effect occurs on the (100) surface and consequently a pattern of inclusions is obtained as shown in figure 3.17, which is a diagramatic simplified representation of figure 3.4.

In conclusion, the growth of lead tantalate is diffusion limited with an interface instability caused by constitutional supersaturation and the combination of these factors leads to a crystal which can only be inclusion free if smaller than 0.3 x 0.3 x 1.2 cm.

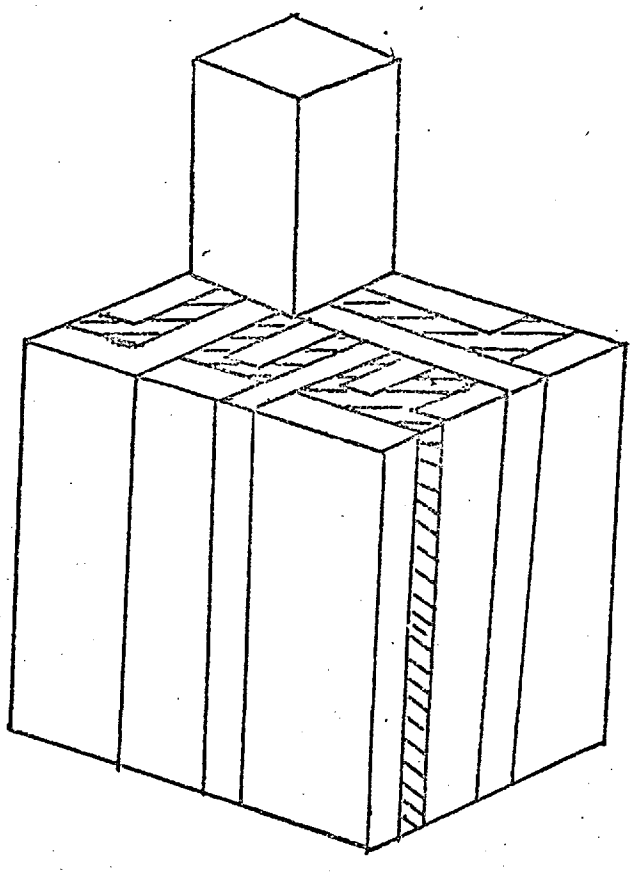

//// inclusión

FIG. 3.17.

CHAPTER IV

4. MEASUREMENT OF THE LINEAR ELECTRO-OPTIC EFFECT IN LEAD TANTALATE

4.1 The Linear Electro-Optic Effect

When an electric field is applied to a crystal there is a change in the refractive indices which is directly proportional to the applied field. The effect was first noted by F. Pockels (1893) in quartz and the effect is sometimes called the Pockels effect. The magnitude of the effect varies with the relative orientation of the electric field to the crystallographic axes of the crystal. If the crystal is isotropic initially, then under the influence of the applied electric field it becomes birefringent.

4.2 The Optical Indicatrix

Before discussing definitions of the electro-optic coefficients, the nomenclature of conventional optics must be established. A crystal can be characterised by the number of independent refractive indices it possesses. An isotropic crystal has one refractive index, a uniaxial crystal has two and a biaxial crystal has three. Whether or not a crystal is isotropic, uniaxial or biaxial is determined by the crystallographic symmetry class to which the crystal belongs. The optical properties of a crystal can be described by the optical indicatrix, which is an ellipsoid of equation:

$$a_{11}x_1^2 + a_{22}x_2^2 + a_{33}x_3^2 = 1 \qquad \ldots \quad 4.1$$

where x_1, x_2, x_3 are the principal axes of the ellipsoid and are directions in the crystal, and

$$a_{ij} = \frac{1}{n_{ij}^2}$$

where n_{ij} is the refractive index in the direction x_j of the crystal. Any

light ray propagated through the crystal is propagated in components, each of which has its electric field polarised parallel to one of the principal axes. In an isotropic crystal $a_1 = a_2 = a_3$ and the ellipsoid becomes a sphere. In a uniaxial crystal $a_1 = a_2$ and the ellipsoid is a body of resolution about the x_3 axis and possesses a circular cross section normal to it. The refractive index in the x_1 direction is called the ordinary refractive index and in the x_3 direction is called the extraordinary refractive index. Biaxial crystals have $a_1 \neq a_2 \neq a_3$ and hence there are three refractive indices.

In general, the axes of the indicatrix are not identical with the crystallographic axes. Referring the indicatrix to the crystallographic axes its equation becomes

$$a_{11}x_1^2 + a_{22}x_2^2 + a_{33}x_2^2 + 2a_{23}x_2x_3 + 2a_{13}x_1x_3 + 2a_{21}x_2x_1 = 1 \quad \ldots 4.2$$

where x_i is the crystallographic axes, $a_{ij} = \frac{1}{n_{ij}}$, where n_{ij} is the refractive index in the x_{ij} direction. The cross terms a_{ij} describe the rotation of the indicatrix relative to the crystallographic axes.

4.3 Definition of the Electro-optic Tensor

The electro-optic tensor is defined by the equation

$$\Delta a_{ij} = r_{ijk} E_k \quad \ldots 4.3$$

where Δa_{ij} is the charge in the coefficient of the optical indicatrix for the applied field, E_k, where r_{ijk} is the electro-optic coefficient. The general electro-optic tensor is a matrix of eighteen elements, but the number of independent coefficients depending on the symmetry of a particular crystal. A monoclinic crystal has all 18 independent coefficients, whereas a cubic crystal has one.

As the subscripts ij are repeated on both sides of equation 4.3,

a reduced form of notation is used. Equation 4.3 becomes

$$\Delta a_i = r_{ik} E_k \qquad \ldots 4.4$$

The convention used is that when ij = 11, then i = 1

ij = 22 i = 2

ij = 33 i = 3

ij = 23 i = 4

ij = 13 i = 5

ij = 12 i = 6

Thus, writing equation 4.4. in full:

$$\begin{pmatrix} \Delta a_1 \\ \Delta a_2 \\ \Delta a_3 \\ \Delta a_4 \\ \Delta a_5 \\ \Delta a_6 \end{pmatrix} = \begin{pmatrix} r_{11} & r_{12} & r_{13} \\ r_{21} & r_{22} & r_{23} \\ r_{31} & r_{32} & r_{33} \\ r_{41} & r_{42} & r_{43} \\ r_{51} & r_{52} & r_{53} \\ r_{61} & r_{62} & r_{63} \end{pmatrix} \begin{pmatrix} E_1 \\ E_2 \\ E_3 \end{pmatrix} \qquad \ldots 4.5$$

4.4 Change of Refractive Index with Applied Electric Field

It is not immediately apparent that equation 4.4. leads to a change in refractive index linearly dependent upon the applied electric field. Consider a field applied in the x_1 direction and a wave normal propagated in the x_3 direction; the equation of the indectrix becomes:

$$\left(\frac{1}{n_1}^2 + r_{11}E_1\right) x_1^2 + \left(\frac{1}{n_2}^2 + r_{21} E_1\right) x_2^2 + 2r_{61} E_1 x_1 x_2 = 1 \qquad \ldots 4.6$$

This is equivalent in a new indicatrix

$$\frac{x_1^2}{n^1_1} + \frac{x_2^2}{n^1_2} + 2r_{61} E_1 x_1 x_2 = 1$$

where the ^{1} indicates the refractive index with the field applied. Now $n_1^1 = (n_1 + \Delta n_1)$ where Δn_1 is the change in the refractive index n_1.

then $$\frac{1}{n_1'^2} = \frac{1}{(n_1 + \Delta n_1)^2} = \frac{1}{n_1^2} + r_{11} E_1 \qquad \ldots 4.7$$

Then, since Δn is small compared to n_1 by binomial expansion of $(n_1 + \Delta n)^2$ equation 4.5 reduces to

$$\Delta n_1 = \frac{-n_1^3 r_{11} E_1}{2} \qquad \ldots 4.8$$

Therefore, there is a change in refractive index directly proportional to the electric field. A similar relationship can be derived for Δn_2. The term $2r_{61} E_1$ is equivalent to a rotation of the indicatrix about the x_3 axis.

4.5 Electro-Optic Effects in Centrosymmetric Crystals

As noted in 4.3, the number of independent values of r_{ij} depends on the crystal symmetry. In centrosymmetric crystals all values of r_{ij} are zero. This may be seen from a consideration of equation 4.7; with the field in one direction a certain value of n_1^1 is obtained, but on reversing the field Δn_1 changes sign and a different value of n_1^1 results. This is inconsistent with the centrosymmetric requirement that the applied field should give the same refractive index in either direction of the electric field. Hence, all values of r_{ijk} must be zero. Electro-optical effects are possible in centrosymmetric materials, but the change in refractive index must be a function of even powers of the applied electric field. In this way symmetry requirements are satisfied and $\Delta n_{ij} = g_{ijk} E k^2$, where g_{ijk} is the coefficient of the second order or quadratic electro-optic effect. The quadratic effect is observed in all materials, though it is usually much weaker than the linear effect in non-centrosymmetric crystals.

4.6 Direct and Indirect Linear Electro-Optic Effect

The electro-optic coefficients can be measured experimentally

under conditions of constant stress or constant strain, which are called respectively the indirect and direct effects. The indirect arises through the addition of piezoelectric strains when the field is applied (All linear electro-optic materials must also be piezoelectric). The piezo-electric strain produces a retardation through the elasto-optic effect. The indirect effect can be greater or less than the direct effect and the latter can only be measured at high frequency or by clamping the crystal.

4.7 Electro-Optic Retardation in Birefringent Crystals

In applications of the linear electro-optic effect light polarised in two components is propagated through the crystal and the components are given a relative retardation by the electric field. Equation 4.6 was derived for light propagated along the x_3 axis and for a field in the x_1 direction, and if the wave is polarised along the x_1 axis and has frequency w it is described in the crystal by

$$A_1 \exp i \left(wt - \frac{2\pi n_1}{\lambda} x_3\right)$$

where λ_o is the wavelength in free space. The phase of the wave depends on n_1. After traversing a length of crystal, L, the change in phase, η, due to the field is $\eta = \frac{-2\pi L}{\lambda_o} \left(n_1 - n_1' \right)$

$$\eta = - \frac{n_1^3 r_{11} E_1 L}{\lambda_o} . 2\pi \qquad \ldots \quad 4.9$$

If E_1 varies sinusoidally, there is a sinusoidal variation in the phase delay.

If the incident wave is polarised at 45^o to x_1, then two equal plane polarised components are propagated at right angles. The emergent beams with $E \neq 0$ are respectively described by

$$\frac{A}{2} \exp i \left(wt - \frac{2 (n_1') x_1}{\lambda_o}\right) \qquad \ldots \quad 4.10$$

and $\frac{A}{2} \exp i\left(wt - 2\pi \frac{(n_2)'}{\lambda_o} x_2 \right)$ ... 4.11

There is a phase difference between these components and they produce a resultant eliptically polarised wave. This resultant can be described by two orthogonally polarised waves referred to any arbitrarily chosen axes. If these axes are chosen as parallel and normal to the incident direction of polarisation, the the components have amplitudes

$$A \cos \frac{\pi L}{\lambda_o} (n_1 - n_2 + \Delta n_1 - \Delta n_2) = A\cos \left(\frac{\Gamma}{2}\right)$$

and $$A \sin \frac{\pi L}{\lambda_o} (n_1 - n_2 + \Delta n_1 - \Delta n_2) = A\sin \left(\frac{\Gamma}{2}\right)$$

Respectively, where Γ is the retardation.

Considering the parallel component, if $\frac{\pi L}{\lambda} (n_1 - n_2)$ is an even multiple of $\pi/2$ the amplitude is zero except for the component due to the electro-optic effect. Using equation 4.8 for Δn the value of this component is

$$\pm \cos \frac{\pi L}{2\lambda_o} (n_2^3 r_{21} - n_1^3 r_{11}) E_1$$

which approximates to

$$1 - \tfrac{1}{2} \frac{L}{2\lambda_o} (n_2^3 r_{21} - n_1^3 r_{11}) E_1$$

Thus, the amplitude modulation is small and contains even powers of E. The same reasoning holds for the other component if $\frac{\pi L}{\lambda} (n_1 - n_2)$ is an odd value of $\pi/4$.

If $\frac{\pi L}{\lambda_o} (n_1 - n_2)$ is an odd multiple of $\pi/4$, then the amplitude for either polarisation is

$$\pm \tfrac{1}{2} \left[1 \pm 2 \sin \frac{\pi L}{2\lambda_o} (n_2^3 r_{21} - n_1^3 r_{12}) E_1\right]$$

$$\approx \frac{1}{2} \left[1 + \frac{\pi L}{\lambda_o} (n_2^3 r_{21} - n_1^3 r_{11}) E_1\right]$$

In this case the retardation is larger and is linear in E. The

condition that $\frac{\pi L}{\lambda}(n_1 - n_2)$ should be an odd multiple of $\pi/4$ is called the optical bias and is achieved either by using a compensator or by utilising the temperature dependence of the crystal's birefringence.

4.8 The Half Wave Voltage

This is a useful measure of the effectiveness of an electro-optic material in device applications. It is the voltage necessary to produce a relative retardation of the π radians between the two components propagated through the crystal. The phase difference between the two components from equations 4.10, 4.11 and 4.8 due to the applied field only is:

$$\eta = \frac{2L}{\lambda_o}(\Delta n_1 - \Delta n_2)$$

$$= \frac{\pi L}{\lambda_o}(n_2^3 r_{21} - n_1^3 r_{11}) E_1$$

If $\eta = \pi$

then $E = \frac{\lambda_o}{L}(n_2^3 r_{21} - n_1^3 r_{11})^{-1}$

If the distance between the electrodes is d, then the half wave voltage V_π is:

$$V_\pi = \lambda_o \frac{d}{L}(n_2^3 r_{21} - n_1^3 r_{11})^{-1} \qquad \ldots 4.12$$

It is desirable from a device viewpoint that V_π be as low as possible. This can be done by choosing a large value of L and a low value of d and large reductions in V_π are then possible. Limitations are imposed on this reduction by the morphology of the grown crystal. In order to quote half wave voltages in a manner independent of the crystal dimensions the half wavelength field path length product $(E.L.)_{\lambda/2}$ is used. This is the product of the field required to achieve a half wave phase difference and the path length of the light through the crystal. Thus:

$$[E.L]\ \lambda/_2 = \lambda_o (n_2^3 r_{21} - n_1^3 r_{11})^{-1} \quad \ldots \quad 4.13$$

4.9 The Dependence of the Electro-optic Coefficient on the Spontaneous Polarisation

Kurtz (1967) has given a theoretical relationship between the linear electro-optic coefficient and the spontaneous polarisation of a ferroelectric material. The refractive index in the visible region is mainly determined by the strong ultraviolet absoption band electrons. The model of the electro-optic effect uses a single electron oscillating in a potential well with an ultraviolet frequency. A small anharmonic perturbation is added to the potential. In the electro-optic effect the d.c. field E(o) is added to the driving optical electrical field E(w,t) of light wave. The equation of motion of the electron is

$$\ddot{x} + R\dot{x} + w_o^2 x + vx^2 = \frac{e}{m} E(w,t) + \beta E(o) \quad \ldots \quad 4.14$$

where R is a damping constant, w_o the electron frequency, w the light wave frequency, v the anharmonic potential, e and m the charge and mass of the electron, and β is a local field parameter. $\beta = \frac{(K+2)}{3}$ where K is the dielectric constant of the material. With no anharmonicity the applied field E(o) merely shifts the equilibrium without affecting w_o. However, using the co-ordinate transformation

$$y = \frac{x - e\beta E(o)}{mw_o^2} \quad \ldots \quad 4.15$$

in equation 4.14, which shifts the origin to a new equilibrium position, a new electron frequency is given by

$$(w_o')^2 = w_o^2 + \frac{2\ ve\ \beta E(o)}{mw_o^2}$$

This gives rise to a field dependence of the refractive index on the electric field as the refractive index varies inversely as $(w_o')^2 - w_o^2$. Solving equation 4.14 one obtains a non-linear susceptibility for

$$P_x^{NL}(w) = \chi_w^{NL}(w + o,w,o)\, E_{x(w)}E(o)$$

where $$\chi_{xxx}^{NL}(w + o,w,o) = \frac{-2\, Noe^3\beta v}{m^2D^2(w)D(o)} \qquad \ldots\ 4.16$$

where $D(w) = w_o^2 - w^2 - 2Rw$. Using the Klienmann relation $r = \frac{4\pi}{n^4}\chi_{NL}$ (Klienmann, 1962) one obtains for r after simplification of equation 4.16

$$r = \frac{(n^2 - 1)^2 \beta v}{2\pi n^4 No\, e\, w_o^2}$$

For a ferroelectric material below its Curie point the local field is augmented by the spontaneous polarisation P_s and replacing the term vx^2 in equation 4.14 by μx^3 one obtains

$$v = \frac{4\pi\, e\, N_o^{2/3} P_s}{m}$$

where $\mu = w_o^2 N_o^{2/3}$

Hence, electro-optic coefficient if given by

$$r = \frac{2}{3}\ \frac{(n^2 - 1)^2}{n^4}\ \frac{KP_s}{mN_o^{2/3}w_o^2} \qquad \ldots\ 4.18$$

4.10 The Electro-optic Tensor for m2m Crystal Symmetry

Lead Tantalate belongs to the same crystal class m2m, and Nye (1960) has given the electro-optic tensor for each crystal class which exhibits the effect. The tensor for the m2m crystal class where the axis is taken as the b axis is: (Johnston, 1969)

$$\begin{matrix} 0 & r_{12} & 0 \\ 0 & r_{22} & 0 \\ 0 & r_{32} & 0 \\ 0 & 0 & r_{43} \\ 0 & 0 & 0 \\ r_{61} & 0 & 0 \end{matrix}$$

An electro-optic effect may, therefore, be observed at in the following combinations of light and field directions:-

light in x_1	field in x_2
light in x_1	field in x_3
light in x_2	field in x_2
light in x_3	field in x_1
light in x_3	field in x_2

Thus, both a traverse effect with field and light orthogonal and a longitudinal effect with field and light parallel may be observed.

4.11 The Apparatus and Procedure for the Measurement of the d.c. Electro-Optic Coefficients in Lead Tantalate.

The apparatus used in the determination was designed and constructed by the Post Office Research Station, Dollis Hill. The apparatus is shown in figure 4.1. The apparatus records the voltage required to rotate the plane of polarisation of the incident wave through 90^{o}, i.e. the half wave voltage. The light source is a model 132 Helium Neon Laser, frequency 6328Å produced by Spectra Physics Inc., with a minimum power output of 1 milliwatt. The laser and the other optical components were mounted on a two metre optical bench. Neutral density filters were used to reduce the intensity of the laser radiation, as a safety precaution and to reduce the signal level from the detector to a suitable value for input into the photodiode amplifier. The polariser and analyser were made of polaroid mounted on rotating frames. The measurement cell is shown in figure 4.1. The electrodes are bress faced with platinum. The lower electrode is earthed. The electrodes were held in a perspex cell, which was filled with benezene to prevent electrical breakdown in the air gap between the electrodes. A quartz wedge compensator which could be adjusted with a micrometer screw was mounted after the cell and was used to correct for

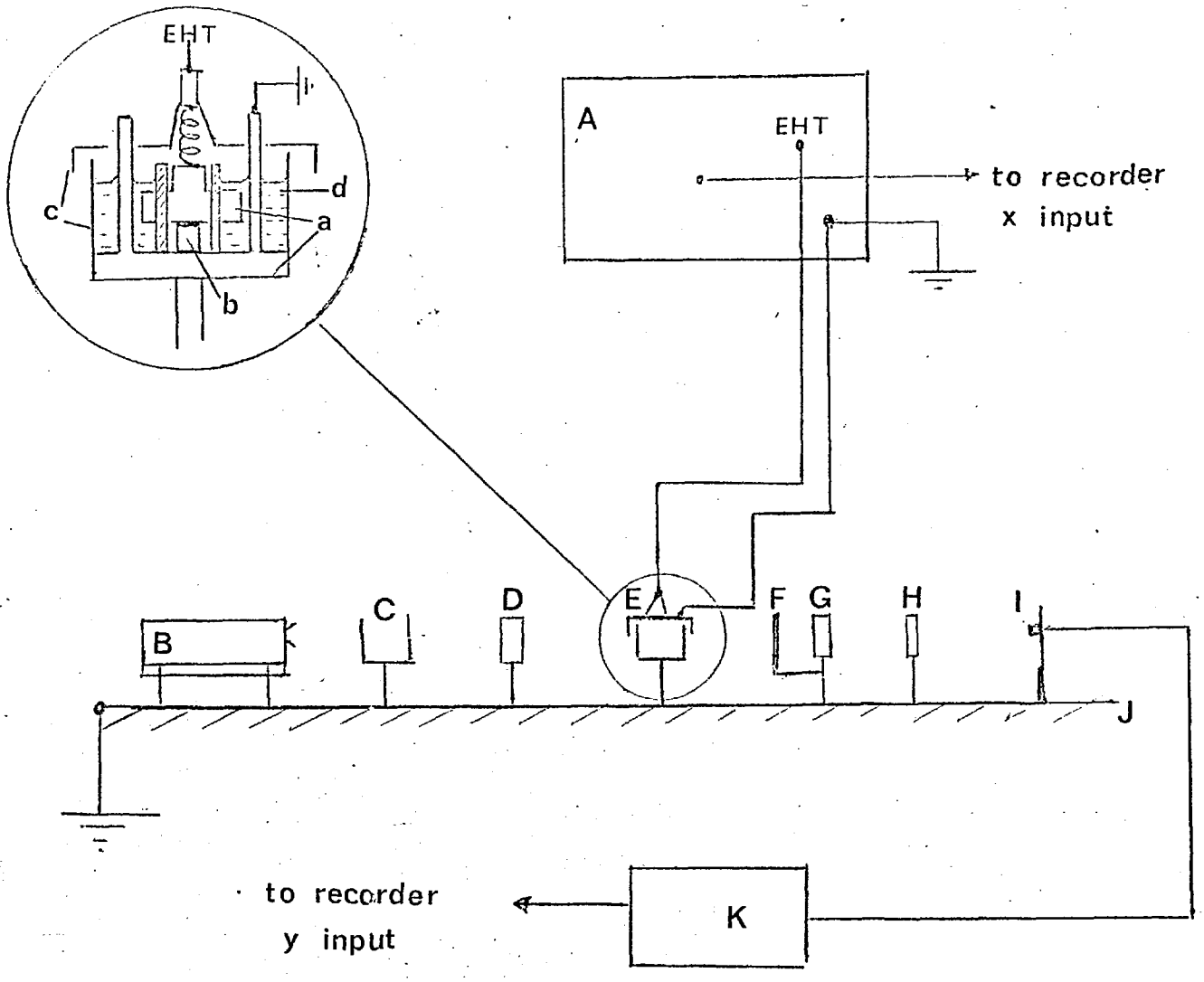

A high voltage generator

B HE-NE laser

C neutral density filter

D polarisor

E crystal holder

F compensator

G analysor

H lens

I photo-diode

J optical bench

K amplifier

a electrodes

b crystal

c perspex

d benzene

FIG. 4.1.

the crystal's natural birefringence, giving either maximum or minimum transmission. After the analyser a focussing lens is used to focus the two light rays from the crystal onto the photodiode detector. A dark paper cone was placed between the lens and the detector to eliminate any effects due to the laboratory lighting. The detector output was connected to a d.c. amplifier, which had an adjustable sensitivity. The amplifier output formed the Y input of an XY chart recorder. The high tension source used was a Brandenburg High Tension generator. The high tension line was connected to the upper electrode of the cell and the generators earth cable to the lower electrode. The voltage could be varied by a manual control. A potential divider circuit in the generator gave an output 10^{-3} of the voltage across the cell. The potential divider circuit output formed the X axis input of the XY recorder.

An electro-optic crystal was placed between the electrodes and the compensator set to give a minimum, polariser and analyser being crossed, and as the voltage was increased an increase in the transmitted light was observed, up to a maximum and the signal then decreased again to the minimum, and so on. A chart trace was recorded. A typical example is shown in figure 4.2 (a). The distance between a maximum and a minimum on the X-axis is the half wave voltage. In the linear electro-optic effect the half wave voltage will be independent of the applied voltage. However, if the crystal exhibits a quadratic effect a decrease in the half wave voltage will be noted for increasing applied voltage, giving a trace of the type shown in figure 4.2 (b).

The lead tantalate crystals used were usually of dimensions 1.5 x 1.5 x 3 mm, the longest dimension being the C axis. The [100] dimension of the crystals was usually longer than the [010] dimension. The crystals were polished on the appropriate surfaces with varying grades of diamond paste down to $\frac{1}{4}\mu$. The crystal dimensions were then

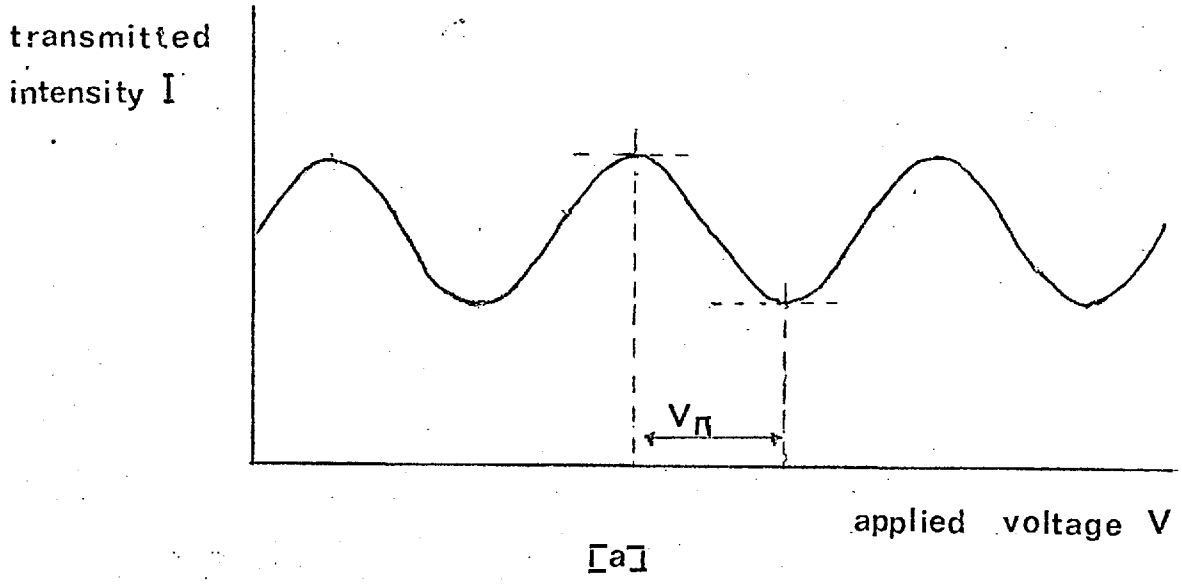

[a]

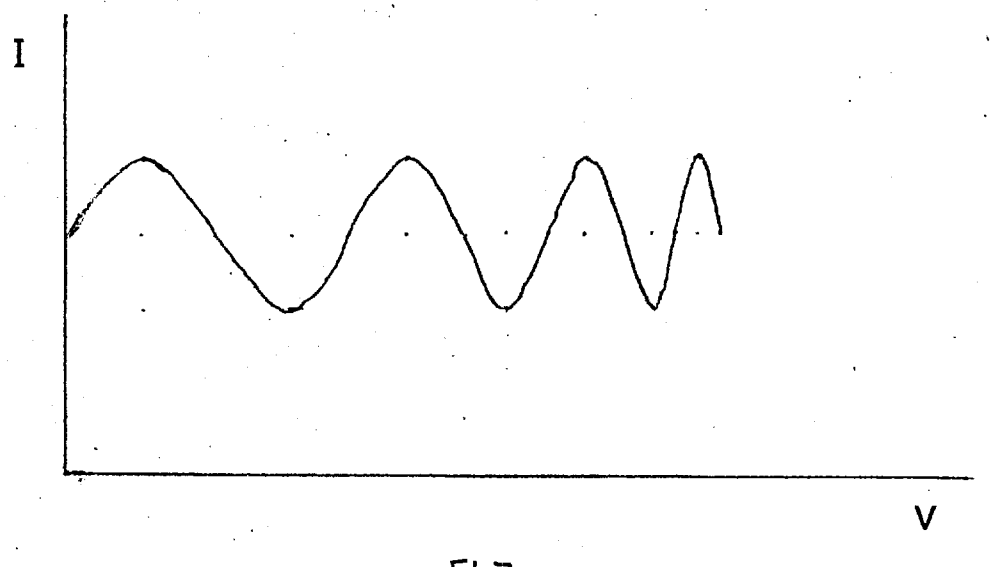

[b]

FIG. 4.2.

measured with a micrometer screw gauge. Silver dag electrodes were painted on the crystal, which was then placed on the lower electrode and aligned in the beam. The upper electrode was then placed on the crystal and the high voltage connections were made. The polariser was set at 45^{o} to the vertical and the analyser was crossed. The ordinary and extraordinary rays from the crystal were focussed with the lens onto the front of the aperture of the photodiode.

The diode was mounted 2.4 cm behind the front aperture and, therefore, the diode stand was moved forward 2.4 cm after the light had been focussed onto the aperture. Recorder and amplifier were then switched on. The compensator was adjusted to give minimum transmission and the voltage was switched on. The voltage was then increased until a series of maxima and minima were obtained. The experiment was repeated at each orientation for different positions of the beam on the same crystal and for different crystals. The calibration of the x axis of the recorder was checked using a standard potentiometer. The average half wave voltage for each orientation was found. A spread in the values of half wave voltages of about 10% of the mean was found. This was probably due to lags in the servo mechanism of the X-Y recorder, which was prone to giving an irregular response.

4.12 Results of Electro-Optic Measurements

The results of the electro-optic measurements for lead tantalate is given in Table 4.1.

Table 4.1

Half wave field path length product for each orientation of a single crystal of lead tantalate $PbTa_2O_6$ measured at $6328^{o}A$.

Table 4.1 continued

Light Direction	Field Direction 100	010	001
100	/	1.14	N.D.
010	/	u.m.	/
001	1.56	0.60	/

/ crystal symmetry indicates no effect

N.D. effect so small in cannot be measured

U.M. unable to be measured with the apparatus

Field wave products are measured in KV.

The refractive index of lead tantalate along the b axis, i.e. n_2, measured by the true and apparent depth method is 1.9 ± 0.5. Using the results in Table 4.1 and this value of n_2 in section 4.12.1. the value of r_{61} is calculated to be 1.49×10^{-8} cm/V.

The retardations due to an applied electric field in the b direction and light in the a and c directions are respectively

$$\Gamma = \frac{2\pi L}{\lambda} \left(n_1^3 r_{12} - n_2^3 r_{22} \right) E_2$$

and $$\Gamma = \frac{2\pi L}{\lambda} \left(n_3^3 r_{32} - n_2^3 r_{22} \right) E_2$$

Since in each case a very low half wave voltage is obtained, and since n_1, n_2 and n_3 are equal to the first decimal place (Subbarao, 1960) then if it may be assumed that r_{12} and r_{32} are small compared to r_{22} an approximate value of $r_{22} = 7.6 \times 10^{-7}$ cm/V is obtained from Table 4.1.

No optical damage due to laser radiation was observed.

4.12.1 The calculation of r_{51}

With light propagated in the C direction, that is with $x_3 = 0$ and with the field in the a direction, the equation of the index elipsoid becomes

$$a_1 x_1^2 + a_2 x_3^3 + 2r_{61} E_1 x_1 x_2 = 1 \qquad \ldots \quad 4.19$$

This indicates that the eliptical section normal to the x_3 axis is rotated through an angle θ as illustrated in figure 4.3. Referring the elipse to new axes x_1^1 and x_2^1 the equation of the elipse becomes

$$a_1^1 x_1^{12} + a_2^1 x_2^{12} = 1 \qquad \ldots \quad 4.20$$

where a_1^1 and a_2^1 are the new coefficients due to the distortion of the elipse by the applied field. Since the axes x_1^1 and x_2^1 are rotated by an angle from the axes x_1 and x_2 the following relationship holds between them. (See figure 4.4)

$$x_1 = \alpha_1 x_1^1 + \beta_1 x_2^1 \qquad \ldots \quad 4.21$$

$$x_2 = \alpha_2 x_1^1 + \beta_2 x_2^1 \qquad \ldots \quad 4.22$$

where α_1, α_2, β_1, β_2 are the direction cosines of the angles between the axes. From figure 4.4

$$\alpha_1 = -\beta_2 \qquad \ldots \quad 4.23$$

and $$\alpha_2 = \beta_1 \qquad \ldots \quad 4.24$$

Substitute for β_1 and β_2 from equations 4.23 and 4.24 in equations 4.21 and 4.22 and then, substituting for x_1 and x_2 in equation 4.19 one obtains

$$x_1^{12} (a_1\alpha_1^2 + a_2\alpha_2^2 + 2r_{61}E_1\alpha_1\alpha_2) + x_2^1 (a_1\alpha_2^2 + a_2\alpha_1^2 - 2r_{61}E_1\alpha_1\alpha_2)$$

$$+ 2r_{61}E_1(\alpha_1^2 - \alpha_2^2 + \alpha_1\alpha_2 \; a_2 - a_1 \;) \; x_1^1 x_2^1 = 1 \qquad \ldots \quad 4.25$$

$a_2 - a_1$ is small compared with unity and, therefore, this term may be neglected in the calculation of α_1. Equations 4.25 and 4.20 are identical and therefore

$$2r_{61}E_1 (\alpha_1^2 - \alpha_2^2) = 0 \qquad \ldots \quad 4.26$$

since there are no $x_1^1 x_2^1$ in equation 4.20.

Therefore $\alpha_1 = \pm \alpha_2$ and from figure 4.3 $\alpha_1 = \cos\theta$ and $\alpha_2 = \sin\theta$, hence $\theta = \pm 45^\circ$ $\qquad \ldots \quad 4.27$

Thus, there is a rotation of the optical indicatrix about the c axis of 45°

when the field is applied, but independent of the magnitude of the field. This solution is only approximate, since if $\alpha_1 = \alpha_2$ exactly the elipse becomes a circle and no electro-optic retardation is possible. Hence $\alpha_1\alpha_2(a_2 - a_1)$ is important in determining the electro-optic properties of the crystal. Since there is a rotation of very nearly 45 degrees and as the polariser had been set at 45° to the initial indicatrix, the amplitudes of the two transmitted components are no longer equal. Hence, total extinction will not be obtained at minima of transmitted intensity. To calculate the retardation the new indicatrix with the field applied is used, the retardation Γ being given by

$$\Gamma = \frac{2\pi L}{\lambda}\left(\frac{1}{\sqrt{a_1}^1} - \frac{1}{\sqrt{a_2}^1}\right) \qquad \ldots \quad 4.28$$

Using $\alpha_1 = \alpha_2 = \theta^1/\sqrt{2}$ in equation 4.25, and letting $a_1 + a_2 = a$, then

$$\Gamma = \frac{2\pi L}{\lambda}\quad\frac{-r_{61}E_1}{a^{\frac{3}{2}}} = -\frac{2\pi}{\lambda}\, n_\alpha^3\, r_{61}\, E_1 \qquad \ldots \quad 4.29$$

where it is assumed that $a^1 >> (r_{61}E_1)$, $a = \frac{1}{n_\alpha^2}$,

From Table 4.1, when L = 1cm and E_1 = 1.56 KV/cm, $\Gamma = \pi$ at $\lambda = 6328^\circ$A, then $r_{61} = 3.$ x 10^{-9} cm/V.

4.13 Discussion of Results

Equation 4.18 gives the electro-optic coefficient in terms of the spontaneous polarisation, dielectric constant and refractive index. Using a value of $P_s = 8 \times 10^{-6}$ coul. cm^{-2}, K = 700 (Subbarao, 1960) and approximate values of $n_o = 1.9 \times 10^{23}$ and $w = 2.5\pi \times 10^{15}$ (Wemple, 1969) (~~Kurtz, 1967~~) and me = 9.1 x 10^{-28} grm, then r = 4. x 10^{-9} cm/Volt. This agrees well with the value $r_{61} = 3.$ x 10^{-9} cm/Volt measured for lead tantalate. The value of r_{22} is larger than this. This is probably due to an enhanced biasing of

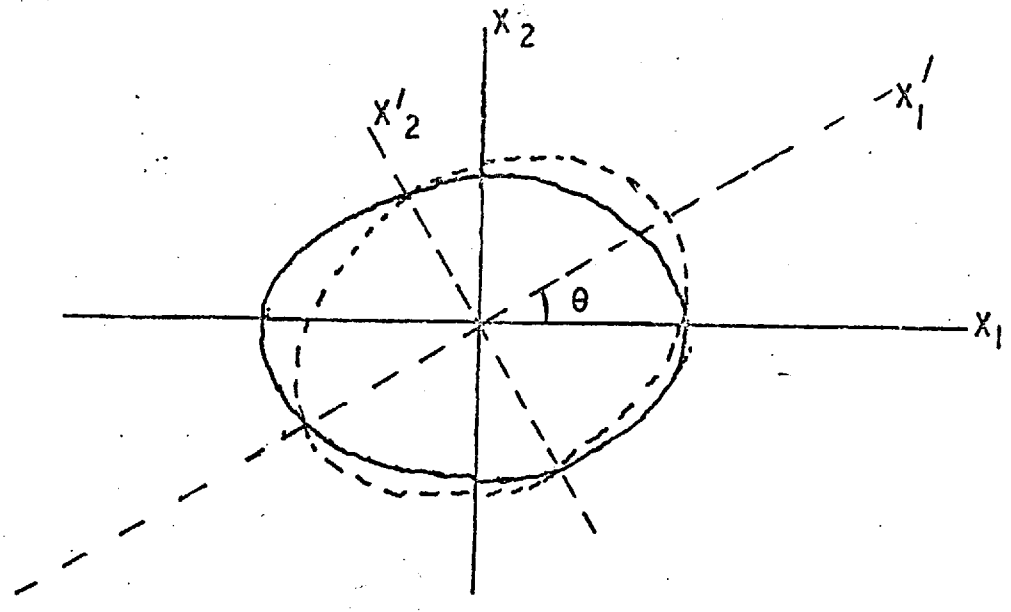

FIG. 4. 3.

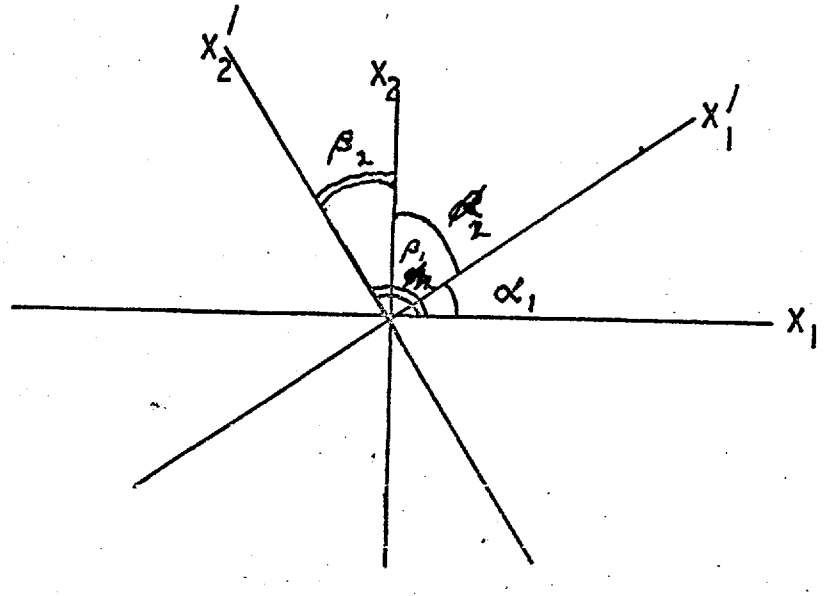

FIG. 4.4.

the quadratic effect when applied electric field and spontaneously polarisation are parallel. That no effect determined by the r_{43} term could be detected from the apparatus is to be expected from the prediction by Miller (1964) that the dielectric constant and hence the electro-optic constant is an order of magnitude less for the c direction than for the a or b.

CHAPTER V

5.0 THE STRUCTURAL AND DIELECTRIC PROPERTIES OF THE TUNGSTEN BRONZE $Pb_6Ti_2Nb_8O_{30}$ FOR VARYING TITANIUM:NIOBIUM RATIOS

5.1 Reasons for the Investigation of $Pb_2Ti_2Nb_8O_{30}$ Type Material

The general formula for a filled tungsten bronze structure material is $(A^1)_2\ (A^2)_4\ (C^1)\ (B^1)_2\ (B^2)_8\ O_{30}$ where A^1 and A^2 are slightly differing sites and are occupied by monovalent or divalent ions. The B sites are occupied by tetravalent or pentavalent ions. The C site is a small one which can accommodate only small monovalent ions such as lithium and for most materials the C site is vacant. Within the requirement of the general formula materials have been investigated which form five distinct groups, which are classified by the valencies of the ions in the structure. The groups are:-

(1) $A_5\ B_{10}\ O_{30}$ e.g. $PbTa_2O_6$, $Ba_{0.5}\ Sr_{0.5}\ Nb_2O_6$

(2) $A_4^{2+}\ A_2^{+}\ B_{10}\ O_{30}$ e.g. $Ba_2NaNb_5O_{15}$

(3) $A_6^{+}\ C_4^{+}\ B_{10}\ O_{30}$ e.g. $K_6Li_4Nb_{10}O_{30}$

(4) $A^{2+}O\ xB_2O_5$ $\quad 1 \leq x \leq 2.5$ e.g. $PbO - 2.5\ Nb_2O_5$

(5) $A_2^{2+}\ A_4^{2+}\ B_2^{4+}\ B_8^{5+}\ O_{30}$ e.g. $Ba_6Ti_2Nb_8O_{30}$

Mant investigations have been carried out on materials in groups (1) to (4). The only investigation of group 5 materials has been the X-ray study of $Ba_6Ti_2Nb_8O_{30}$ by Stephenson (1965), who concluded that ferroelectricity was probable in this structure. As lead is a more highly polarisable ion, a requirement of ferroelectric materials, than barium, the material $Pb_6Ti_2Nb_8O_{30}$ should also be ferroelectric. If the titanium-niobium ratio is varied, then the Curie point of the material should also vary because of the different numbers of Ti-O and Nb-O bonds which possess different polarisations. In order to vary this ratio a charge compensating ion must be added. Burns (1968) has shown that the addition of lanthanum to a

ferroelectric tungsten bronze reduces its Curie temperature. This is desirable as Miller's rule has established that the dielectric constant is directly proportional to the electro-optic coefficient. When measured near the Curie point of a material where the dielectric constant is large the half wave voltage will be low. Thus, it should be possible to synthesize a material of tungsten bronze structure with suitable dielectric and electro-optic properties.

This investigation was undertaken as a secondary project in order to evaluate the fifth group of tungsten bronze structures as a source of possible electro-optic materials.

5.2 X-ray Analysis of the Materials

The specimens for analysis by the X-ray powder diffraction technique were prepared by firing the appropriate mixtures of the constituent oxides. A charge of 25 grms was weighed out, mixed with 10 cm^3 of distilled water and placed in a ball mill. The charge was milled for sixteen hours, then filtered and dried. Approximately one gram of material was then placed on a platinum sheet and heated in an oxy-hydrogen flame until molten. The molten charge was allowed to cool, ground with a pestle and mortar and then refired. This process was repeated several times. The final product was then examined by Debye-Scherrer powder diffraction technique. Figures 5.1(a) and 5.1(b) show the results. To simplify identification, a standard specimen of lead niobate $PbNb_2O_6$ was similarly prepared, yielding the ferroelectric orthorhombic tungsten bronze structure which was identified by comparing the d spacings with those given in the ASTM index. The lead-rich members of the series were found to have structures similar to that of lead niobate. For compounds containing less lead than $Pb_3La_3Ti_5Nb_5O_{30}$ a different structure was obtained as seen in figures 5.1(a) and 5.1(b). Few lines were visible for these compounds, and the structure

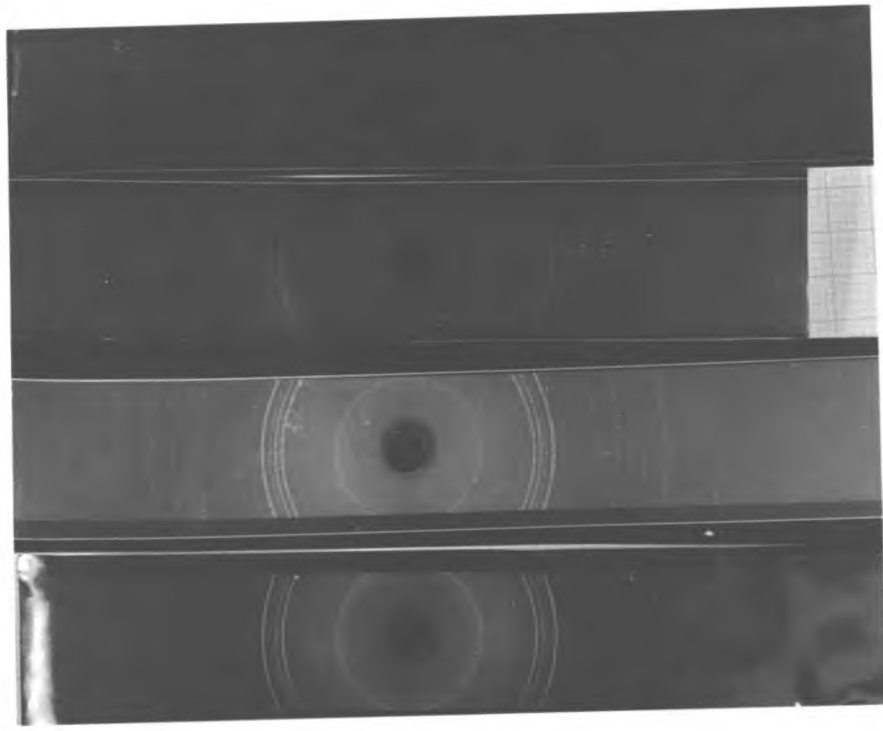
$PbNb_2O_6$
$Pb_6Ti_2Nb_8O_{30}$
$Pb_5LaTi_3Nb_7O_{30}$
$Pb_4La_2Ti_4Nb_6O_{30}$

(a)

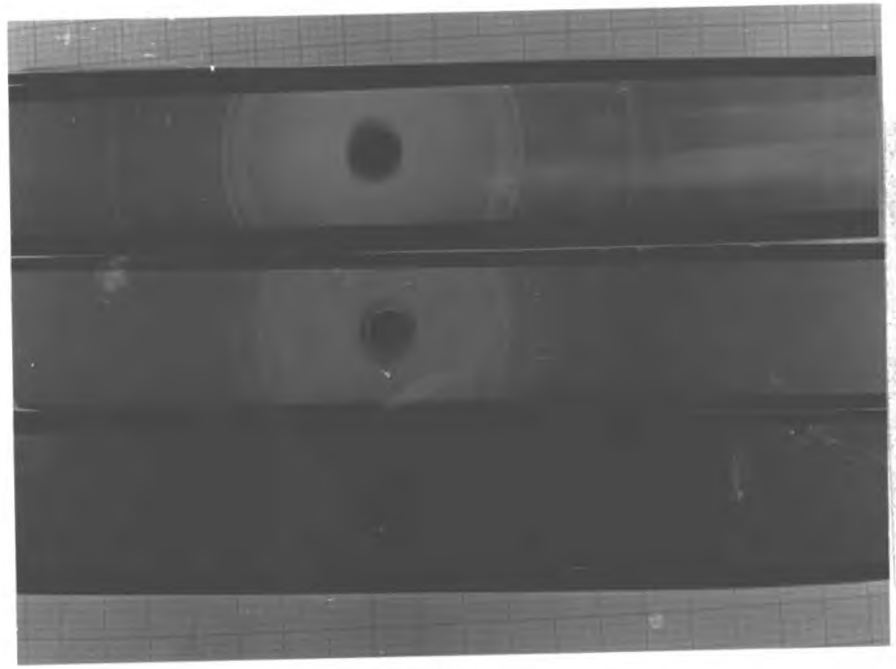
$Pb_3La_3Ti_5Nb_5O_{30}$
$PbLa_5Ti_7Nb_3O_{30}$
$La_6Ti_8Nb_2O_{30}$

(b)

FIG. 5.1.

could not be identified by comparison with known materials. No unreacted components were present, nor were any known binary combinations of them.

5.3 The Structure of the $Pb_6Ti_2Nb_8O_{30}$ Series

The d spacings of each of the first five strong lines for each X-ray photograph was calculated from the measurement of the diameter of each line on the photograph. No correction was made for film shrinkage, as only the low angle lines, which are the least accurate, were visible on the film. The index of each line was deduced by comparison with the standard lead niobate photograph, and using the d spacings given by Roth (1957). The lattice spacings measured in Angstroms for each composition are given in Table 5.1.

Table 5.1

The lattice spacings of the first five strongest lines in $Pb_6Ti_2Nb_8O_{30}$. type materials.

$Pb_6Ti_2Nb_8O_{30}$	$Pb_5LaTi_3Nb_7O_{30}$	$Pb_4La_2Ti_4Nb_6O_{30}$	$PbLa_5Ti_7Nb_3O_{30}$	$La_6Nb_2Ti_8O_{30}$	(h.k.l)
3.440	3.187	3.173	3.43	3.413	150
2.941	3.030	3.001	3.232	3.307	131
2.848	2.911	2.905	2.930	2.995	440
2.700	2.756	2.756	2.689	2.757	350
2.548	2.582	2.573			060

As ceramic discs were used as the source material the lines on the photograph were broadened due to the compositional variations typically found in specimens prepared in this way. Because of this doublets, due to the orthorhombic structural deformation, were not resolved for lead niobate or for any of the other materials. Hence, it was necessary to use a tetragonal cell to calculate the lattice parameters. There was insufficient

evidence to decide if in fact their structure was orthorhombic or tetragonal. The lattice parameters were calculated for each material and are shown in figure 5.2. The series appears to divide into two parts with a phase boundary near the composition $Pb_3La_3Ti_5Nb_5O_3O$. Little change is observed in the c parameter on varying the Ti:Nb ratio. This may be expected, since the O-Ti and O-Nb bonds are of similar lengths in tungsten bronze materials (Stephenson (1965); Jamieson, (1968)). The a parameters are smaller than for $PbNb_2O_6$, which is consistent with the smaller diameter of La compared with Pb.

5.4 Determination of the Melting Point as a Function of Composition

In order to prepare ceramic discs for dielectric studies the melting point of each composition was determined using a Griffin and George Hot Stage Microscope. The heating element was a platinum 5% rhodium/ platinum 20% rhodium thermocouple junction. The element was heated by a chopped electric current which allowed the thermocouple temperature to be monitored in between the heating pulses. The temperature of the thermocouple could be set manually and its value was displayed on an accurately calibrated scale.

To determine the melting point of each specimen a small amount of material was placed on the thermocouple, which was then clamped in position on the microscope. The thermocouple temperature was increased until the material became molten. The temperature was then decreased to solidify the material. Again, the temperature was increased and the melting point was then taken as the temperature at which the solid material was in equilibrium with its liquid. The initial melting of the material was necessary to ensure complete reaction of the oxides. The measurement of melting point was performed several times for each composition and the average taken. The melting point as a function of temperature is shown in

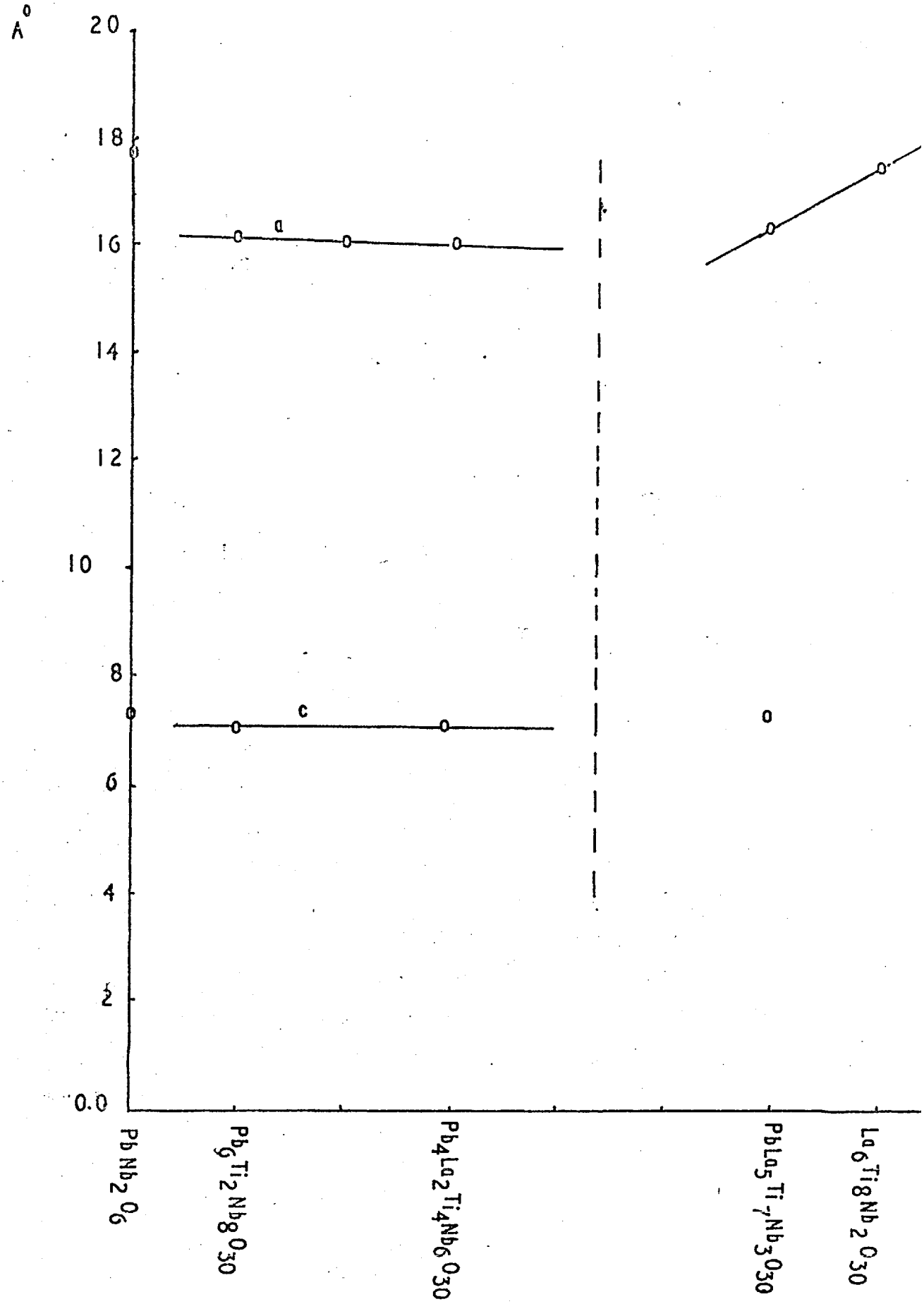

FIG. 5.2. THE LATTICE PARAMETERS OF $Pb_6 Ti_2 Nb_8 O_{30}$ TYPE MATERIALS

figure 5.3.

5.5 Preparation of Ceramic Discs

Sintered discs of each composition were fired in the following manner. About 2g of material was placed in a 1 cm internal diameter cylindrical die and hydraulically pressed at three tons indicated pressure. The disc was then removed and the die cleaned to remove material adhering to the sides. The discs were fired initially for sixteen hours at a temperature 0.6 Tm, where Tm was the melting temperature. The firing temperature was then increased subsequently until a dense, impervious disc was obtained. The weight loss on sintering was in all cases less than 2%. Table 5.2 gives the firing temperature for each disc. A number of discs of each composition were fired at a time. One disc was crushed and examined by the X-ray powder photography to ensure the correct phase had formed.

Table 5.2

The firing temperature for sintering $Pb_6Ti_2Nb_8O_{30}$ type materials.

Material	Firing temperature
$Pb_6Ti_2Nb_8O_{30}$	1160°C
$Pb_5LaTi_3Nb_7O_{30}$	1180°C
$Pb_3La_3Ti_5Nb_5O_{30}$	1200°C
$PbLa_5Ti_7Nb_3O_{30}$	1220°C
$La_6Ti_8Nb_2O_{30}$	1240°C

5.6 Measurement of the Dielectric Constant as a Function of Temperature

The dielectric constant was determined using a capacitance bridge technique. Dielectric anomalies indicating ferroelectricity were found in

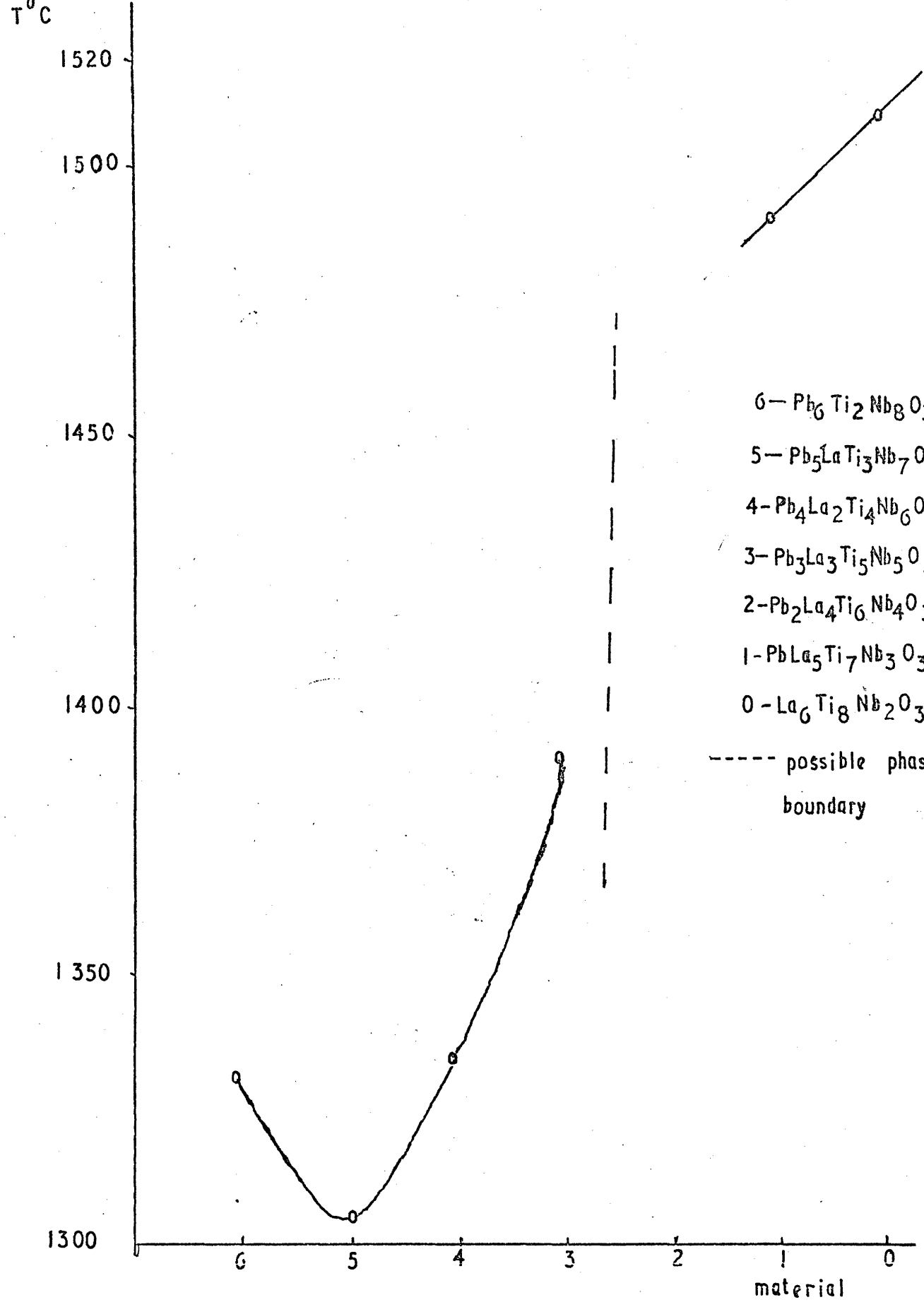

FIG. 5.3. THE GRAPH OF THE MELTING POINTS OF $Pb_6Ti_2Nb_8O_{30}$ — TYPE MATERIALS.

materials that were lead rich. No anomalies were found in materials with lead contents less than $Pb_3La_3Ti_5Nb_7O_{30}$.

The results showed a weak anomaly at 670°C for $Pb_6Ti_2Nb_8O_{30}$, a reproducible large anomaly at 375°C for $Pb_5LaTi_3Nb_7O_{30}$ and evidence of an anomaly below room temperature for $Pb_3La_3Ti_3Nb_7O_{30}$.

With the exception of $Pb_5LaTi_3Nb_7O_{30}$ a wide variation in results was observed for different discs of the same material. This was probably due to an imcomplete reaction of the oxides and the difficulty of achieving a uniform composition for such complex materials. However, the fact that no ferroelectric behaviour was found for lanthanum rich members of the series is consistent with the observation that these materials did not possess the ferroelectric lead niobate structure. To confirm the existence of ferroelectricity it was clearly necessary to prepare single crystals of the lead rich members of the series.

5.7 The Growth of Single Crystals

From the dielectric study the material $Pb_5LaTi_3Nb_7O_{30}$ exhibited the most sharp dielectric anomaly. As it had a melting point of 1305°C and appeared to melt coherently, it was capable of preparation as single crystals by the Czochralski technique. However, when molten, the material rapidly lost lead oxide by evaporation. An attempt to encapsulate the melt by floating boric oxide, B_2O_3, on the surface was made to suppress the evaporative loss of PbO - undesirable because of its toxicity and because of the change in melt composition. This attempt was unsuccessful, as lead oxide diffused into the boric oxide layer, which then mixed with the melt within a period of about an hour, after which lead oxide was again evolved. No satisfactory method of overcoming this problem was found, and the Czochralski technique was discarded as being unsuitable for the preparation of lead rich members of the series.

The high temperature solution technique was then employed, as this offers the advantage that the growth could be carried out at a constant temperature by evaporation of the solvent. With such complex materials, temperature variations would not only result in a variation in the crystal composition, but might also lead to the precipitation of secondary phases within the crystal. The problem was to find a volatile solvent which did not react irreversibly with the solute. In order to test the solvent a trial run was carried out in a 30ml platinum crucible using a solute solvent ratio of 1:5 by weight. The first two solvents to be used were lead fluoride and lead oxide. Both precipitated an unwanted pyrochlore type phase, rich in lead oxide. The next solvents tried were molybdenum triodixe, lithium molybdate $Li_2Mo_2O_7$ and lithium molybdate, Li_2MoO_4. The first two of these precipitated lead molybdate over a wide range of compositions and solution temperatures. Using Li_2MoO_4 as solvent, a mixture of lead molybdate and the desired tungsten bronze phase was precipitated. However, the results were inconsistent, as seen when an experiment was repeated, additional phases were present and the tungsten bronze phase absent. In order to obtain a more easily reproducible system the slow cooling technique with a non-volatile solvent was used. The solvent used was potassium carbonate and the tungsten bronze phase was precipitated. However, a pyrochlore phase was also present in the crystals and sometimes only this phase formed. The temperature and composition at which the pyrochlore phase formed could not be determined from the experimental results as the solution was cooled over a range of temperatures.

Thus, there appeared to be two problems in the preparation of $Pb_5LaTi_3Nb_7O_{30}$ from solution. One is the reaction of the component oxides with the solvent, and the other the phase change from tungsten bronze to pyrochlore structure. The first problem may be overcome by a series of trial and error experiments with possible solvents. The second may be

overcome by a study of the phase diagram of the $PbO-La_2O_3-TiO_2$ Nb_2O_5 system. A protracted series of tedious experiments is, therefore, necessary before single crystals can be prepared. As this study was undertaken as a topic of secondary interested, extended work of this kind could not be undertaken and the investigation ended.

5.8 Conclusion

From the structural and dielectric evidence, the series divides into two parts, each possessing differing structure and properties. The lead rich part is ferroelectric and possesses a structure very like the orthorhombic tungsten bronze structure. There is no evidence for ferroelectricity in the lanthanum-rich part and the structure is not tungsten bronze. The phenomenon of two structural types in a series of solid solutions of varying composition has been previously observed by Subbarao (1960), who studied the systems $Pb(Ta,Nb)_2O_6$, $(Pb,Ba)Nb_2O_6$ and $(Pb,Sr)Nb_2O_6$. In each case two different structural groups were found with structures similar to the end members.

CHAPTER VI

6. CONCLUSIONS AND FUTURE WORK

6.1 The Growth of Single Crystals of Lead Tantalate

The control of the growth of optical quality single crystals is the principal barrier to the development of new and improved non-linear optical materials. The high quality of crystals obtainable from high temperature solution growth makes this an attractive technique for the preparation of optical materials, but very little work of a fundamental nature has been directed to the study of either the properties of high temperature solutions or the mechanism of crystal growth by this technique. In the present work a systematic investigation of the properties of lead tantalate solutions has been made. It has been shown that the variables which determine the principal mechanisms in crystal growth can be measured, and in particular the thermobalance has been used effectively for the solubility and diffusivity measurements. Density, viscosity and heat capacity of the solution have been measured by conventional techniques.

The theoretical model for estimating solubilities proposed by Cobb (1969) has been tested with the experimentally measured solubilities. Good agreement was obtained for lead tantalate dissolved in lead vanadate, $Pb_2V_2O_7$, but the theory had only a poor predictive value where there was interaction between solvent and solute as for solutions in bismuth borate and PbV_2O_6.

The measurement of solution properties made possible the growth of single crystals of lead tantalate by controlled nucleation on a single seed. In this was a crystal 1 x 1 x 1 cm could be grown. However, the crystals were of very poor quality even when the optimum slow cooling programme was used. The crystal growth was found to be diffusion limited and this led to instability of the interface due to constitutional supersaturation. The effect of local heating of the interface by the liberated heat of crystallisation

was found to be negligible. It was deduced that the maximum size of good quality crystal that could be grown under diffusion limited conditions was 1.0 x 0.3 x 0.3 cm. It was found that rotating the seed crystal marginally improved the quality of the grown crystal and it was deduced that higher rotation rates would further improve crystal quality.

The crystal gorwth experiments were successful in producing crystals of good optical quality with dimensions 4 x 2 x 1 mm which were suitable for electro-optic measurement.

6.2 The Measurement of the Transverse Linear Electro-Optic Effect in Lead Tantalate

Lead tantalate possesses a large transverse electro-optic effect for light propagated in the [001] direction and the field applied in the [010] direction, the half wave voltage being 600V for a cube of material. An approximate value of $r_{22} = 7.2 \times 10^{-7}$ cm V^{-1} and a measured value of $r_{61} = .3 \times 10^{-9}$ cm V^{-1} were determined. Good agreement was found between this value of r_{61} and that given theoretically by Kurtz (1967). Its low half wave voltage makes lead tantalate a promising material for device applications. A crystal of dimensions 1.2 x 0.3 x 0.3 cm, that is the largest that could be grown using the apparatus in this study, would possess a half wave voltage of 150V which may be generated in standard electronic circuits.

6.3 Properties of $Pb_6Ti_2Nb_8O_{30}$ Type Materials

The series of compounds based on $Pb_6Ti_2Nb_8O_{30}$ was shown to possess tungsten bronze structures in either the orthorhombic or tetragonal form. The series exhibited a typical phenomenon of tungsten bronze solid solutions in dividing into two structural types, the lead rich being ferroelectric, and the lanthanum rich, non-ferroelectric. An adequate method of growing

single crystals was not found due to the high volatility of lead oxide, the reactive nature of the component oxides with common high temperature solvents and the formation of a pyrochlore phase at certain temperatures.

FUTURE WORK

6.4 The Growth of Lead Tantalate and its Non-Linear Optical Properties

As lead tantalate is a good electro-optic material it may be expected to strongly exhibit other non-linear electro-optic phenomena. In particular, it should be a good source for second harmonic generation as it should possess a large coefficient of second harmonic generation and it should exhibit non-critical phase metching due to its tungsten bronze structure. A measurement of its S.H.G. coefficients should, therefore, be valuable.

It is desirable to grow larger crystals of lead tantalate than those obtained in this study. A possible method is to 'pull' the crystal from high temperature solution as described by Elwell (1968), in the growth of nickle ferrite crystals. This method has the advantage that growth occurs in one direction. Thus, growth could be achieved in the [001] direction with only a small growth rate in directions normal to it. This corresponds to the normal growth, which is anisotropic for lead tantalate. The slow growth rates used would enhance the stability of the interface to constitutional supersaturation (Mullin, 1964). In addition, the rotation of the crystal necessary in this technique would increase the crystal quality as predicted in section 3.3.

REFERENCES

Bardsley, W., Callan, J. M., Chedzey, H. A. Hurle, O. J. T., Solid State Elect. 3, 142, (1961)

Becker, R., Doring, W., Ann. Phys. 24, 552 (1935)

Bennema, P., Thesis (Ph.D) Tech. Univ. of Delft, 1965

Bergman, J. G., Kurtz, S. K., Mat. Sci. Eng., 5, 235, (1970).

Billings, B. H., J. Opt. Soc. Am., 39, 797, (1949)

Bloembergen, N., Non-Linear Optics, W. A. Benjamin, New York, (1965)

Bloom, H., Chemistry of Molten Salts. W. A. Benjamin (1967)

Bockris, J. O'M., White, J. L., Mackenzie, J. D., Physicochemical Measurements at High Temperatures, Butterworths, (1959)

Brice, J. C. (I), J. Cryst. Growth I, 218, (1967)

Brice, J. C. (II), ibid. I, 161, (1967)

Brice, J. C. ibid. 6, 9, (1969)

Burns, G., D. F. O'Kane, Geiss, E. A., Scott, B. A., Solid. Stat. Comm. 6 223, (1968)

Burton, W. K., Cabrera, N., Frank, F. C., Phil. Trans. A243, 299, (1951)

Carlson, A., Growth and Perfection of Crystals, p. 421., John Wiley (1958)

Chen, see Bockris (1959)

Cobb, C. M., Wallis, E. B., Final Report AFCRL-67-0196, 1967

Cobb, C. M., Wallis, E. B., Final Report AFCRL-69-0126, 1969

Elwell, D., Smith, S. H., J. Mat. Sci., 2, 297, 1967;

Elwell, D., Smith, S. H., J. Cryst. Growth, 3, 4, 471, 1968.

Elwell, D., To be published (1970).

Emmenegger, F., Nitsche, R., Miller, A., J. Appl. Phys. 39, 3039, 1968

Fawsitt, Proc. Roy. Soc. A80, 290, (1908)

Francombe, M. H., Lewis, B., Acta. Cryst. 11, 696, 1958)

Frank, F. C., Dis. Faraday Soc., 5, 48, (1949)

Garrett, C. G. B., IEEE, J. QE, 4, 70, (1968)

Geiss, E. A., Burns, G. B., O'Kane, D. F., Smith, A. W., Appl. Phys. Lett, 11, 233, (1967)

Geusic, J. E., Levinstein, H. J., Rubin, J. I., Singh, S., van Uitert, L. G., Appl. Phys. Lett. 11, 269, (1967)

Goldstein, S., Modern Developments in Fluid Mechanics, O.U.P., (1950)

Hahn, R. B., Webster, F. J., Inorganic Qualitative Analysis, van Nostrand, New York, (1963)

Hill, V. G., Harker, R. I., J. Electrochem. Soc., 113, 1333, (1966)

Hurle, D. J. T., Solid. Stat. Elec. 3, 37, (1961)

Ismailzade, I. G., Sov. Phys. (Cryst), 4, 518, (1959)

Ismailzade, I. G., Ibid, 10, 535, (1966)

Jakob, M., Heat Transfer, John Wiley, New York, (1953);

Jamieson, P. B., Abraham, S. C., Bernstein, J. L., J. Chem. Phys. 48, 5048, (1968)

Janz, G. J., Molten Salts Handbook, Academic Press, New York, (1967)

Johnston, A. A., Appl. Phys. Lett., 7, 195, (1965)
Johnston. A.R. Nakamura. T. J. Appl. Phys. 40. 3656. (1969).
Kaminow, I. P., Turner, E. H., Procc. IEEE 55, 1374, (1966)

Kaminow, I. P., Johnston, W. D., Phys. Rev. 160, 518, (1967)

Kaye, G. W., Laby, G. H., Physical & Chemical Tables, Longmans Green, London, 1959

Kelly, R. L., Phys. Rev. 151, 721, (1966)

Kleinman, D. A., Phys. Rev. 126, 1977 (1962)

Knudsen, J. G., Katz, D. L., Fluid Dynamics and Heat Transfer, McGraw Hill (1958)

Kohman, G. T., Art and Science of Growing Crystals, ed. J. J. Gilman, John Wiley, (1963)

Kurtz, S. K., Robinson, F. N. H., Appl. Phys. Lett, 10, 62, (1967)

Laudise, R. A., see Kohman (1963)

Levich, V. G., Physicochemical Hydrodynamics, Prentice Hall (1962)

Mackenzie, J. D., see Bockris, (1959)

Miller, R. C., Appl. Phys. Lett, 5, 17 (1964)

Mullins, W. W., Serkerka, R. F., J. Appl. Phys. 34, 323, (1963)

Nernst, W., Z. Phys. Chem. 47, 52 (1904)

Nye, J. F., Physical Properties of Crystals, OUP, London, (1960)

Pockels, F., Abhandhungen der Geseilschaft der Wissenchaften, zu Gottingen, 39, 1, (1893)

Pockels, F., Lehrbuch der Kristalloptik Leipzig (1906)

Roth, . Acta. Cryst. 10, 437, (1957)

Roy, R., White, W. B., J. Cryst, Growth, 3,4,33 (1968)

Rubin, J. I., van Uitert, L. G. Levinstein, H. O. J., J. Cryst. Growth 1, 315, (1967)

Smolenskii, G. A., Agranovskaya, A. I. Sokl. Acad. Nauk, SSR, 97, 237, 1954

Spencer, E. G., Lenzo, P. V., Ballmann, A. A., Proc. IEEE, 55, 2074, (1967)

Stephenson, N. C., Acta. Cryst. 18, 496, (1965)

Stranski, I. N. Z, Phys. Chem, 136, 259 (1928)

Strickland-Constable, R.F. Kinetics of Crystallisation, Academic Press, New York, (1967)

Subbarao, E. C., J. Am. Ceram. Soc. 44, 92, (1961)

Subbarao, E. C., Shirane, G., Jona, F., Acta. Cryst. 13, 226, (1960)

Tammann, G., States of aggregation, van Nostrand, (1925)

Tammann, G., Kristallisieren und Schmelzen, Leipzig (1903)

Tiller, W. A., J. Cryst. Growth, 2, 69, (1968)

Tyrrell, H. J. V., Diffusion and Heat Flows in Liquids, Butterworths, London (1961)

van Uitert, L. G. Singh, S., Levinstein, H. J., Appl. Phys. Lett, 11, 161, (1967)
Geusic, J. E. Bonner, W. A.

Volmer, M., Schulze, W., Z. Phys. Chem, 139, 156, (1931)

Volmer, M., Trans Faraday Soc. 28, 359, (1932)

Wemple, S. H., Di Domenic, M., J. Appl. Phys. 40, 720, (1969)

Whipps, P. W., Private Communication

White, E. A. D. (I), Techniques in Inorganic Chem. IV, 31, (1965)

White, E. A. D., Brightwell, J. W. II, Chemistry in Industry, 1662- 1965.

White, J. L. see Bockris (1959)

Wood, J. D. C., Private Communication

Zwicker, B., Scherrer, P., Helv. Phys. Acta. 16, 414, (1943)

Zwicker, B., Scherrer P., Ibid 17, 346, (1944)

APPENDIX A

THE DEFINITION OF DIMENSIONLESS NUMBERS

Dimensionless numbers are used in the solution of problems where the fluid mechanical equations which define the system under study are so complex that direct analytical solution is impossible. The well known principle of similarity is used in the solution. In a geometrical problem, if there are n triangles which are similar, and if the lengths of sides a_1, b_1, c_1 of the first triangle and of the a sides of the other triangles are known, then the lengths of the b and c sides of all the others may be found by multiplying by the ratio of a_n/a_1. By the same principle, if the fluid flow through two systems is similar, then if a relationship is true in one system it will be true in the other. In this way relationships between variables may be established experimentally for a simple system and then generalised for the solution of more complex problems. The two systems are similar if the dimensionless numbers specifying the systems are equal.

The value of the application of this principle can be seen in the case of flow through an infinite tube of diameter L. The flow along the tube in the one dimension is characterised by the Navier Stokes equation:

$$\rho \frac{\partial V_x}{\partial t} + V_x \frac{\partial V_x}{\partial x} = -\frac{p}{x} + \frac{4}{3}\mu \frac{\partial^2 V_x}{\partial x^2} \quad \ldots\ (A1)$$

where ρ is the density of the fluid, μ the ~~kinematic~~ dynamic viscosity, p the pressure at the point x and V_x the velocity of flow. This equation cannot be solved analytically. For two systems to be similar they must exhibit geometrical, kinematic and dynamic similarity. Geometrical similarity exists if the surfaces in the two systems in contact with the fluid are similar, i.e. both infinite tubes or infinite plane surfaces. Kinematic similarity occurs if all combinations of products and ratios of lengths and distances in the Navier Stokes equation have the same proportionality

constants. Thus:

$$V_x \frac{\partial V_x}{\partial x} = C_1 \frac{V_m^2}{L} \quad \text{.... (A2)}$$

and

$$\frac{\partial^2 V_x}{\partial_{\partial x^2}} = C_2 \frac{V_m}{D} \quad \text{.... (A3)}$$

Dynamic similarity occurs if the ratio of the different forces in the equation are the same. That is,

$$\rho V_x \frac{\partial V_x}{\partial x} = C_3 \mu \frac{\partial^2 V_x}{\partial x^2} \quad \text{.... (A4)}$$

C_1, C_2, C_3 are dimensionless constants found for one system. From (A2), (A3) and (A4) then, (ν is the kinematic viscosity)

$$\frac{V_m L}{\nu} = \frac{C_2 C_3}{C_1} = C. \quad \text{.... (A5)}$$

C is known as the Reynolds number N_{Re} and any two systems with the same Reynolds number will have similar flows. Thus, a Reynolds number of 2300 in any systems corresponds to the transition form lamellar to turbulent flow.

This method may be applied to the problem of convective heat transfer, where the relevant equations are more complex than the Navier Stokes equation. The relevant equations are:

$$dq = -k\frac{\partial t}{\partial n} \quad dA = h\,\theta s\, dA \quad \text{.... (A6)}$$

$$\rho \frac{\partial V_z}{\partial t} + V_x \frac{\partial V_z}{\partial x} + Vy \frac{\partial V_z}{\partial y} + Vz \frac{\partial V_z}{\partial y} =$$

$$\mu \left(\frac{\partial^2 V_z}{\partial x^2} + \frac{\partial^2 V_z}{\partial y^2} + \frac{\partial^2 V_z}{\partial z^2} \right) + g\beta\theta\rho \quad \text{.... (A7)}$$

$$\frac{\partial V_x}{\partial x} + \frac{\partial V_y}{\partial y} + \frac{\partial V_z}{\partial z} = 0 \quad \text{.... (A8)}$$

$$\rho Cp \frac{\partial \theta}{\partial t} + v_x \frac{\partial \theta}{\partial x} + v_y \frac{\partial \theta}{\partial y} + v_z \frac{\partial \theta}{\partial z} = k \left(\frac{\partial^2 \theta}{\partial x^2} + \frac{\partial^2 \theta}{\partial y^2} + \frac{\partial^2 \theta}{\partial z^2} \right) \quad \ldots\ (A9)$$

where dq is the heat flow across and element dA of surface with normal in direction n, k is the thermal conductivity of the fluid, h the coefficient of convective heat transfer, θs the temperature difference across the surface, Cp the heat capacity of the fluid, θ the fluid temperature at the point x,y,z, β the coefficient of expansity, g the acceleration due to gravity and the other terms have been previously defined.

Assuming that a similar geometry exists for two systems designated by subscripts 1 and 2, then if the systems are similar the following relations hold:

$$\begin{aligned}
x_2 &= \lambda x_2; \quad y_2 = \lambda y_2, \; z_2 = \lambda z_1, \; L_2 = \lambda L_1 \\
t_2 &= \rho t_1 \\
\theta_2 &= \phi\theta_1, \quad \theta s_2 \quad \phi\theta s_1 \\
v_{x2} &= \omega\, v_{x1} \quad \text{etc.} \\
g_2 &= \xi g_1 \\
p_2 &= \psi p_1 \\
\beta_2 &= \chi\beta_1 \\
\rho_2 &= \partial\rho_1 \\
\mu_2 &= \eta\mu_1 \\
Cp_2 &= \varepsilon\, Cp_1 \\
k_2 &= Kk_1
\end{aligned} \quad \ldots\ (A10)$$

Rewriting (A7) for cases 1 and 2

$$\rho_1 \frac{\partial v_{z1}}{\partial t_1} + v_{x1} \frac{\partial v_{z1}}{\partial x_1} + v_{y1} \frac{\partial v_{z1}}{\partial x_1} = \mu_1 \left(\frac{\partial^2 v_{z1}}{\partial x_1^2} + \frac{\partial^2 v_{z1}}{\partial y_1^2} + \frac{\partial^2 v_{z1}}{\partial x_1^2} \right)$$

$$+ g_1 \beta_1 \rho_1 \theta_1 \quad \ldots\ (A11)$$

and $$\rho_2 \frac{\partial v_{z2}}{\partial t_2} + v_{x2} \frac{\partial v_{z2}}{\partial x_2} + v_{y2} \frac{\partial v_{z2}}{\partial x_2} = \frac{\partial p_2}{\partial z_2} + \mu_2 \left(\frac{\partial^2 \sigma_z}{\partial x_2^2} + \frac{\partial^2 v_z}{\partial y_2^2} + \frac{\partial^2 v_{z2}}{\partial z_2^2} \right)$$

$$+ g_2 \beta_2 P_2 \theta_2 \qquad \ldots\ (A12)$$

Now, substituting for $x_2 = \lambda x_1$, $v_{x2} = w v_{z1}$ etc in A12

$$\sigma\rho_1 \left[\frac{\omega}{\mathcal{P}} \cdot \frac{\partial v_{z1}}{\partial x_1} + \frac{\omega^2}{\lambda} \left(\frac{\partial v_{z1}}{\partial x_1} + \frac{\partial v_{z1}}{\partial x_1} + \frac{\partial v_{z2}}{\partial y_1} \right) \right] = \frac{-\psi}{\lambda} \frac{\partial p_1}{\partial z_1} + \frac{\eta_\omega}{\lambda 2} \mu \left[\right.$$

$$\left. \frac{\partial^2 v_{x1}}{\partial x_1^2} + \frac{\partial^2 v_{y1}}{\partial x_1^2} + \frac{\partial^2 v_{z1}}{\partial z_1^2} \right] + \xi\chi\sigma\phi g_1 \beta_1 \rho_1 \theta_1 \qquad \ldots\ (A13)$$

(A13) and (A11) must be identical and this only occurs if

$$\frac{\sigma\omega}{\mathcal{P}} = \frac{\sigma \omega^2}{\lambda} = \frac{\psi}{\lambda} = \frac{\eta_\omega}{\lambda^2} = \varepsilon\chi\sigma\phi \qquad \ldots\ (A14)$$

Other relations may be found in the same way using equation (A9)

$$\frac{\sigma\varepsilon\phi}{\mathcal{P}} = 1 \frac{\sigma\varepsilon\phi}{\lambda} = \frac{K\phi}{\lambda^2} \qquad \ldots\ (A15)$$

From,(A14) and (A15) the following relations hold

$$\eta = \lambda \sigma \qquad \ldots\ (A16)$$

$$\mathcal{P} = \frac{\lambda}{\omega} \qquad \ldots\ (A17)$$

$$\psi = \omega^2 \sigma \qquad \ldots\ (A18)$$

$$\eta^2 = \lambda^3 \phi \xi \sigma^2 \chi \qquad \ldots\ (A19)$$

$$K = \eta_\varepsilon \qquad \ldots\ (A20)$$

Equation (A16) yields

$$\frac{\rho_1 L_1 v_1}{\mu_1} = \frac{P_2 L_2 v_2}{\mu_2}$$

As previously defined (A5) this is the Reynolds number. Hence, one requirement for similarity of heat flow is that both systems should possess the same Reynolds number.

Equation (A.18) yields $\frac{\rho_1 v_1^2}{P_1} = \frac{\rho_2 v_2^2}{P_2}$

that is, the ratios of kinetic energy to pressure must be constant in similar systems. $\frac{\rho v}{P}$ is called the Euler number and is of little significance in problems of free convection.

Equation (A17) yields $\frac{t_1 v_1}{L_1} \quad \frac{t_2 v_2}{L_2}$ which is an obvious requirement for similarity.

Equation (A19) yields

$$\frac{g_1 \beta_1 \rho_1^2 L_1^3 \theta_{51}}{\mu_1^2} = \frac{g_2 \beta_2 \rho_2^2 L_2^3 \theta_{32}}{\mu_2^2} \qquad \ldots\ (A21)$$

This is termed the Grashof number N_{Gr}, and is important because it is a measure of the driving force for convection, i.e. $g\beta\Delta\theta$ against the viscous forces apposing convection $\nu = \mu/\rho$.

Equation (A20) yields $\frac{\mu_1 Cp_1}{k_1} = \frac{\mu_2 Cp_2}{k_2}$

and the relation $\frac{\mu Cp}{k}$ is called the Prandtl number, N_{Pr}, and can also be expressed as $N_{Pr} = \frac{\nu}{\alpha}$ where α is the thermal diffusivity. The Prandtl number relates the thermal flow to the momentum flow. If the Prandtl number equals unity, then isotherms and streamlines are identical.

A further relation may be derived from equation (A6) if $h_2 = ih_1$ then one obtains $\frac{K}{\lambda} = i$, that is $\frac{h_1 L_1}{k_1} = \frac{h_2 L_2}{k_2}$. The dimensionless $\frac{hL}{k}$ is called the Nusselt number, N_{Nu}. The Nusselt number contains the coefficient of heat transfer by convection, h, which is the quantity that has to be determined for the solution of many heat flow problems.

The heat flow problem has been reduced to three variables, i.e. the Prandtl, Grashof and Nusselt numbers, of which only two are independent.

Thus, $N_{Nu} = \phi\ (N_{Gr}, N_{Pr})$ where ϕ is some power function of N_{Gr} and N_{Pr}.

The principle of similarity may also be applied to systems in which the concentration of a moving fluid solution varies in time. The equations of mass transfer are

$$\frac{\partial m}{\partial t} = -D \frac{\partial c}{\partial n} \qquad \ldots\ (A21)$$

$$\text{and } \frac{\partial c}{\partial t} + v_x \frac{\partial c}{\partial x} + v_y \frac{\partial c}{\partial y} + v_x \frac{\partial c}{\partial z} = D\left(\frac{\partial^2 c}{\partial x^2} + \frac{\partial^2 p}{\partial y^2} + \frac{\partial^2 c}{\partial z^2}\right) \qquad \ldots\ (A22)$$

$$\frac{\partial c}{\partial x} + \frac{\partial c}{\partial y} + \frac{\partial c}{\partial z} = 0 \qquad \ldots\ (A23)$$

where c is the concentration at the point x, y, z and D, the coefficient of diffusion. These equations are exactly similar to equations (A6), (A8), (A9) and equation (A7) also applies to the mass transfer problem, except the term $g\beta\theta\rho$ is replaced by $g\beta\Delta\rho$ where $\Delta\rho$ is the change in density imposed by the concentration differences. Hence, it is possible to derive Prandtl, Grashof and Nusselt numbers for the mass transfer where the appropriate thermal variables are replaced by their mass equivalent. Thus, the Prandtl number becomes $N_{Pr} = \frac{\nu}{D}$ and is usually called the Schmidt number N_{Sc}. The Grashof number becomes $\frac{g\Delta\rho L^3}{\mu^2}$ and the Nusselt number $\frac{Lb}{\delta}$, where b is the coefficient of mass transfer defined by $\frac{\partial m}{\partial t} = b(C_S - C_o)$ and δ is the thickness of the mass boundary layer, C_s and C_o are the concentrations at the surface and bulk respectively.

A further dimensionless number is obtained from equation (A22) in the following way. Dividing through by $CoVL^2$, where Co is the bulk concentration, V and L a characteristic fluid characteristic fluid velocities and lengths, then (A22) becomes (A23)

$$V_x \frac{\partial C}{\partial X} + V_y \frac{\partial C}{\partial Y} + V_z \frac{\partial C}{\partial Z} = \frac{D}{VL}\left(\frac{\partial^2 C}{\partial X^2} + \frac{\partial^2 C}{\partial Y^2} + \frac{\partial^2 C}{\partial Z^2}\right)$$

where $V_x = \frac{v_x}{V}$, $X = \frac{x}{L}$, $C = {}^{c}/Co$ etc.

The term $\frac{VL}{D}$ is dimensionless and is called the Peclet number, $N_{Pé}$ This number determines the relative importance of fluid motion to pure diffusion in the mass transfer process. The thermal equivalent is $\frac{VL}{\alpha}$ where $\alpha = \frac{\rho Cp}{k}$ the thermal diffusivity, and measures the relative importance of convection to conduction in heat transfer. At large Péclet numbers the fluid motion terms are dominant.

Table A1 summarises the principal dimensionless numbers for both heat and mass transfer systems.

Dimensionless number	Symbol	Thermal	Mass
Reynolds	N_{Re}	$\frac{VL}{\nu}$	$\frac{VL}{\nu}$
Péclet	$N_{Pé}$	$\frac{VL}{\alpha}$	$\frac{VL}{D}$
Prandtl	N_{Pr}	$\frac{\nu}{\alpha}$	-
Schmidt	N_{Sc}	-	$\frac{\nu}{D}$
Grashof	N_{Gr}	$\frac{g\beta\theta L^3}{\nu^2}$	$\frac{g\Delta\rho L^3}{\rho\nu^2}$
Nusselt	N_{Nu}	$\frac{hL}{k}$	$\frac{Lb}{\delta}$

For an 8 mole % solution of lead tantalate at 1160°C.

Table A2 lists the values of the relevant dimensionless number using the data derived in Chapter 2.

Table A2

Number	Value
N_{Re}	10^4
$N_{Pé}$	31.8×10^6
N_{Sc}	3.06×10^3
N_{Pr}	0.513
N_{Gr} (Thermal)	19×10^6

APPENDIX B

THE DERIVATION OF THE RELATIONSHIP BETWEEN THE SOLUBILITY OF A REFRACTORY OXIDE AND THE TEMPERATURE OF SOLUTION

The derivation of solubility follows from a consideration of figure B.1, in which a cycle of the states of the oxide is shown. Pure solid oxide is in equilibrium with the solution at temperature T ^{o}K, where N moles of oxide is the saturated concentration in solution at temperature T ^{o}K. To derive the solubility N moles of pure oxide are melted at temperature T with a free energy charge ΔG_F and then mixed with the solvent with a free energy charge $\Delta G_S = 0$.

By standard thermodynamics

$$\Delta G_M = RT \ln K = RT \ln \frac{\gamma N}{a_o} \quad \ldots\ (B1)$$

where K is the equilibrium constant, γ the activity coefficient of the oxide in the solution and a_o is the activity of the oxide in the pure molten state. This pure molten state is taken as the reference state for the free energy change and therefore, $a_o = 1$.

If ΔG_M is known, then N can be found, but ΔG_M cannot be deduced from first principles. However, considering figure B1, the total free energy change aroung the cycle must be zero. Therefore

$$\Delta G_M = -\Delta G_F \quad \ldots\ (B2)$$

ΔG_F may be derived by standard thermodynamics.

$$\Delta G_F = (\Delta H_M)_T + T\,(\Delta S_M)_T \quad \ldots\ (B3)$$

where $(\Delta H_M)_T$ and $(\Delta S_M)_T$ are the heat and entropy of mixing at the temperature T. If ΔH and ΔS are the heat and entropy of mixing at the melting point Tm and ΔCp is the difference in heat capacity between solid and liquid oxide, then

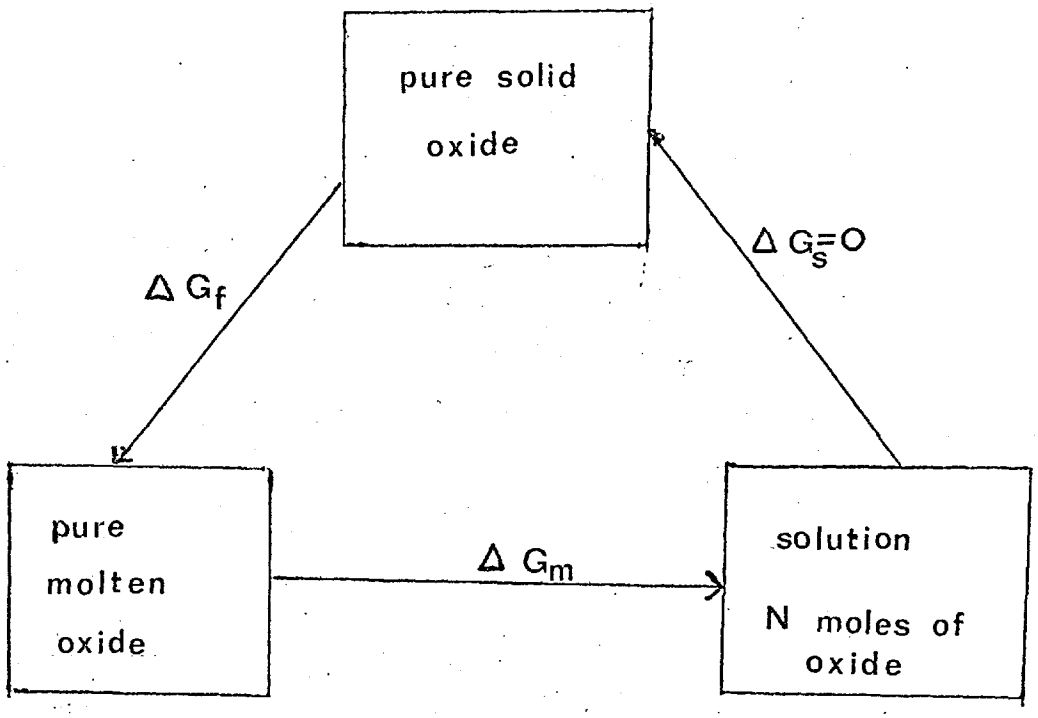
pure solid oxide
ΔG_f
$\Delta G_s = 0$
pure molten oxide
ΔG_m
solution
N moles of oxide

FIG. BI.

$$(\Delta H_m)_T = \Delta H_m + \int_{T_m}^{T} \Delta Cp\, dT \cong \Delta H_m + Cp\,(T-T_m) \qquad \ldots.(B4)$$

$$(\Delta S_m)_T = \Delta S_m + \int_{T_m}^{T} \frac{\Delta Cp}{T}\, dT = + \frac{\Delta H_m}{T_m} + \Delta Cp\ \ln \frac{T}{T_m} \qquad \ldots.(B5)$$

Substituting from B2, B3, B4 and B5 into equation B1, then

$$\log \gamma N = \left(\frac{\Delta H_m}{RT_m} - \frac{\Delta Cp}{R} \right) \left(\frac{T_m}{T} - 1 \right) + \Delta Cp\ \ln \frac{T_m}{T} \qquad \ldots.(B6)$$

If the solution is ideal $\gamma = 1$ and

$$\log N = \left(\frac{\Delta H_m}{RT_m} - \frac{\Delta Cp}{R} \right) \left(\frac{T_m}{T} - 1 \right) + \Delta Cp\ \ln \frac{T_m}{T}$$

If the solution is regular then

$$\text{Log } N = \left(\frac{\Delta H_m}{RT_m} - \frac{\Delta Cp}{R} \right) \left(\frac{T_m}{T} - 1 \right) + \Delta Cp\ \ln \frac{T_m}{T} + \frac{\Delta H'}{RT}$$

where $\Delta H'$ is the heat of mixing and $\Delta H' = RT \ln \gamma$.